technische universität
dortmund

TÜRK-ALMAN ÜNİVERSİTESİ
TÜRKISCH-DEUTSCHE UNIVERSITÄT

Werkstoffprüftechnik
Prof. Dr.-Ing. habil. Frank Walther
www.wpt-info.de

Technische Universität Dortmund
Fakultät Maschinenbau
Fachgebiet Werkstoffprüftechnik
Prof. Dr.-Ing. habil. Frank Walther

Fatigue resistant design of an aerostat's mooring station

Master Thesis
February 2018

Name: Özgün Sarıoğuz
Matr. No.: 189964

Supervisors:

Prof. Dr.-Ing. habil. Frank Walther

Asst. Prof. Dr. Mehmet Gökhan Gökçen

15.02.2018

The result of the thesis presentation of Özgün SARIOĞUZ, who is registered in the joint graduate program Manufacturing Technology between Turkish-German University and Technical University Dortmund with the registration number 1561011102, titled "Fatigue Resistant Design of an Aerostat's Mooring Station" held on 15.02.2018 at 10.00 is presented below.
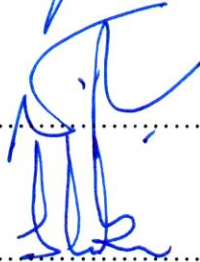
| ☒ Successful | ☐ Extension (3 months) | ☐ Unsuccessful |

Thesis Presentation Committee:

Prof. Dr.-Ing. habil. Frank WALTHER
(Co-advisor)

Assist. Prof. Dr. Mehmet Gökhan GÖKÇEN
(Co-advisor)

Assist. Prof. Dr. Selim COŞKUN
(Member)

Assist. Prof. Dr. Mehmet İPEKOĞLU
(Member)

Assist. Prof. Dr. Ali Bahadır OLCAY
(Member)

technische universität dortmund

Materials Test Engineering
Prof. Dr.-Ing. Frank Walther
www.wpt-info.de

Master thesis

Name:	**Özgün Sarioguz**
Company:	**OTONOM TEKNOLOJI**
Supervisor:	**M.Sc. Shafaqat Siddique** **Dr. Mehmet Gökhan Gökcen**
Title:	**Fatigue resistant design of an aerostat's mooring station**

Aerostat is a lighter-than-air system, consisting of a Helium-filled balloon and a mooring station, which is used for terrain-scaled measuring and monitoring applications. As they remain in service at higher altitudes for several weeks to months, they are subjected to dynamic forces for long periods due to varying wing magnitudes and directions at these altitudes. The mooring station of the aerostat, which is connected to the balloon with a tether during service and with ropes during landing, consisting of mainly metallic components, is affected by the dynamic loading; therefore, the fatigue mechanisms should be taken into consideration for the design of the mooring station.

This work aims at developing a fatigue-resistant design for components of the mooring station i.e. tether crane, flying sheave, rope connection arm as well as park tower. These components will be analyzed based on the maximum force expected during the flight and parking positions calculated based on the wind speed. Steel alloys ST37, ST44 and ST52 as well as aluminum alloy Al5083 will be considered to generate Woehler curves from the static FEM analysis based on wind speed. An appropriate method will be selected for calculation of fatigue strength by mean stress corrections. The mechanical properties of the materials required for fatigue simulations i.e. tensile strength, hardness and Young's modulus will be extracted from the existing literature for the used materials. Static FEM analysis will then be used to generate maximum and minimum loads for theoretical design of Woehler curves by nCode for each component, such that they are considered having safe life for 1E6 cycles. The sensitive parts i.e. flying sheave made of Al5083 and tower crane made of ST44 will be tested under fatigue loading up to 1E6 cycles, where they should turn as run-outs corresponding to the design. For testing of these parts, holder and ground connection platforms will be designed and manufactured, and will be connected to the ground so that all parts can be tested at the same loading conditions.

This study will be carried out at company "OTONOM TEKNOLOJI" in Ankara, and will be supervised jointly by supervisors from TU Dortmund University, Germany and Turkish-German University in Istanbul, Turkey.

Dortmund, 20.11.2017

(Prof. Dr.-Ing. Frank Walther)
Department of Materials Test Engineering (WPT)

Istanbul, 20.11.2017

(Dr. Mehmet Gökhan Gökcen)
Turkish-German University

Abstract

Aerostat is a lighter-than-air system, consisting of a Helium-filled balloon and a mooring station, which is used for terrain-scaled monitoring applications. During the service at higher altitudes for several weeks to months, the mooring station is subjected to dynamic forces for long period by varying wind magnitudes and directions. The metallic components of the mooring station, which are connected to the balloon with a tether during service and with ropes during landing, are affected by these dynamic loads; therefore, the fatigue mechanisms should be taken into consideration. In the scope of this thesis project, both a previously designed and the new fatigue resistant designed mooring stations of accordingly 14 m and 17 m aerostats were analysed depending on their fatigue behaviour. The fatigue behaviour of the mooring stations were analysed by CAE software ANSYS R16.2 and nCode DesignLife 11.0. Besides, life curves and fatigue strengths for the components of fatigue resistant designed mooring station of 17 m aerostat were analytically generated with the help of equations presented by the former academic works. The CAE analyses and analytical generated curves were then verified by the cyclic loading tests for the two mooring station components, flying sheave and tower crane section. For comparison, fatigue safety factors, which were calculated depending on the determined fatigue limits of the components, were utilized.

CAE fatigue analysis comparison of the two mooring station designs have shown that, despite an increase in the load range by 50% the large mooring station of 17 m balloon has not shown any significant decrease in fatigue safety factors parallel to this load range increase. The safety factors by analytically generated life curves of the fatigue resistant designed mooring station components were lower than those found by the CAE fatigue analysis and the highest similarity to CAE fatigue analysis results was seen by the analytical generated S-N curve results, which are accepted as more accurate due to more comprehensive parameter usage. In the cyclic load tests of the two components, made of accordingly steel and aluminium, no failure was observed. The results of the thesis work therefore have shown, fatigue resistant design of the mooring station and all the analysis methods within, were reliable and the components were suitable to use under dynamic loads. For future aerostat design projects, use of this fatigue resistant design approach is recommended together by improving it with more comprehensive cyclic load tests with higher frequencies between 20-50 Hz and up to 10^8 cycles both for the components and specimens.

Table of Contents

Abbreviations and symbols

Abbreviation	Definition
Al	Aluminium
CAD	Computer Aided Drawing
CAE	Computer Aided Engineering
CFD	Computational Fluid Dynamics
Cr	Chromium
FEA	Finite Elements Analysis
FEM	Finite Elements Method
FLE	Fatigue Limit Equation
HB	Brinell Hardness
HCF	High Cycle Fatigue
HRC	Rockwell Hardness
HV	Vickers Hardness
LCF	Low Cycle Fatigue
LTA	Light-Than-Air
Max.	Maximum
Min.	Minimum
Mn	Manganese
MSC	Mean Stress Correction
SF	Safety Factor
SRF	Surface Retention Factor
UTS	Ultimate Tensile Strength

Symbol	Unit	Definition
σ_a	MPa	Stress amplitude
σ_v	MPa	Equivalent (von Misses) stress
σ_m	MPa	Mean stress
σ_{max}	MPa	Maximum stress
σ_{min}	MPa	Minimum stress
σ_e	MPa	Endurance limit
σ_u	MPa	Ultimate tensile strength
σ_y	MPa	Yield tensile strength
σ_f'	-	Fatigue strength coefficient
ε_f'	-	Fatigue ductility coefficient
b	-	Fatigue strength exponent
c	-	Fatigue ductility exponent
N_f	Cycle	Number of cycles to failure

1 Introduction

Technical problems -or requirements, confronted in the industry, make scientific research projects have a great importance, for all of the developing fields of technology today. It is also possible, on the other hand, conducting scientific works, within the design and engineering projects of products or of processes, in order to simultaneously achieve these technical difficulties. One such field of these design and engineering projects is the aerostat technology.

Aerostat is a currently developing technology which can be described as a lighter-than-air (LTA), modern observation vehicle, which consists of a helium filled balloon and a mooring station. It is especially used in terrain-scaled monitoring applications, where an online monitoring system can be held at high altitudes for long durations. The semi-flying, semi-static device consists of two main components as a tethered Helium balloon and a mooring station. The balloon is the main part, named as aerostat, which executes flight and observation duties during the service while the mooring station is the component on which the aerostat is tethered, is also benefited during the take-off and landing duties especially when maintenance of the aerostat is required.

Figure 1.1: An aerostat example by Craftsmen Industrial [Cra10]

Owing to the aerostatic characteristic of the vehicle, great dynamic loads can be seen on mooring stations, which are emerged by winds acting on aerostats during flight as well as during the maintenance activities on the ground. These dynamic forces might cause such

dynamic load related material failures as metal fatigue, especially within the mooring station which is most particularly built by metallic components.

Due to this problem, a design work with scientific methodology against metal fatigue of the components are precisely required, which take these dynamic forces as well as fatigue behaviour of the mooring station components into consideration, in order to produce safe and reliable aerostat vehicles which will not fail during the service.

Depending on this issue, the thesis work will cover a scientific fatigue resistant design approach in the design project of 17 m aerostat, and a comparison with the older mooring station design of 14 m aerostat according to their predicted fatigue behaviour. Firstly, all the relevant technical information on aerostats and aspects of fatigue will be presented in Chapter 2. The motivation and goals will then be clearly described in the Chapter 3. In Chapter 4, loading characteristics of the aerostats, mooring stations and fatigue related material properties of the mooring station components will be given. In Chapter 5, setup and results of CAE – fatigue analysis of the two mooring station designs will be explained. While Chapter 6 demonstrates analytical prediction of fatigue life of the 17 m aerostat mooring station components, in Chapter 7 the results of cyclic loading – or service - tests of the two of these components will be described. All of the presented results will be discussed in the end according to the given aims and motivations of the thesis work in Chapter 8.

The results of this thesis work is hence accepted to have great influence, especially, on fatigue resistant aerostat designs in the future, which focus on dynamic loads affecting the metal components of the mooring station. This thesis project, indeed, can be standardized and used in the future fatigue resistant design and engineering projects on aerostats.

2 State of the art

2.1 Aerostat technology

2.1.1 Introduction

Aerostat can principally be described as a balloon, containing helium, which has aerodynamic characteristic, as also implied in the name, is as well as statically tethered to a mooring station in the ground. The capability to lift is obtained by buoyancy, caused by helium inside the balloon. Through the tether, which connects the aerostat to mooring station, the balloon can send and receive data while being kept at a specific altitude –or position from the ground. The mooring station has several duties as supplying power to the aerostat, conducting the take-off, landing and maintenance activities [Pet05].

The first commercial design project on aerostats was made in 1990s, by TCOM, with a special fabric material for balloon, which provides both flexibility and fluid conservation. It was designed with a size which lets number of users up to two to four people, successfully complete both filling, deflation and flight operations. A spun airfoil was in fact the base of the geometry in the design. For the other sections of the balloon beside the main surface, such as hull, fins, ballonet and reinforcements, again this fabric material was used. Through the hull, helium was also deployed inside the fins [Pet05].

The hardware and equipment on the aerostat was basic, which are ropes with eye splices and commercial joints. In order to protect aerostat pitch angle from disturbance of a variation in the weight of the payload, the confluence lines are used for the suspension of weight. By a steadily blowing fan, the ballonet was able to remain the stall pressure. The inflation and deflation processes were quickly made via a set of ring and the plate bolted on it [Pet05].

The mooring station was placed on the back of a long vehicle on the other hand, which included such components as a tether winch, a generator and slip rings, which are used to supply power and execute data transfer between the aerostat. The tether, which connects the aerostat to the mooring station, was made of commercially reachable materials. During the maintenance on the ground level, the aerostat, however, had to be placed on another area than the long vehicle, by a cable bridle. All further designs have applied this concept, and improved it with tests. Many modifications were made to enhance flight effectivity of the aerostat, such as changing the fabric material in order to provide better rigging, therefore better reliability [Pet05].
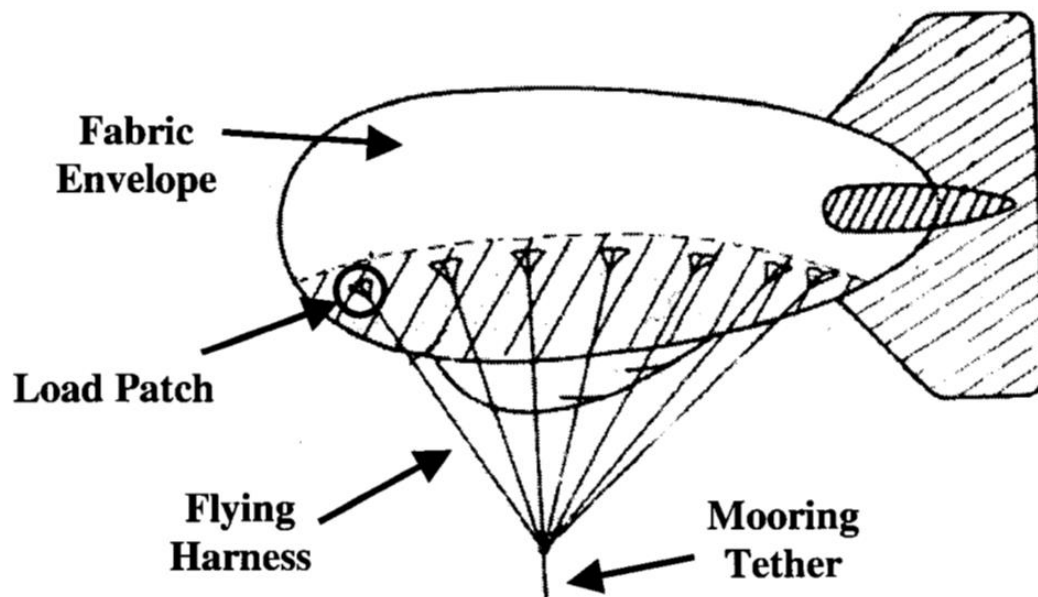
Figure 2.1: Sketch of a basic aerostat [Mil05]

There are, in fact, two major types of Light-Than-Air (LTA) platforms, which are aerostats and airships. They are both filled with a gas, mainly helium, to lift in the air, while aerostats are tethered to a mooring station on the ground, airships freely move. Without a propulsion system, aerostats are only connected to the ground via a long, strong data cable, named as tether. The main tasks of the tether can be named as firstly, holding the aerostat, which is loaded by monitoring, and data transmitting equipment as well as sensors, in a specific area in the specific altitude and also supplying power to aerostat and providing the data transfer. Airships are however directionally controlled devices with self-propulsion and are even able to fly manned [GAO-13-81].

The aerostats have actually been used by the Department of Defence of The United States (U.S.) since 1978 on the borders, for such monitoring activities as drug detection. Not only in defence but also in civil activities, the aerostats were used to monitor air pollution, and atmospheric and geographical changes. Beginning from the year 2009, aerostats were utilized by the Environmental Protection Agency of U.S. Government in order to obtain samples from the air, to investigate emission for example during forest fires. They were also used by the U.S. Department of Commerce's National Oceanic and Atmospheric Administration, for logging wind speed magnitudes and directions. Moreover, aerostats are considered nowadays by the U.S. Department of Homeland Security's U.S. Customs and Border Protection to be utilized for security activities at the borders. Until now, the utilization of LTA platforms in civil activities was actually seriously rare, comparing to that in defence and military. Even though the utilization of commercial airships today are limited only to advertisement and touristic activities, the new interests have occurred to deploy airships for

transportation activities, especially in regions, where transportation with modern vehicles are problematic, such as between Canada and Alaska [GAO-13-81].

Source: U.S. Army.

**Figure 2.2:** An aerostat used by the U.S. Army [GAO-13-81]

The interest of U.S. Department of Defence on aerostats has especially increased due to the inability of air defence of enemies, and cost-efficiency of LTA for heavy-lift cargo operations especially in maintenance costs [GAO-13-81].

Source: U.S. Navy.

Figure 2.3: An airship utilized by the U.S. Navy [GAO-13-81]

As stated frequently above, within the commercially designed aerostats, a payload is deployed in high altitudes which have specific monitoring, data transmitting and other electronic equipment. These can be summarized as surveillance radars with varying size and abilities, Signal Intelligence (SIGINT) Collection, gyro-stabilized daylight, low-light as well as infra-red video cameras, direct television and FM radio broadcast and relays, VHF / UHF, Ground Control Intercept (GCI), microwave communications, and varying environmental monitoring equipment, which all can be seen in the system integration schematic presented in the below **Figure 2.4** [Gaw07].
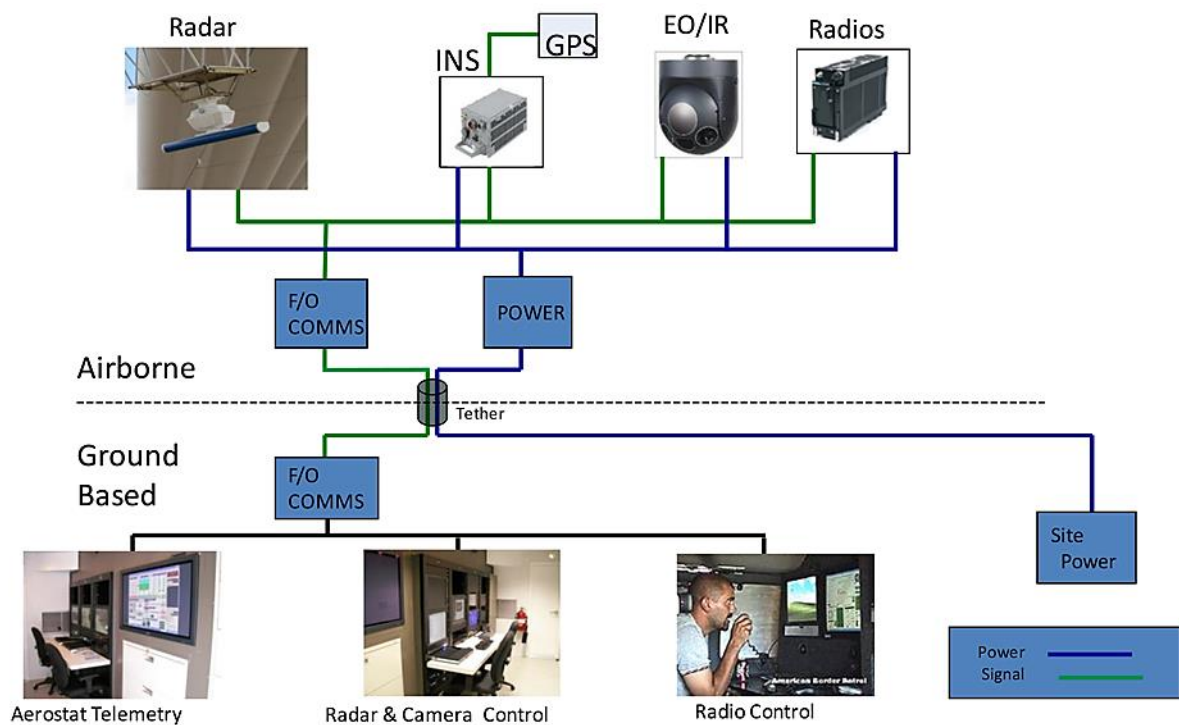
Figure 2.4: System integration of an aerostat system [Kra11]

The data obtained from the equipment in the payload, can be simultaneously processed or displayed in the ground control platform [Kra11].

In the design process of aerostats, on the other hand, the specific parameters, presented in the **Table 2.1** below, are required [Gaw07].

Table 2.1: Design parameters of aerostats [Gaw07]

Input Parameters	SI Unit	Typical Value
Payload	[kg]	7.00
Floating Altitude (From Sea Level)	[m]	740.81
Spot Altitude from Sea Level	[m]	560.00
Design Wind Speed	[m/s]	15.00
Off Standard Temperature	[C]	20.00
Operational Time	[days]	15.00
Diurnal Temperature range	[C]	10.00
Free Lift Permissible	%	15.00
Permissible Reduction in Altitude	±DH	5.00
Constant Parameters		
Contained Gas Initial Purity	[%]	99.50
Option for Envelope Material (PVC-1, Other-2)	PVC	1.00
Rate of Gas Permeability thru Envelope fabric	[ltr/m2/day]	2.50
PoE Cable Specific Length	[kg/m]	0.04
Low Loss Cable Specific Length	[kg/m]	0.00
Elastic Strip Specific Length	[kg/m]	0.02

Available PVC Fabric density	[kg/m2]	0.21
Permissible Blow by and Excess Length for all the cables Design altitude	AGL %	20.00
Centre of pressure for Aerostat (0.3-0.35)	[-]	0.33
Options		
Profile Configuration (NPL-1, GNVR-2, SAC-3, Optimum-4, TCOM360Y-5)	SAC	3
Petal Configuration (1-Single, 2-Double)	Double	2
Rear Gore Petals (No. of Petals)	[-]	10.00
Front Gore Petals	[-]	20.00
Contained Gas (He-1, H2-2)	Helium	1
Include Integrated Balloonet OR Elastic Strips (Ballonet-1,El Strip-2)	El. Strip	2

2.1.2 Mooring station

The base of the mooring systems, as seen in an example in **Figure 2.5** below, is a small trailer, with similar look to a boat, can possibly be made of steel or aluminium. The rotating platform is specifically placed onto a trailer via a strong bearing system containing slip rings. All the required equipment, machines and devices are placed onto or within this rotating platform which are essential to control the aerostat [Pet05].

**Figure 2.5:** A mooring station example [Cra10]

The launch and landing activities are conducted by the winch while tower is required to securely hold aerostat during maintenance on the ground level. A user can control the tether, nose and close haul winches on the winch control station, simply by joysticks. If necessary, a generator can also be placed onto the platform, to supply required amount of power, when especially there is no mains electricity. During the maintenance on the ground level, specifically to resupply the lost helium or to repair equipment, the platform let user reach the aerostat as well as loaded equipment on it [Pet05].

The bumper rails are constructed, on both sides of the platform, to contact the balloon and protect it from damaging by hitting sharp edges, in case of serious wind cases, during maintenance on the ground [Pet05].

In the both sides of the flying sheave, spreader beams are placed to supply connection points for tether lines and to redirect the landing ropes. Electric landing rope winches, on the other hand, are especially essential for the take-off and landing operations [Pet05].

The platform is such designed, so that the payload will be placed at the end, mostly inside a cradle, when the aerostat is moored to the station. Another important mechanism in the system is the ability of platform to rotate. According to the changes in wind direction, the platform will rotate with the aerostat, so that aerostat will not be affected by winds affecting on its sides. By this way, the stresses occurred on platform and within the ropes will always

be at the minimum level, thus, the equipment will be protected. Lastly, the ladders, placed on the both sides, are used to make the platform accessible by users [Pet05].
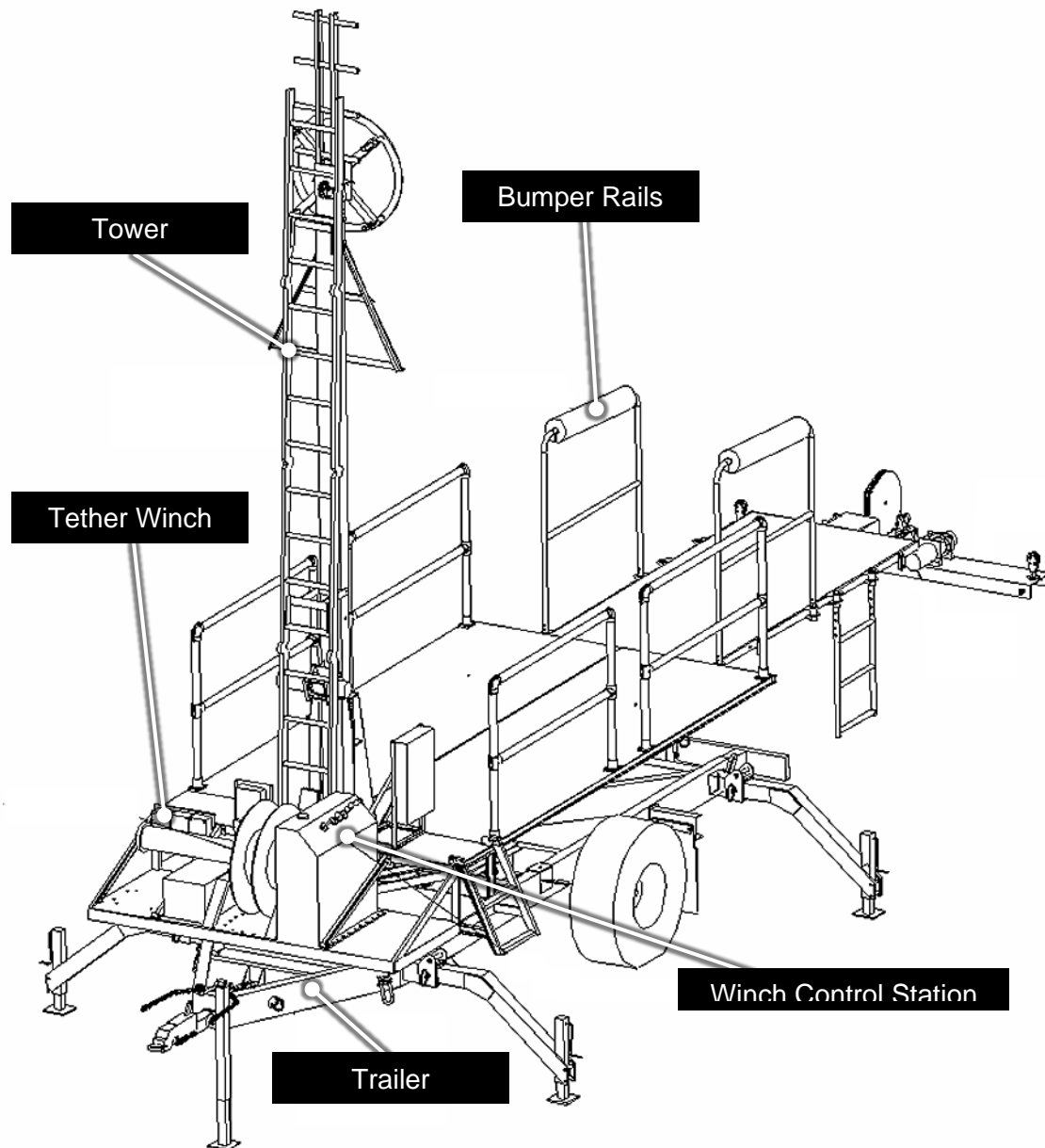
Figure 2.6: A basic mooring station design [Pet05]

2.1.3 Cautions

There are several major risks of hazard while operating such LTA devices as aerostats and airships. Firstly, weather, most specifically, high wind conditions generate the highest threat to these devices. In order to protect an aerostat system, especially the payload and mooring station from failure, the flight must be stopped, the platform level must get closer to the ground, and placed inside the mooring station, in case of any approaching dangerous weather conditions during the flight of an aerostat. For airships, dangerous weather

conditions under high wind velocities, bring about a difficulty of control the vehicle as well as an increase in the energy consumption [GAO-13-81].

Beside of the problematic weather conditions described above, the fabric of the balloons can also be easily damaged by bullets and other projectiles in case of an attack in the war zones or under combat missions. One solution to this problem would be lowering the helium pressure within the envelope, so that the inside pressure will be a bit higher than the atmospheric pressure. Thus, the gas leaks from damaged holes will be much slower, even the fabric shall be repaired within the planned maintenance time [GAO-13-81].

2.2 Fatigue

2.2.1 Introduction

Fracture may occur within components or mechanical systems, which undergo cyclic loads applied in many number of cycles, even by loads lower than they can resist when applied once as static. The most common example to this is the fracture seen when bending a thin rod repeatedly in reverse directions. This kind of failures is caused by the phenomena, named, fatigue. The most common structures, which are affected by repeated loading, and thus tend to fatigue, are bridges, cranes, towers, railways etc. Within metallic components, which are under the influence of cyclic loading, fatigue is caused by progressive expansion of the micro-cracks [Kum09].

There are four main stages of fatigue defects:

– Micro-crack initiation, at the regions with concentrated stresses
– Crack propagation
– Fatigue fracture

The progress of crack growth can be seen in **Figure 2.7** below. Fatigue defects are described by number of cycles, and it takes time until determining a predicted defect phenomena. There are basically two types of fatigue failure, which are categorized according to the required number of cycles until the fracture, high cycle (HCF) and low cycle (LCF) fatigues. While LCF is described for the ruptures observed after number of cycles between a few cycles to thousands, HCF is used to categorize fractures seen after more than thousands even few millions number of cycles.
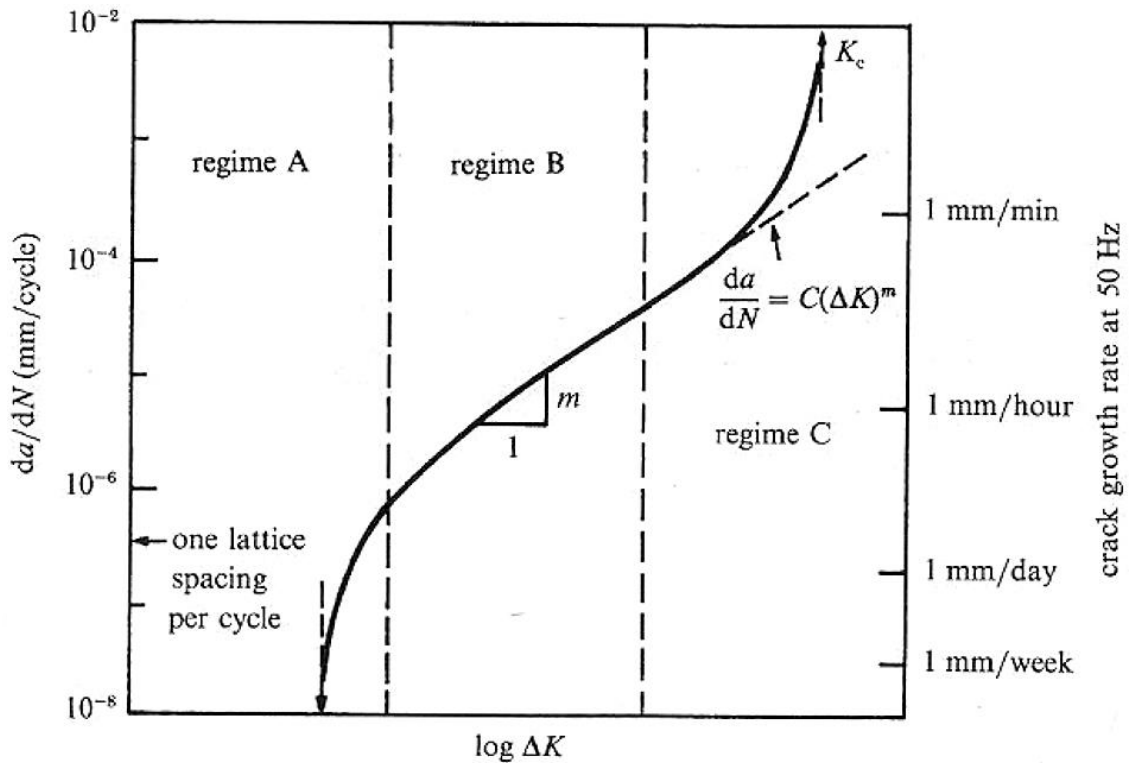
Figure 2.7: Fatigue growth in three regimes [Ram14]

The technical properties and terms used to define stress cycles, caused by these cyclic loads are given in the next chapter, which are essential when researching fatigue failures or making designs against fatigue.

2.2.2 Stress cycles

The major factors resulting fatigue ruptures are basically high values of maximum tensile stresses, varying and fluctuating type of cyclic loading, and adequate number of cycles of the cyclic stress. Despite the large variety, there are three main types of stress cycles as accordingly given in **Figure 2.8** below, fully reversed, tension-tension, and random. Within the fully reversed, or tension-tension or compression-compression cycle types, the stresses are observed with a sinusoidal character. While maximum and minimum stresses in fully reversed are equal to each other, in tension-tension, or compression-compression types, they are different [ASM08].
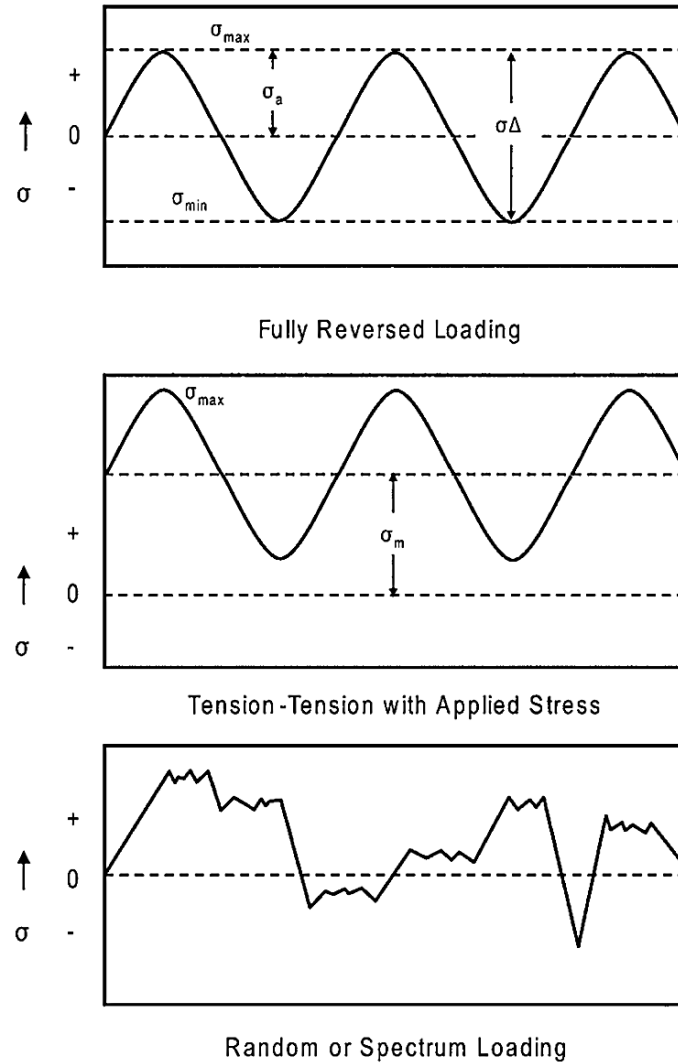
Figure 2.8: Three main types of stress cycles [ASM08]

Among the main parameters of the stress cycles [ASM08]:

σ_m is the mean stress, the σ_a is the stress amplitude, $\Delta\sigma$, stress range and, R, stress ratio.

Constant stress range:

$$\Delta\sigma = \sigma_{max} - \sigma_{min} \tag{2.1}$$

Mean stress:

$$\sigma_m = \frac{\sigma_{max} + \sigma_{min}}{2} \tag{2.2}$$

Stress amplitude:

$$\sigma_a = \frac{\Delta\sigma}{2} = \frac{\sigma_{max} - \sigma_{min}}{2} \tag{2.3}$$

Stress ratio:

$$R = \frac{\sigma_{min}}{\sigma_{max}} \qquad\qquad \textbf{(2.4)}$$

Maximum stress:

$$\sigma_{max} = \sigma_m + \sigma_a \qquad\qquad \textbf{(2.5)}$$

Minimum stress:

$$\sigma_{min} = \sigma_m - \sigma_a \qquad\qquad \textbf{(2.6)}$$

Comparing to stresses generated by single applied static loads, cyclic stresses are more hazardous for the metallic components or systems. The components, or systems assembled by metallic components, may represent fractures under these repetitive loads. By increasing number of repetitive cycles, the acceptable stress decreases. Despite the applied stress which is below the yield strength of the material, therefore is in the elastic region, these locally generated stresses may result in local plastic deformations, and thus micro-cracks. These cracks progressively grow within the structure, until the part totally fractures. Bader et al. stated that, for fatigue, applied life cycles have more importance than the load frequency. The components which undergo repetitive loadings during service, generally represent a fatigue character, which is more influenced by mean stress [Bad14].

2.2.1 Mean stress correction (MSC)

Even though cyclic stresses are the most commonly observed under full reverse loadings with zero mean stress, in the real cases it is the opposite, as mostly non-zero mean stresses are observed within the cyclic stress histories of structures. Mean stress correction (MSC) methods are, therefore, used to solve the effects of non-zero mean stresses on fatigue, rather than applying too many fatigue tests, which take too much time, to solve different fatigue behaviours under varying mean stress cases. The mean stresses are most frequently categorized, or defined by the parameter, R, the ratio of the minimum applied stress to the maximum applied stress in a stress cycle, which are all presented in the **Figure 2.9** below within the history of fully reversed cyclic stress [Bad14].
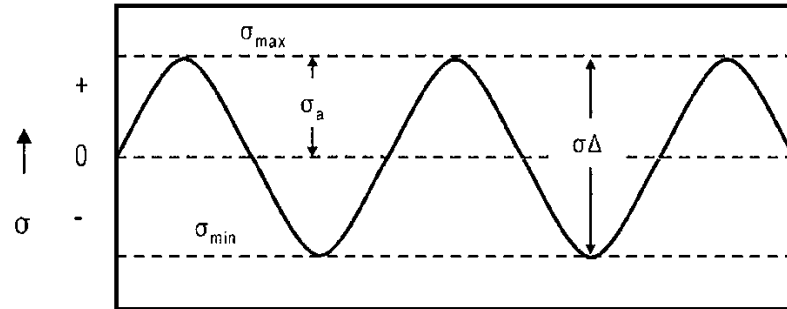
Figure 2.9: Cyclic stress parameters [ASM08]

In the fully reverse loading cases, the mean stress are, as explained, equals to zero. In this type of cycle types, which are also named as completely reversed cycling, the "R" ratio is equal to -1. For the cases of zero mean stresses, the allowable stress amplitude on a specific life cycle is called the effective fatigue limit. On the other hand, the allowable stress amplitude will decrease, when the mean stress increases. The mean stress can increase until the material's tensile strength, when the allowable stress amplitude will become zero [Bad14].

There are many approaches given to the literature to determine effects of mean stress on fatigue life. The three major methods which are utilized to determine fatigue life of components under cyclic loadings are presented by Goodman, Soderberg, and Gerber, as given the mathematical descriptions below [ASM08].

In which, σ_m is the mean stress, σ_e is the fatigue endurance limit, σ_u is the ultimate tensile strength, and finally σ_y describes the material's tensile yield strength [Bad14].

Goodman's theory:

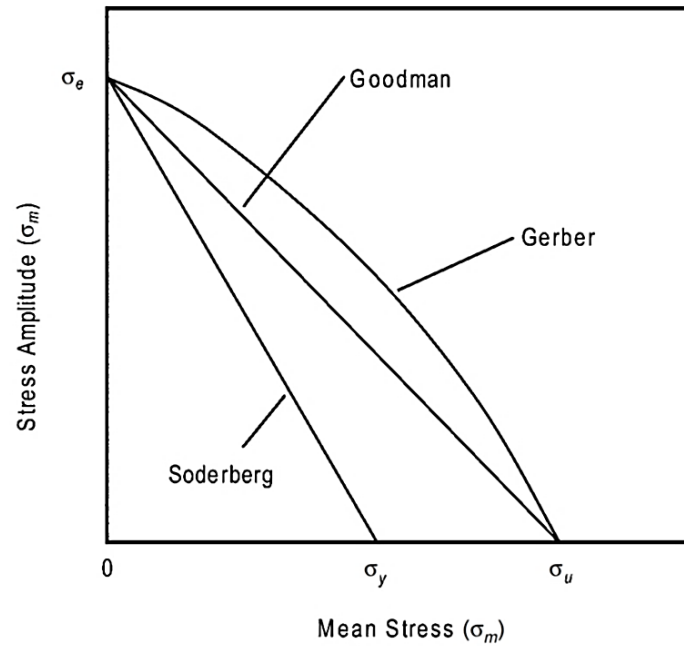$$\frac{\sigma_a}{\sigma_e} + \frac{\sigma_m}{\sigma_u} = 1 \tag{2.7}$$

Soderberg's theory:

$$\frac{\sigma_a}{\sigma_e} + \frac{\sigma_m}{\sigma_y} = 1 \tag{2.8}$$

Gerber's theory:

$$\frac{\sigma_a}{\sigma_e} + \left(\frac{\sigma_m}{\sigma_u}\right)^2 = 1 \tag{2.9}$$

The graphical comparison of these equations is shown in the **Figure 2.10** below.

Figure 2.10: Comparison of the three major mean stress correction methods [ASM08]

Among the three main MSC methods, with graphical representation above, Goodman is the most adequate for materials with brittle structure. Moreover, it is not bounded under a negative mean stress. Gerber, however, is bounded under negative mean stresses, but is mostly used for materials, which has ductile characteristic. According to the experiment results in the literature, the real case is actually mostly found between Gerber and Goodman. Lastly, Soderberg represents the most conservative life curves, and is also not bounded as Goodman under a negative mean stress [Bad14].

2.2.2 Stress-Life (S-N) curves

The fatigue behaviour of the materials is most frequently characterized by life curves, or stress-life curves, also called S-N curves, in which the amplitude of applied stress (S) is drawn according to the number of cycles until the rupture (N), mostly in semi-logarithmic scale [Kum09]. One common example of S-N curves is demonstrated in the below **Figure 2.11**, as the S-N curve of AISI 4340 alloy steel [Boa90].

In the S-N curve of AISI 4340 steel in the below **Figure 2.11**, it can be observed that the fatigue life increases by the applied stress amplitude reduces. After a limit, around 10^7 life cycles in the graph, the curve becomes straight, and decreases less by the increase in life cycles. This limit is named as "fatigue endurance limit". To demonstrate fatigue behaviour, a linear curve is more preferred than the original scale, which is generated by using the log scales of both of the axes. This approach was actually built by Woehler, with the **Equation 2.10** below, where "m" and "C" are the case related coefficients [Kum09]:
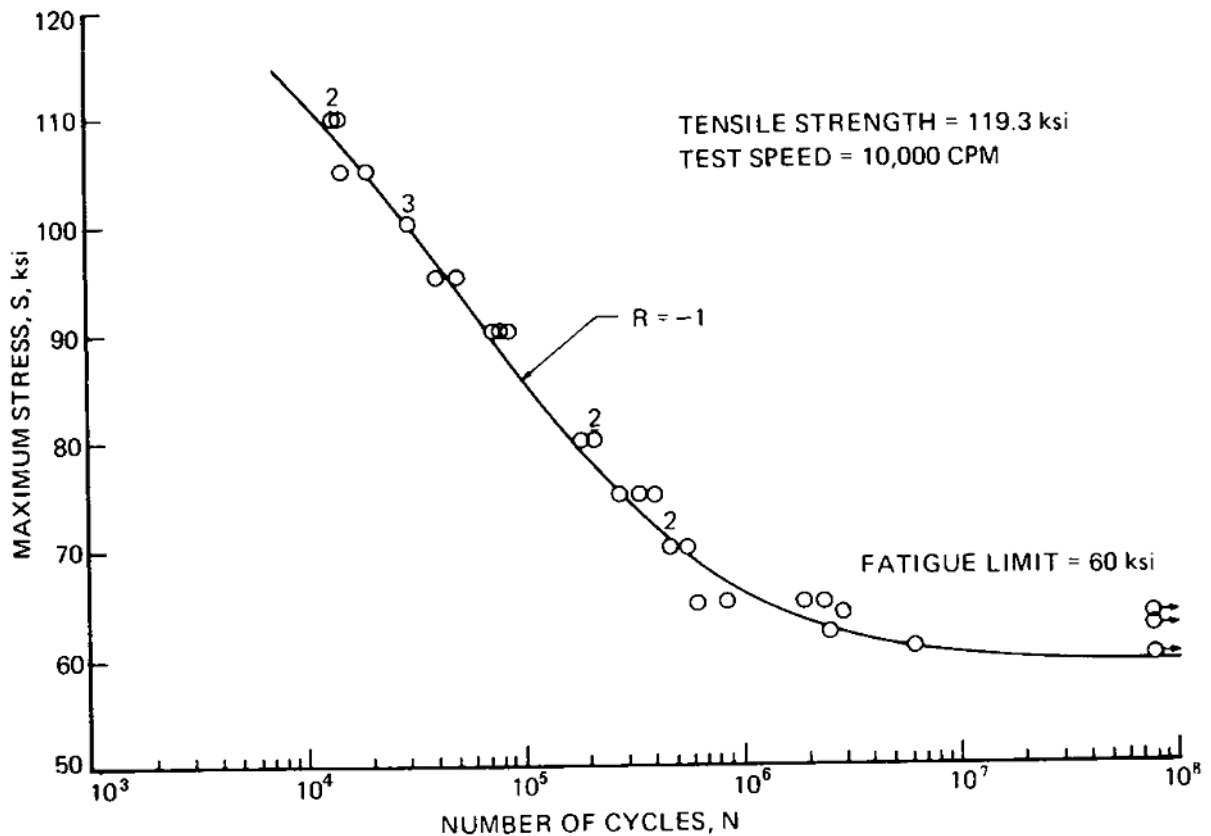
$$\log N = \log C - m\log S \tag{2.10}$$

Figure 2.11: A typical S-N curve for steels [Shi00]

As stated, S-N curves represent the correlated effect of cyclic stress and number of cycles on fatigue behaviour of a material which is repetitively loaded. The curve, therefore fatigue behaviour of materials, is influenced by such factors as mean stress, frequency, kind of stress cycles, temperature, and environmental conditions. However, among many efforts, to determine an analytical expression for the S-N curves, Basquin's relation has been the most preferred approach, by which an mathematical explanation of the S-N curve can be generated for specific number of cycles to failure, both in low or high cycle fatigue without requiring too many information. This method, thus, allows predicting the fatigue life analytically by knowing less information than other methods. The mathematical expression of the Basquin's curve is given in the **Equation 2.11** below as [Boa90]:

$$\sigma_a = aN_f^b \tag{2.11}$$

Where; σ_a is the fatigue stress amplitude in MPa and N_f represents the number of cycles to failure. In the equation, "a" and "b" are the respectively material and geometry related constants. While "a" is the fatigue endurance coefficient, has a value approximately around material ultimate tensile strength, "b" is the fatigue strength exponent. Through the utilization

of least squares method which is used to obtain linear curve by taking logarithmic scale of power law, S-N curve is then determined [Boa90].

The points on S-N curves are named as fatigue strengths of components, which are defined as the maximum allowable stress, which component can undergo at the respective number of cycles. The term fatigue strength is especially essential for fatigue behaviour characterization of the non-ferrous metals, as they do not show a fatigue limit to consider in design processes, and fatigue strength according the specific number of cycles is the only parameter for evaluating the applied cyclic stress. Fatigue strength is also utilized more commonly than fatigue limit, when estimating fatigue life of low-alloy and carbon steels [Boa90].

Fatigue limit, or endurance limit, is also named as fatigue endurance limit, is a term specifically used for ferrous metals, which describe a point in S-N curve, after what, max. allowable stress does not reduce anymore by any increase in number of cycles. After the point of fatigue limit, S-N curve gets flattened and remain at the same allowable stress value despite number of cycles rises infinitely. The fatigue limit is believed as especially unique for carbon and low-alloy steels. Even though it is widely applicable for the cases under variable-amplitude loading, the cases under periodic overstrains can show great differences in terms of long-life resistance of component, which is more similar to real cases [Boa90].

A more detailed representation of S-N curves can be seen in the **Equation 2.12** below, which is determined from a research of Roessle and Fatemi on analytical fatigue life determination of steels [Roe00]:

$$\frac{\Delta\sigma}{2} = \sigma'_f (2N_f)^b \qquad\qquad \textbf{(2.12)}$$

Where, "$\Delta\sigma/2$" is the axial stress amplitude, "$2N_f$" represents the number of cycles to failure, while "b" is the axial fatigue strength exponent. For determination of all stress life, as well as strain-life curves of materials, fatigue strength coefficient as well as the fatigue strength exponent must be first known, while within the strain-life determinations fatigue ductility coefficient as well as fatigue ductility exponents are also required [Poe11].

In the same research of Roessle and Fatemi, fatigue strength coefficients are tried to be related to the material hardness, depending on data fits obtained by tests conducted on varying steel specimens. In the research, the axial fatigue strength coefficient, σ'f, and the axial fatigue ductility coefficients, εf', of are determined by Brinell hardness (HB) of respective steels as given in the **Equation 2.13** below [Roe00]:

$$\sigma'_f = 4{,}25\,(HB) + 225 \qquad\qquad \textbf{(2.13)}$$

The fatigue strength exponent, b, and fatigue ductility exponent, c, were on the other hand determined from the research of Poeppelman respectively as -0.09 and -0.56, after analysing the results obtained by 69 steels with varying mechanical properties [Poe11].

2.2.3 Fatigue limit prediction for steels

As described in the previous section, fatigue endurance limit is the maximum stress value, under which, components will not fail in an infinite number of cycles, which can only be applied to such specific metallic materials as steel and titanium [Kos93].

Determination of such endurance limit is not possible on the S-N graphs generated by Basquin's or similar methods. It is, however, mostly assumed that fatigue limit is the fatigue strength of a material at 10^6 number of cycles in an analytically generated S-N curve [Bad14].
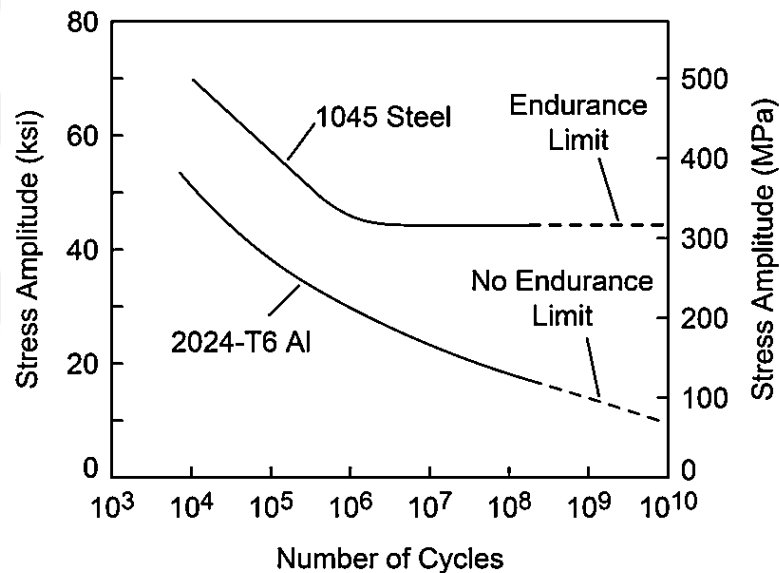
Figure 2.12: S-N curve comparison of steel and aluminium materials [ASM08]

In most of the cyclic loading cases, component is affected by high number of cycles, such as 10^7 and analysed by high cycle fatigue. During the service life, machine parts as connecting rods, crank shafts and helical springs undergo number of cycles which even exceeds 10^{10}. The fatigue life of railways and bridges, on the other hand, is predicted as around 10^8 number of cycles. Mostly, predicted fatigue limit is accepted as the fatigue strength of the component according to the last cycle of its service life. Many researches in 1990s have shown that the materials do not represent an infinite endurance limit as believed that they have a definite fatigue limit in their fatigue life. Due to this finding, many investigations were conducted to obtain fatigue strength, σ_w, of the metallic components with analytical models as well as experiments, which are affected by high number of cycles compared to other high cycle regimes, named as gigacycle regimes [Ban13].

Most of the fatigue strength prediction approaches in the literature are based on size factors of dangerous non-metallic defects. A fatigue investigation by measuring of defects with critical sizes is complicated. On the other hand, experimentally determination of component S-N curves in high cycle regimes is highly time and energy consuming. Thus, it is necessary to create an analytical fatigue strength approach for the components affected in gigacycle regimes, which only requires obtainable material properties, and is not dependent on defect sizes but it is also adequately accurate. One approach is an ultimate strength and Vickers hardness dependent prediction method developed by Bandara et al., for steels under gigacycle regimes. Within the research, the analytical model was also validated by experimental data of forty five steels with varying properties. Another model was also developed to predict fatigue strength of steels and steel alloys, by using data from number of experiments exceeding hundred, applied in varying number of cycles of high cycle regime and on different steels [Ban13].

The first analytical approach in the research of Bandara et al., named as the first fatigue limit equation (FLE1), was independent of the factor area but an accurate and reliable relation model was built for area, dependent on the ultimate strength. The model FLE1 can be seen in the **Equation 2.15** below:

$$(\sqrt{area})^{1/6} = \left(\frac{14}{\sigma_u{}^2}\right)^{1/6} \quad \textbf{(2.14)}$$

$$\sigma_w = 0,001\,(Hv + 120)(155 - 7LogN_f)\,\sigma_u{}^{1/3} \quad \textbf{(2.15)}$$

This model is used to predict fatigue strength of medium and high strength steels in gigacycles regimes. The accuracy of the model was verified by data obtained by experiments on varying steels.

In the second analytical model, can be described as the second fatigue limit equation (FLE2), a global approach was applied for steels and alloys, dependent on the experimental fatigue strength data of forty five steel and nine alloys with various properties. This model is even less complicated than the first equation, which only requires, number of cycles, Nf, and ultimate tensile strength, σ_u, while the parameters γ and η are respectively determined as 0,707 and 1,214. The units of the factors of σ_w and σ_u are given in MPa, while the Nf range is between 10^6 to 10^{10} cycles. The FLE2 equation is given in below **Equation 2.16** [Ban13].

$$\sigma_w = \frac{\gamma\sigma_u{}^{\eta}}{LogN_f} \quad \textbf{(2.16)}$$

2.2.4 Factors effecting fatigue

There are various factors affecting the fatigue life of components, which depend both on environmental as well as structural factors, which can be summarized as below:

- Loading amplitude (constant or variable)
- Cyclic stress ratio, R, and stress range, $\Delta\sigma$
- Mean stress, σ_m
- Geometry and size of the part
- Concentrated stresses in local points
- Corrosion or aggressive environment [Shi00]
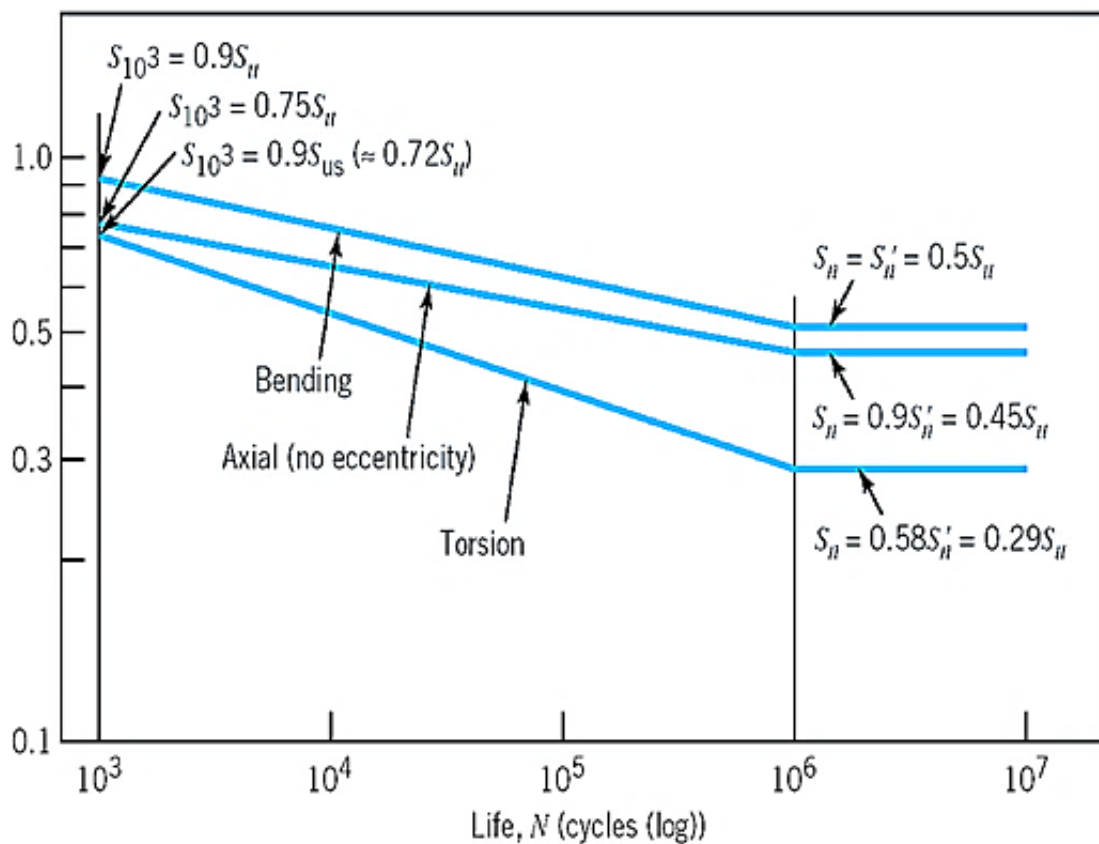
Figure 2.13: Effect of stress type on life curves [Tho05]

According to the chart above in **Figure 2.13**, an initial fatigue strength which is approximately equal to the ultimate tensile strength, which is presented as Su, is reduced up to 0.5 Su for cyclic loading under bending, and 0.45 Su under axial cyclic loading. As presented, while the fatigue is the highest under torsional cyclic loads, it is the least under bending. Under axial loads, on the other hand, the effect of fatigue on life is between torsion and bending, however, the aim of the life curve (applied stress amplitude per number of cycles to failure) seems to decrease less than all others.

As already introduced, surface quality of materials have a great influence on fatigue. The effect of surface quality on fatigue is described –or rated- by a factor called surface retention factor, SRF [ASM08]. In below **Figure 2.14**, a generalized change of SRF of metals according to a change in ultimate tensile strength, hardness and manufacturing operation can be seen. As seen, the more quality in surface of the material brings about a higher SRF. For materials having UTS of approximately 400 MPa, the SRF values vary respectively for the mirror-polished surfaces 1,0, machined surfaces 0,8 and forged surfaces around 0,5. On the other hand, for materials having the same sort of surface quality, by an increase in hardness –or UTS-, SRF will decrease.
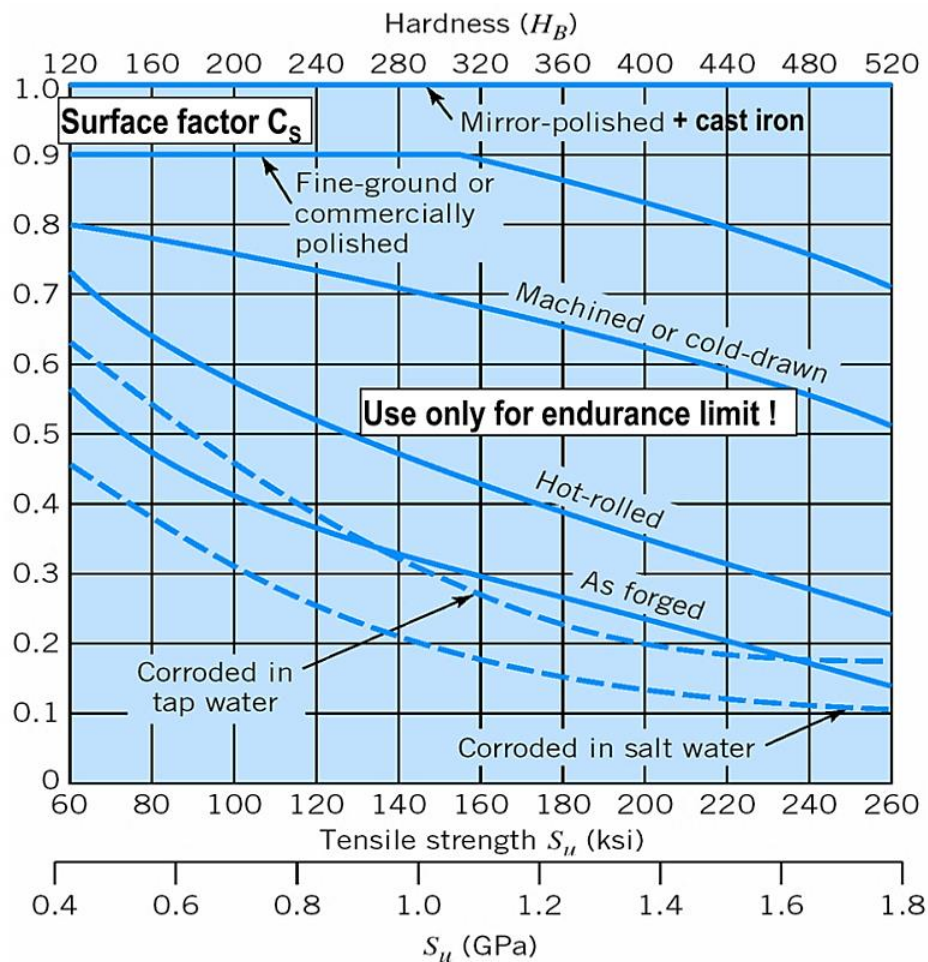
Figure 2.14: Effect of surface finish and UTS on fatigue [Tho05]
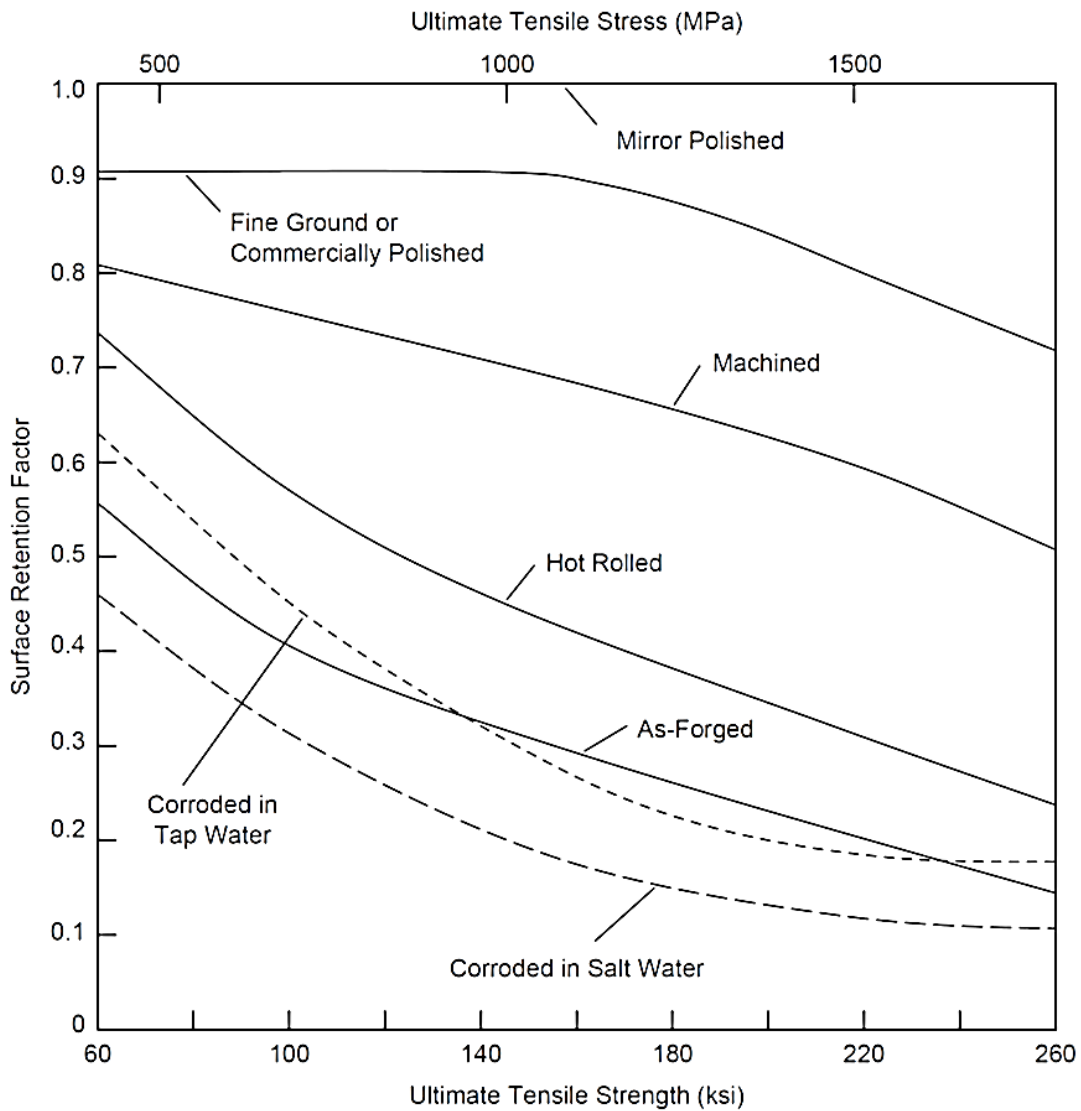
Figure 2.15: Effect of surface finish on fatigue of steels [ASM08]

For steels, the change of SRF by UTS is demonstrated above in **Figure 2.15**. As seen, the curves are very similar to those in previous **Figure 2.14**, which generally presents effect of surface finish on fatigue behaviour of metallic materials.

In **Figure 2.16**, the effect of geometry (type of hole in structure) on fatigue behaviour is presented. As clearly given in the life curves, a structure with tight fit fastener in cold worked hole presents the highest fatigue life due to the surface quality and generated compression stress on the surface, while structures with reamed open hole have shown the shortest fatigue life.

2024-T851 Al
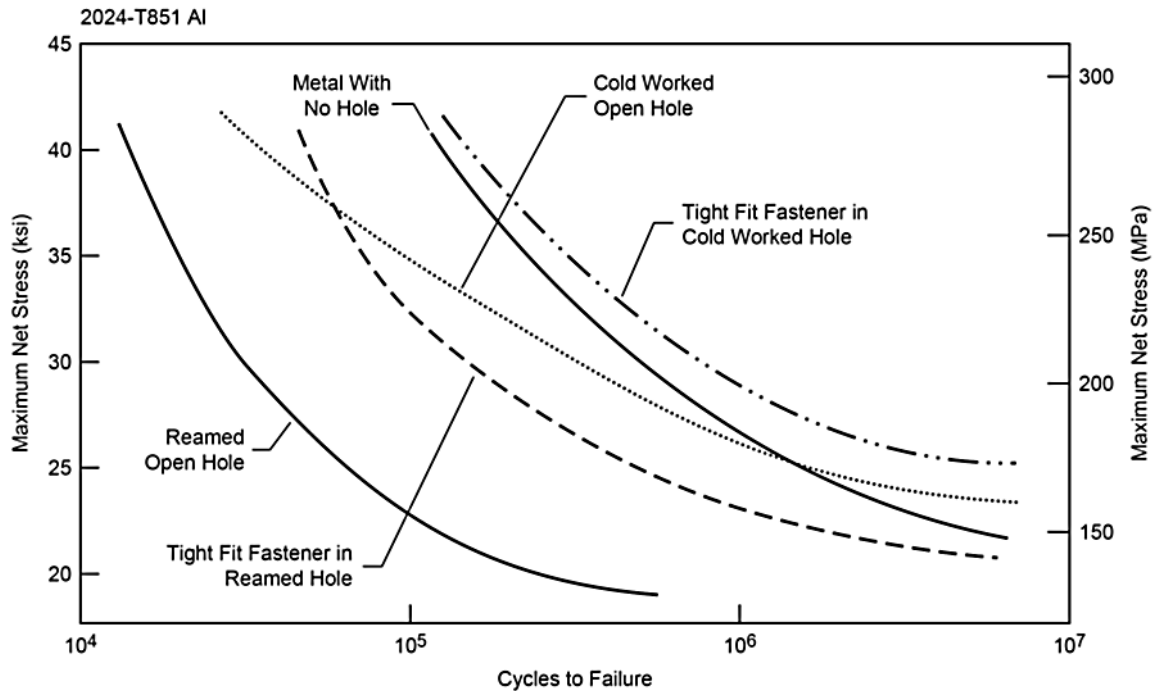
Figure 2.16: Fatigue life improvement with cold working [ASM08]

Besides, in the **Figure 2.17** below, the negative effect of corrosion on fatigue life can clearly be seen.
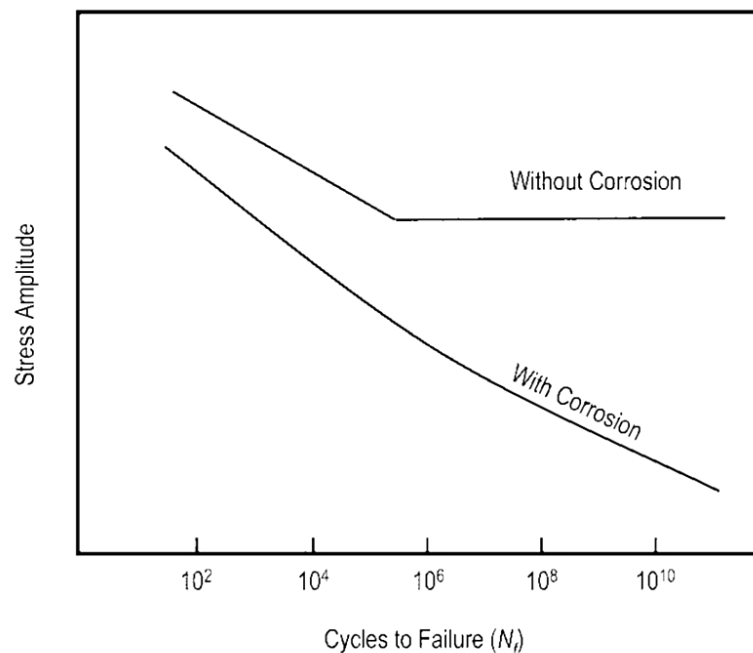
Figure 2.17: Effect of corrosion on fatigue performance [ASM08]

Lastly, according to the research of Guennech et al., the effect of cyclic loading frequency on fatigue behaviour can be seen in below **Figure 2.18** [Gue13]. As given very similar effects

was observed between 0,2 and 2 Hz, similar but perceivable difference between 2 and 20 Hz, and a great difference between 20 kHz and all the others.
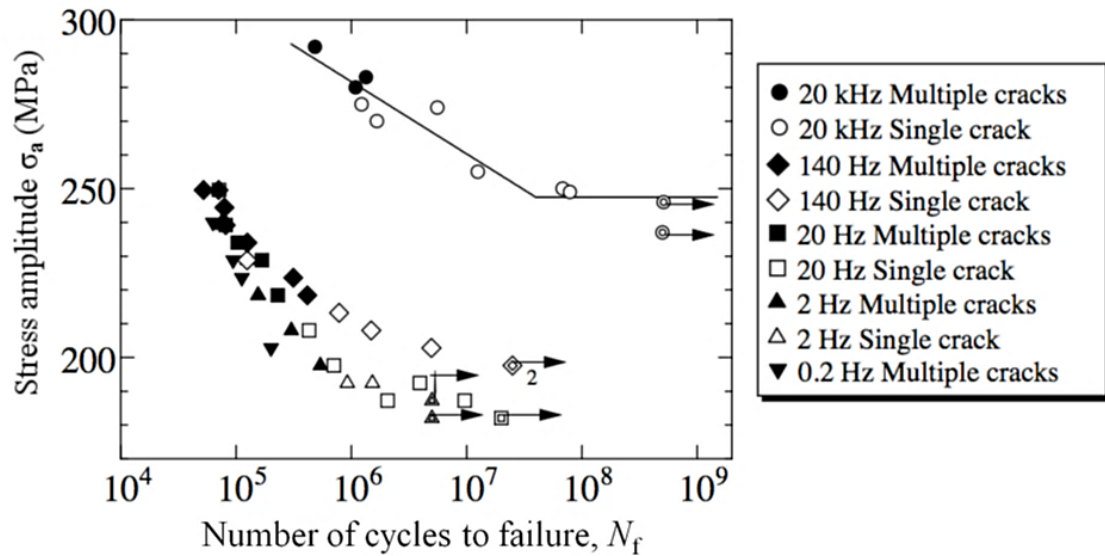
Figure 2.18: Effect of frequency on fatigue life [Gue13]

2.2.5 Fatigue resistant design

The fatigue behaviour of components may be improved via the improvements in the design as well as manufacturing stages. In fact, if there is no significant failure within the material structure, fatigue life of components are more dependent on the presented fatigue life considerations in design, production and maintenance stages. The most reliable and cost effective improvements to be made for fatigue resistant designs can be summarized as:

- Reducing stress concentrators by improving the geometrical design
- Not having any surface failures by cold working operations
- Avoiding imperfections, interstitial atoms or decarburizing operation on the surface
- Omitting tensile stress generation on surface in manufacturing, heat treatment or thermal joining opeartions
- Improving the application of fastening or joining operations according to fatigue behaviour
- Protecting the structure from corrosion, erosion, chemical influence, such surface defects as cracks during service [Boa90]

2.2.6 Fatigue design methodologies

During the last two centuries, varying fatigue design methodologies have been discussed in order to obtain the most reliable design methodology considering fatigue. As a summary, four

major types of fatigue design methodology with various aspects can be presented, which are infinite-life design, safe-life design, fail-safe design, damage-tolerant design [Boa90].

Infinite-Life Design: As the oldest type of fatigue design methodology, infinite-life designs focus on keeping the maximum stress amplitudes of cyclic loadings below a certain fatigue strength of the material. This is clearly a methodoly dependant on material S-N curves. Any residual failure such as cracks, or flaw are also avoided. It can be more appropriate to use if cyclic stresses remain only below yield strength of the material, and the material has such a certain fatigue endurance limit as in steels. Even though there are more superior design methodologies, which were developed later, it is the most simple, basic and economical method, specifically applied where periodic test or monitoring of the structure is not feasible. On the other hand, it brings about heavier designs and more material costs than others, since it represents the most conservative solution [Boa90].

Safe-life design: The method assumes the structure as initially failure-free and will have a finite life with generated critical flaws. It is more applicable for components under cyclic stresses exceeding yield strength and thus, generating plastic strains. For this condition, a more strain dependant descriptions are made which result in requirements of the solution which are based on the factors, strain (ε) and number of cycles (Nf). The defect is defined by observation of a small flaw or related finding depends on a critical response of loading. The defect can also be determined as rupture [Boa90].

Fail-Safe Design: The idea behind fail-safe design method is that although there will may be fatigue defects within the structure, they will be repaired simultaneously before the rupture. This is especially applied in aerospace and aircraft industries, where infinite-life designs with high factor of safeties cannot be utilized due to the great weight concerns. Within the fail-safe designs, various load paths and flaw inhibitors are placed in the structure. In this way, the alternative load paths will take the loading, if the main load path fails, and the fracture of the structure will be prevented. To be able apply this method, a reliable verification method as well as defect inspection must be incorporated [Boa90].

Damage-tolerant design: As the newest method, damage-tolerant design can be defined as the improved fail-safe method. By this methodology, it is also assumed that structures may include flaws, and the growth rate of these cracks can be inspected by fracture mechanics. By inspecting the structure periodically, it can either be repaired or removed depending on the stage of determined crack growth rate [Boa90].

Despite the great efforts on fatigue resistant design methods, fatigue fractures are still seen with a critical amount. Therefore, it is necessary to apply cycle tests on components before

utilizing them in service, under the exact or the most similar conditions they will be used in service [Boa90].

2.2.7 Fatigue crack inspection by temperature

Along with the many developed methods to inspect defects inside the metallic structures or machine components, infrared thermography method is one of the most simple and effective, using a thermoelasticity heat generation equation for determining cracks within the structures as well as measuring applied stresses [Nis12].

As known, temperature reduces, if gasses are adiabatically expanded, and the opposite happens, in case of an adiabatic compression. For solids, the similar case can be observed, depending on a rapid stress increase. This effect is specifically named as thermoelasticity. The **Equation 2.17** below is used to represent the thermoelasticity effect in metals, as well as other homogeneous materials:

$$\Delta T = -K \, T \, \Delta\sigma \qquad\qquad (2.17)$$

In which, "$\Delta\sigma$" represents the difference in the applied principal stresses, "T" the absolute temperature and "K" is coefficient of thermoelasticity. The thermoelastic coefficient, K, has an unique value per material, it is such as for mild steels, equal to $3{,}5 \times 10^{-12}$ Pa^{-1}.

Within the defect inspection and stress determination by the thermoelasticity effect, the first factor, ΔT, is called as minute temperature change, and is the measurement value obtained by infrared temperature sensor. The applied stress, $\Delta\sigma$, can then be obtained via calculation of the above **Equation 2.17**. Moreoveri if a crack is generated within the measured part of the body, then an amount of stress will be concentrated at the tip of the flaw. Depending on this method, this generated stress can also be obtained by the increase in temperature.

2.3 Finite elements analysis (FEA)

FEA is an analysis method, which applies a numerical solution approach named as finite element method (FEM) in order to solve engineering problems for the field problems, where analytical solutions are not capable.

The term FEA was first introduced to the literature by Clough in 1960. At those years, this method was used to solve engineering problems in varying fields of stress analysis, fluid flow, heat transfer, and the others, by an approximation. After the publication of the first source about FEM by Zienkiewicz and Chung in 1967, the FEM has started to be used for problems, seen in a variety of engineering fields between the late 1960s and 1970s. The well-known FEA software such as Abaqus, Adina, ANSYS etc. were also first appeared in 1970s.

The reasons behind the use of FEA with a rapid increase and in variety of fields can be counted as:

- Applicability on complex geometries
- Simplicity to use in different engineering fields such as solid mechanics, dynamics, heat transfer, fluids, electrostatic and more
- Ability to solve difficult restraints, as indeterminate structures
- Ability of use for such complicated loadings as nodal loads, element loads which are caused by pressure, thermal or inertial forces or time/frequency dependent loadings

On the other hand, the following aspects are considered as downsides of the FEA:

- Inability of generating a closed-form solution
- Limitation to producing only approximation to problems
- Existence of inherent errors
- Possibility of damages, resulting solution to fail, caused by user mistakes

The main principle behind the FEA can be described as, breaking a structure into number of pieces, which are called elements, and then joining these elements by the points, called nodes, which hold these elements connected to each other. After describing the elements and the nodes, the analysis is finalized by solving some algebraic equations, the number of degrees of freedom (DOF). The origin of the name, finite element method, comes from its difference from the infinite continuum methods, since FEM uses finite elements, continuum methods are applied on infinite elements [Wec04].
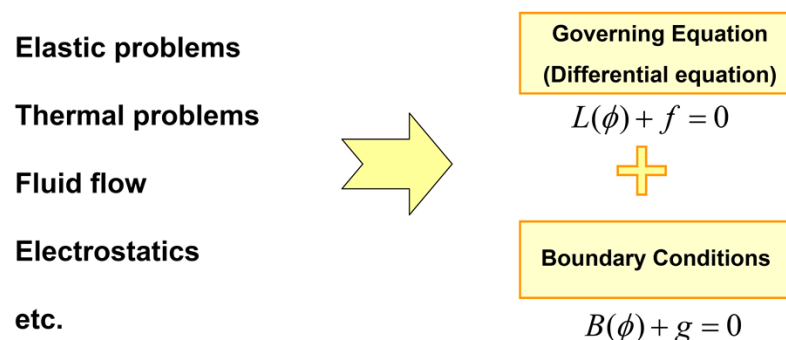
Figure 2.19: The principle of FEA [Wec04]

In FEM, a great number of engineering problems can be solved by governing equations and boundary conditions as seen given in the **Figure 2.19** above. Even though the governing equations can be generated and presented by calculation, the solution is impossible without use of a computer. The governing equation is defined by the **Equation 2.18** given below:

$$K\,u = F \qquad\qquad\qquad (2.18)$$

Where "K" is the property, "u" defines behaviour, and "F" represents the action. The various input parameters and variables of the governing equations can be seen below in **Figure 2.20**.

	Property $[K]$	Behavior $\{u\}$	Action $\{F\}$
Elastic	stiffness	displacement	force
Thermal	conductivity	temperature	heat source
Fluid	viscosity	velocity	body force
Electrostatic	dialectri permittivity	electric potential	charge

Figure 2.20: Governing equation variables [Wec04]

In FEM, the piecewise polynomial interpolations are used to interpolate field quantity in the whole structure via connecting elements each other, by a piecewise procedure. Then set of simultaneous algebraic equations, described for the nodes, are solved.

Preprocess

Process
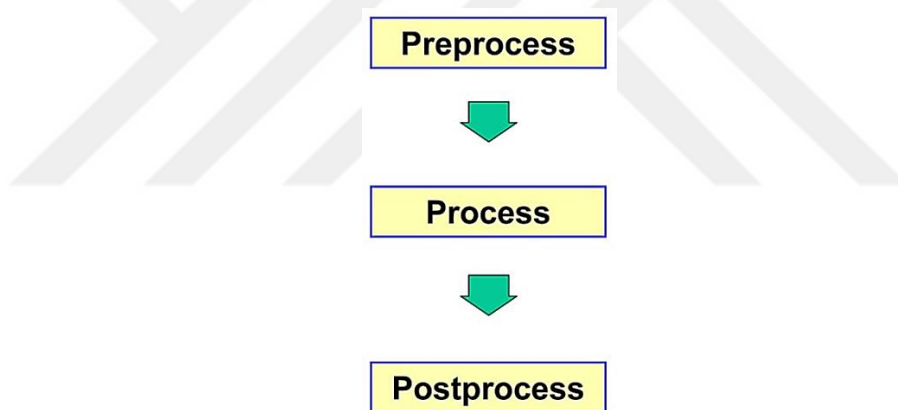
Postprocess

Figure 2.21: Three stages of FEA

FEA, which is made through frequently used software tools, has three main steps as pre-process, process and the post-process, which flows as presented in the **Figure 2.21** above. In pre-process step, user first builds a FE model. Computer is then utilized for applying numerical analysis in the process step. In the last stage, post-process, the results are read and interpreted [Wec04].

In the pre-process step, the analysis type must first be selected among such analysis types as:

- Structural Static Analysis
- Modal Analysis
- Transient Dynamic Analysis

- Buckling Analysis
- Contact
- Steady-state Thermal Analysis
- Transient Thermal Analysis

Afterwards, the type of element must be chosen among the below variants:

- 2D or 3D
- Linear or quadratic
- Truss, beam, shell, plate of solid

Then, material properties as Young's Modulus, E, Poisson's Ratio, p, etc. are given. After the above described steps, the nodes and elements are generated by meshing, which is a specific term used to describe element creation in FEA. Lastly, boundary conditions and loads are assigned onto this meshed body with given material properties. The meshing, or element generation stage, can be better understood in the below **Figure 2.22** [Qi06].
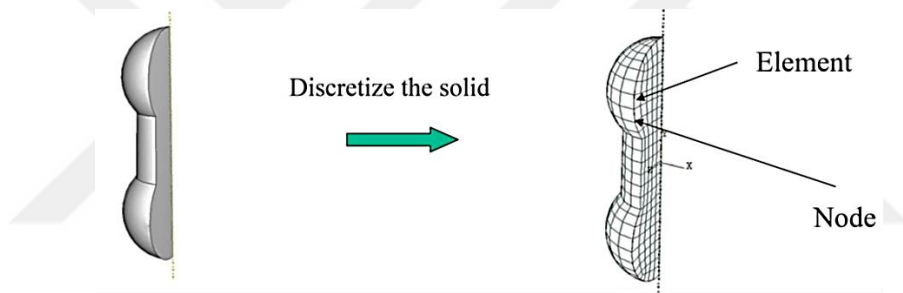
Figure 2.22: Element generation, meshing in FEA [Qi06]

After completion of the above steps, computer is used for the process step, in order to solve described boundary equations and then generate the results. And then lastly, in the post-process stage, the related analysis results can be analysed, which can be counted as displacement, stress, strain, natural frequencies, temperature or time histories.

Within the static structural analyses, stress, strain and displacement results are the most essential among others. The stress results are mostly displayed and interpreted as equivalent, or von Mises stress, with the **Equation 2.19** given below:

$$\sigma_v = \sqrt{\frac{1}{2}\left[(\sigma_1 - \sigma_2)^2 + (\sigma_2 - \sigma_3)^2 + (\sigma_3 - \sigma_1)^2\right]} \quad \textbf{(2.19)}$$

The equivalent stress is calculated through maximum, minimum and middle principal stresses, as presented in the **Equation 2.19** above as σ_1 and σ_2 and σ_3. Among these three principal stresses at the node in the solution, the σ_1 is the algebraically maximum and σ_3 is

the algebraically the minimum, and the σ_2 is algebraically the middle. When the stress case is uniaxial, the only unknown will be σ_1, where [Qi06]:

$$\sigma_2 = \sigma_3 = 0 \qquad\qquad\qquad \textbf{(2.20)}$$

$$\sigma_v = \sigma_1 \qquad\qquad\qquad \textbf{(2.21)}$$
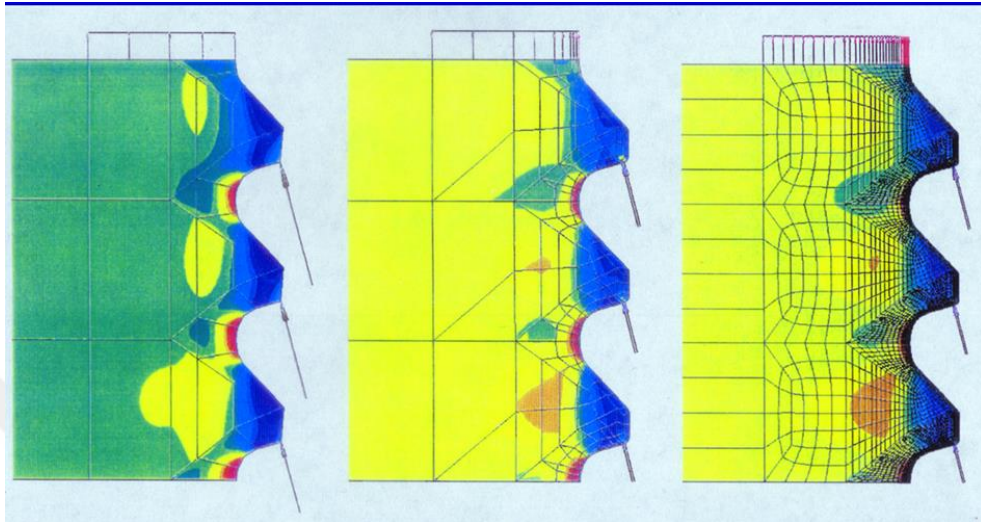
Figure 2.23: Accordingly; Coarse Mesh, Converged Mesh, Reference Mesh [Mit09]

Accuracy is one of the most important aspects while evaluating FEA solutions, since fatigue investigations, or life predictions, can only success with an accurate determination of the surface stresses, especially at the regions which are of crucial importance [Mit09]. The accuracy caused by varying mesh types can be seen in the **Figure 2.23** above.

After building, processing, and resulting of FEA, despite all the above described simplicities and capabilities used within the process steps, the following disadvantages of FEA as the approximation of the geometry and the assumption of field quantity as a piecewise polynomial over element, must be carefully considered in the end, which are accordingly presented in the **Figures 2.24** and **2.25** below.
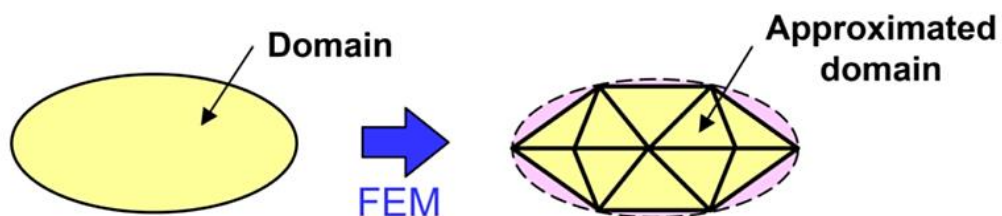
Figure 2.24: Geometry approximation
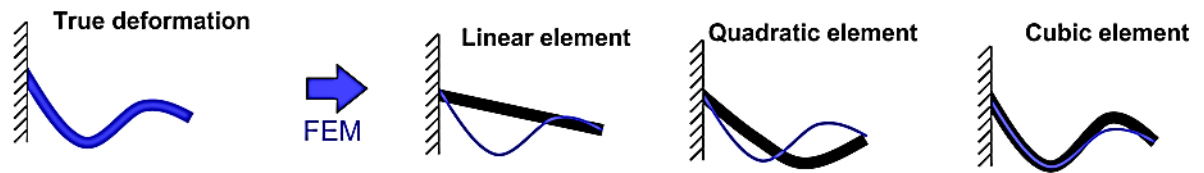
Figure 2.25: Assumption of the field quantity as a piecewise polynomial

Beside of the disadvantages given above, these negative aspects should also be taken into consideration when applying a FEA:

- Applying relatively simple integration methods as Gauss Quadrature
- Limitation of computer, having only finite digits (π= 3.14159265)
- Complexities of calculation, such as too much difference in stiffness [Wec04]

3 Overview and motivation

Within this thesis work, an aerostat's mooring station, which is affected by dynamic loads during the service, is planned to be fatigue resistant designed via a comprehensive literature research, CAE fatigue analyses, analytical life calculations and verification by cyclic load tests within the design project of the aerostat at the firm Otonom Teknoloji. In addition, a further CAE fatigue analysis will be applied onto the former mooring station design of a 14 m long aerostat. The analysis results from both of the mooring station designs will also be compared and discussed.

For the standardized fatigue-resistant design process, firstly fatigue resistant design criterion and fatigue design methodologies are determined through a literature search, to be able to apply on the design of mooring station components. Afterwards, the fatigue related mechanical properties of the used materials and the worst possible dynamic load scenarios by CFD, which aerostats undergo, will be generated for the both former and new fatigue resistant mooring station designs of accordingly 14 m and 17 m balloons. After the fatigue resistant design of the new mooring station, fatigue analyses will be utilized for the fatigue behaviour prediction of the two mooring station designs of 14 m and 17 m balloons by CAE fatigue analysis, via software Ansys Mechanical and nCode DesignLife. After obtaining the fatigue related safety factors from CAE fatigue analyses for the two different mooring stations, by a further analytical approach, life curves and fatigue strengths for the fatigue resistant mooring station components of the 17 m balloon will be generated and the related fatigue safety factors will be presented. The analytically obtained fatigue safety factors will then be compared by CAE generated safety factors and the results will be discussed. From all of the fatigue behaviour analysis of the two mooring stations, it is expected to obtain fatigue safety factor values above 2,0, to be able to eliminate all the risks of failure within an infinite-life design methodology.

After fatigue behaviour analysis of the mooring stations by CAE and analytical life curve generations, two main components of the fatigue resistant designed mooring station, tower crane made of steel and flying sheave made of aluminium, will be manufactured for the aim of cyclic loading tests and tested under the worst loading condition up to 10^6 life cycles. A cyclic loading test setup will therefore be manufactured within the facility for the component design verification purposes.

4   Analysis specifications

The CAE fatigue analyses in this thesis work are planned accordingly for the new fatigue resistant and the former mooring stations of accordingly 17 m and 14 m balloons. The analyses are not only applied onto the designed and manufactured components in the facility, which are the tower, flying sheave and rope connection arm but also onto the ready taken component, tether crane, which are all affected by the dynamic loads, as attached to the mooring station, during service. While tower and rope connection arm are the components which undergo dynamic loads during parking position of the balloon on the ground, flying sheave and tether crane are affected by dynamic loads directly during the flight of the balloon at high altitudes.
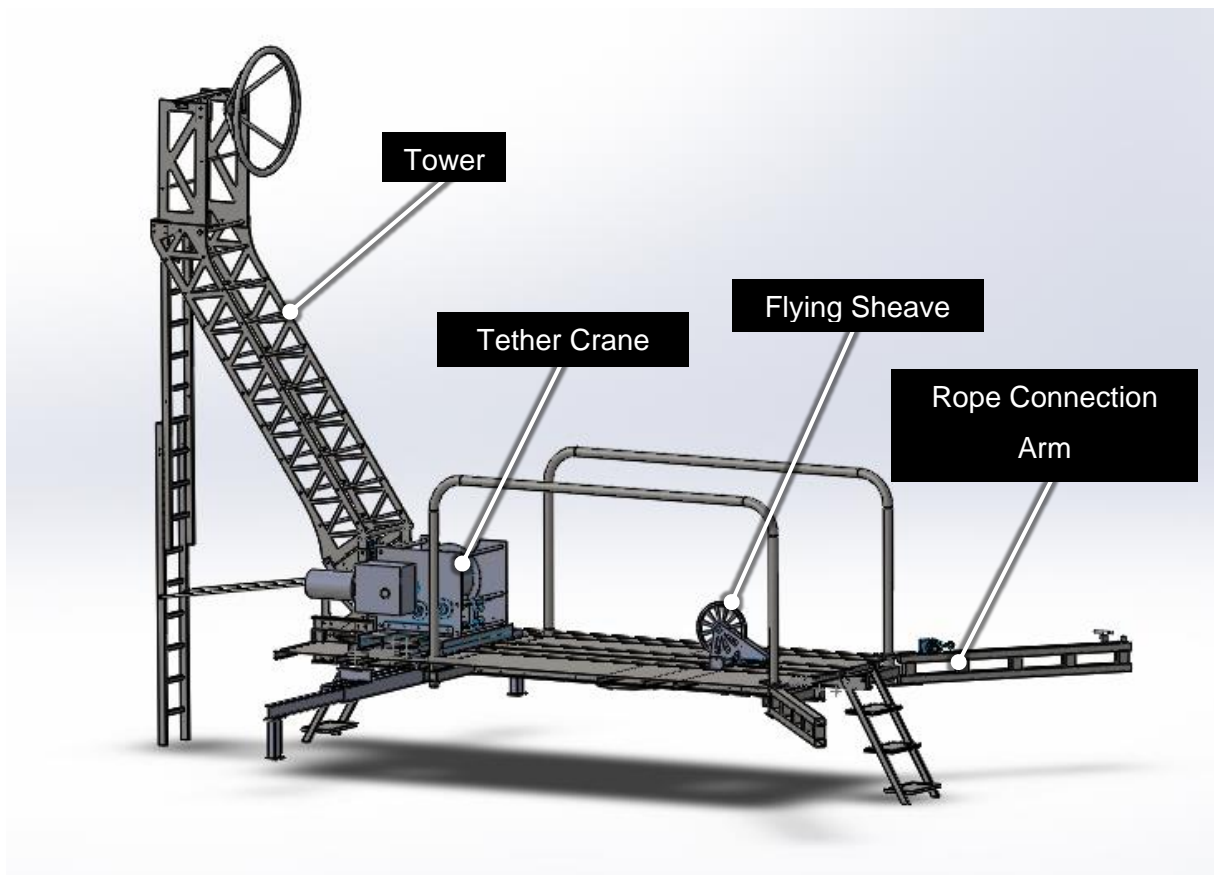
Figure 4.1: 3D CAD of the mooring station of the14 m long balloon

Since cranes are not specific machines, but used almost in all of the fields of industry with great variety of products and accessibility today, according to the required properties, the component is therefore not designed within the project, but ready taken, according to the required properties for both of the mooring stations. However, a CAE analysis of the component is still required, to be able to sure about analysis results.
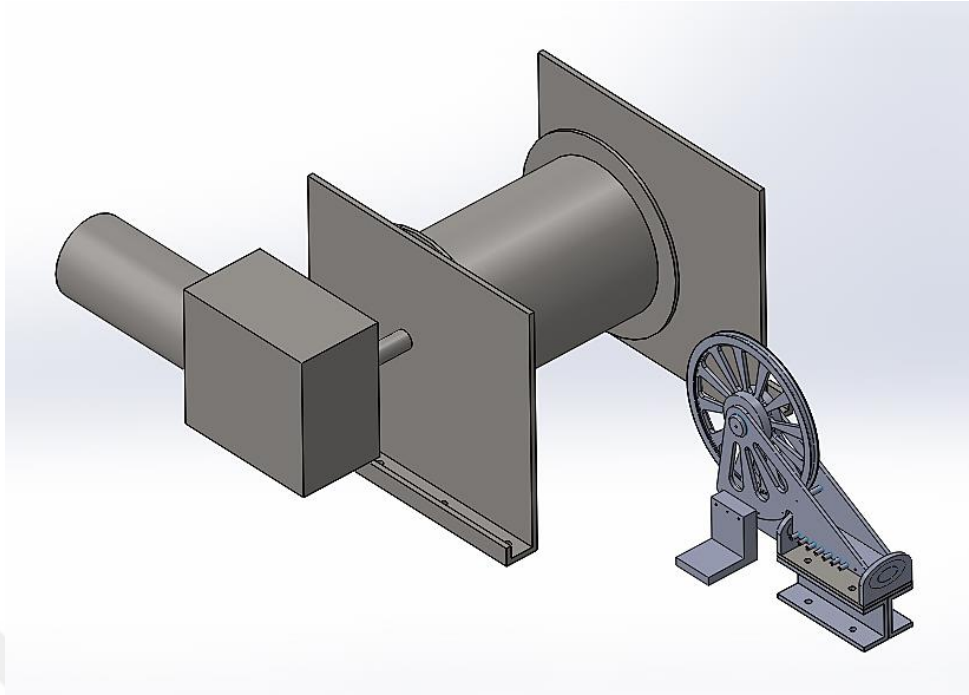
Figure 4.2: 3D CAD views of the tether crane and flying sheave of the small mooring station

CAE and analytical fatigue analyses in the project work however do not cover joints of bolts and nuts within or between these components since these were in-supplier tested ready taken products, of which fatigue consideration is made by safety factors already in the design phase without any requirement for a complex analysis.

The major analysis parameters for mooring station components can be counted as cyclic loading parameters by wind speed measurement, fatigue related material properties, and surface factors (SRF), which all be used in CAE fatigue analysis as well as analytical curve generation sections.

4.1   Wind speed - load calculations

The dynamic loads affecting the mooring station components are caused precisely by winds, acting on balloon during the service at high altitudes. Even though dynamic loads can be seen by high magnitudes, there will only be tension on the components of the mooring station, due to the unidirectional load affected to mooring station by the ropes or the tether. The worst (max. possible) loading case condition must therefore be found according to the worst possible wind speed conditions.

The worst possible loading cases by the worst possible wind scenario are created for both the aerostat design with 14-m balloon and the the design with 17-m balloon since an increase in the surface area of the balloon lets the force increase, which is taken by mooring station components. The dynamic loading case of the mooring station is accepted as a cyclic loading with constant amplitude for the fatigue analyses, since a vibration-like dynamic

loading will be unnecessarily complex and would not present the worst case despite its similarity to the real condition.
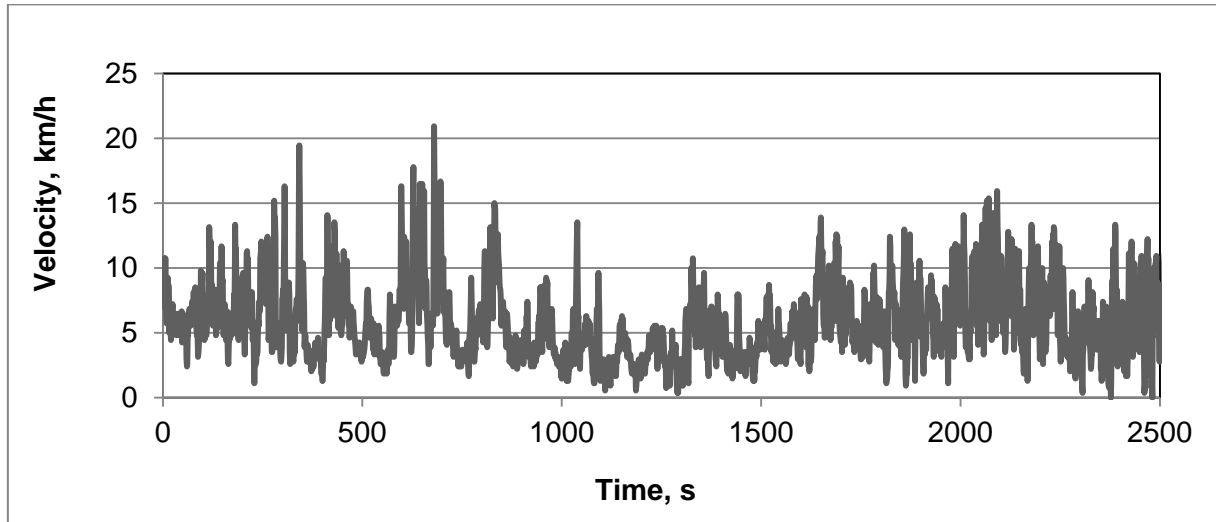
Figure 4.3: Wind speed measurement results in open air

In the first step of the calculation, the range of wind speed, the difference between max. and min. values, is found by the wind speed measurements in the open air, as seen in the **Figure 4.3** above, between 0,37 and 20,93 km/h with a magnitude of 20 km/h. The wind speed measurements were completed in June 2017 in Ankara, Gölbek at an altitude of 300 m from ground, with max. possible measurement capacity of 40 mins. Although the duration is not capable of representing real worst case during the service, the main aim of the measurement is to generate an estimated frequency and speed range value in order to create a similar cyclic loading case. However, to be able to finally generate the worst wind case, an offset value of 50 km/h is added to the min. and max. values, in order to set the maximum wind speed to the highest possible wind value of 70 km/h, by protecting the measured natural wind speed range. The reason of accepting 70 km/h as the highest possible wind, is that, depending on the angle of attack of the aerostats (10°), the ready taken tether of the aerostats is only capable of service under the maximum possible wind speed value of 70 km/h. In case of exceeding this value, the mission of aerostat will be terminated and be immediately landed, therefore the aerostats will never be used under wind speeds higher than 70 km/h.

After applying the offset value, max. and min. values are both increased by 71 and 51 km/h, which are accepted as max. and min. values of wind speed acting on the balloon in the worst case in order to calculate max. and min. cyclic loading values for the fatigue analysis, which are presented in the **Table 4.1** below.

Table 4.1: Wind speed cases depending on measurements

	MAX.	MIN.
Measured wind speed range, m/s	5,81	0,10
Measured wind speed range, km/h	20,93	0,37
Range in the worst case, km/h	70,93	50,37

By using the maximum and minimum wind speed values, found by the worst possible wind scenario, max. and min. values of cyclic loading (Force, N) are found as seen in the **Table 4.2** below, both for the 14 m and 17 m balloons (Length, L) by the CFD analysis for the each.
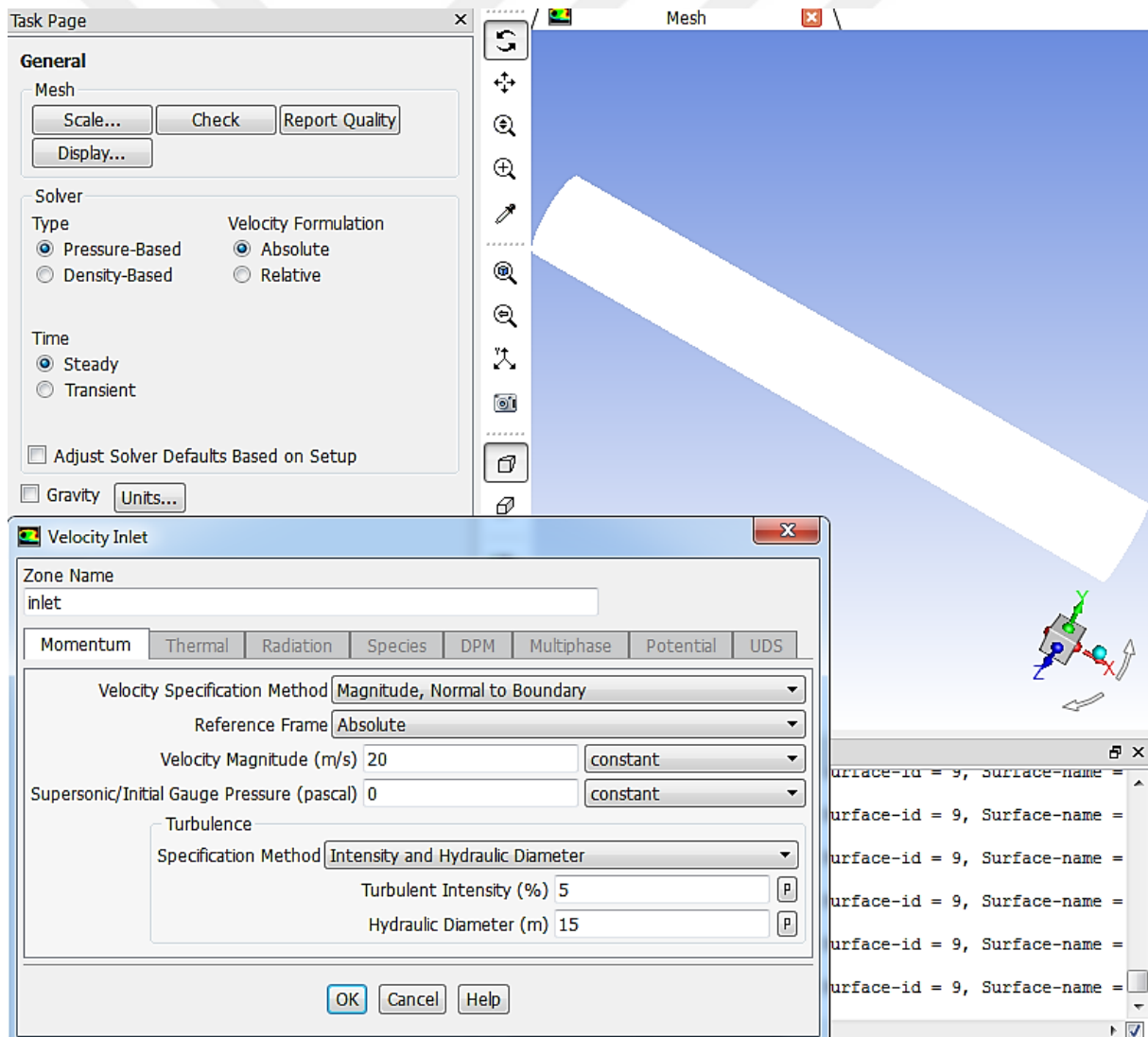
Figure 4.4: Details of CFD analysis

The details of the CFD analysis can be seen in the **Figure 4.4** above. It was a steady state, pressure-based analysis, which uses absolute velocity. Velocity was specified by magnitude, as a constant of 20 m/s. The turbulent intensity and hydraulic diameter values were accordingly entered as 5 % and 15 m. According to the analyses, the cyclic loading cases for 14 m and 17 m aerostats were found accordingly as 3611 - 2060 N; 5308- 3006 N as presented below.

Where, L, is the length of the aerostat, V, is the wind speed, S_ref, is the affected surface, and, Rho, is the air density.

Table 4.2: Wind speed – load calculation parameters

L, m	17	17	14	14
V, m/s	20	14,44	20	14,44
V, km/h	71	51	71	51
S_ref, m^2	50,86	50,86	34,5	34,5
Rho, kg/m^2	1,11	1,11	1,1	1,1
Force, N	5307,77	3006,09	3611,11	2059,92

Depending on the open air wind measurement data, the frequency of the dynamic load is also determined, according to the highest frequency obtained from the measurement data. The highest wind speed frequency was seen between the 2066th and 2070th seconds, as one life cycle per 4 seconds, therefore as 0,25 Hz. According to the highest frequency, 10^6 life cycles are calculated as 46,3 days, which means, if there are cyclic loads, acting as the worst case, and with the highest frequency in a duration of 10^6 cycles, the mooring station must resist them more than one and a half months.

4.2   Material properties

The materials used both in the mooring station of 14 m balloon as well as in the 17 m balloon, are all made of steel and aluminium which are the most frequently used metals in machine design works in the industry. The materials used in the mooring station components are, accordingly, hot rolled non-alloy construction steels with the standard DIN EN 10025, which are S235JR, S275JR and S355JR, an AISI 420 stainless steel and an Al 5083-H111

untempered Al-alloy. The mechanical properties of all of the materials can be found in the below tables, both obtained by manufacturer catalogues and former related academic works. The properties from former academic works are used not only to prove the reliability of the information given by manufacturers, but also to obtain some other required fatigue related properties which are not included in the manufacturer catalogue.

For the required fatigue properties of steels, the fatigue strength coefficients, σf', of all steels are simply obtained by the **Equation 2.13** [Roe00], depending on the mechanical properties presented in this section, while the fatigue strength exponent, b, is taken as -0.09, depending on the research of Poeppelman [Poe11], which are all explained in detailed in the state of the art.

For the components made of aluminium 5083, on the other hand, these properties are taken from the research of Higashida et al. [Hig78].

4.2.1   Steels DIN EN 10025-P2 S235JR, S275JR and S355JR

−   Chemical composition and microstructures

Table 4.3: Chemical compositions of S235JR, S275JR and S355JR from manufacturer [Erd15]

	S235JR	S275JR	S355JR
C	0,17 max.	0,21 max.	0,24 max.
Mn	1,4 max.	1,50 max.	1,60 max.
P (max.)	0,04	0,04	0,04
S (max.)	0,04	0,04	0,04
Si			0,55
N (max.)	0,012	0,012	0,012
Cu (max.)	0,55	0,55	0,55
Ceq (max.)	0,35	0,4	0,45
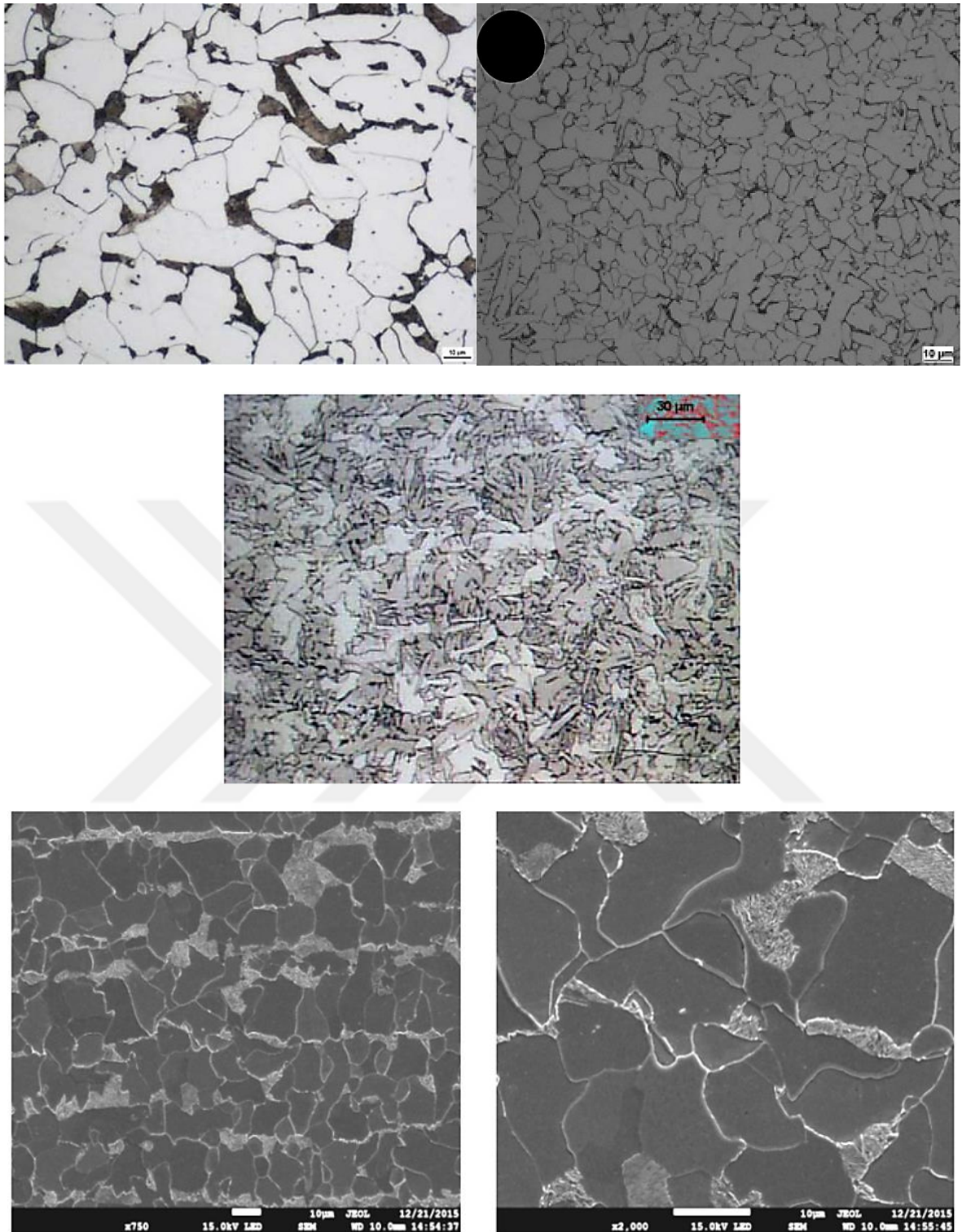
Figure 4.5 (a) and (b): Microstructures of S235JR accordingly by [Kos12] and [Kuk14], **Figure 4.5 (c):** Microstructure of S275JR (500x) [Bap11], **Figure 4.5 (d) and (e):** Microstructure of S355JR steel [Dzi16]

– Mechanical properties

Table 4.4: Mechanical properties of accordingly S235JR, S275JR, S355JR [Erd15]

Brinell Hardness, HB	104 - 154	122 - 162	140 - 180
Yield Strength (min.), MPa	235	275	355
Tensile Strength, MPa	360 - 510	430 - 580	510- 680
Specimen thickness, mm	3 – 40	3 – 40	3 – 40

These hot rolled structural steel profiles were not specifically strengthened by a heat treatment therefore, as shown as in the micrographs above in **Figure 4.5**, have a ferritic-pearlitic microstructure. With a C content below 0,2 % and a Mn content max. 1,4 %, S235JR seems to be a formable material however with the lowest strength, while S275JR and S355JR are seemed to have higher hardness, ultimate and yield tensile strength values with C contents over 0,2 % and with Mn contents accordingly max. 1,5 and 1,6 %.

Table 4.5: Mechanical properties of S235JR taken from academic work [Sko14]

Elasticty Modulus, GPa	215
Poisson's Ratio	0,30
Yield Strength (min.), MPa	281
Tensile Strength, MPa	441

The mechanical properties presented by the research [Sko14] for steel S235JR above, were presented after a statistical analysis of the test results, depending on Annex D "Design assisted by testing", Eurocode PN – EN 1990 methodology. The values yield and ultimate tensile strengthes were calculated depending on normal distribution of the all results. Depending on these given mechanical properties, required fatigue strength coefficient, σf' is calculated as 773,25.

The material properties in the below **Table 4.6** are taken from the academic work [Kta12], in which a S275JR metal sheet were tested by uniaxial tensile testing (NF A 03-151) in order to find properties as elasticity modulus, Poisson's ratio, tensile yield and ultimate tensile strengths. The required fatigue strength coefficient, σf', is thus calculated as 862,5.

Table 4.6: Properties of S275JR taken from academic work [Kta12]

Elasticty Modulus, GPa	210
Poisson's Ratio	0,30
Yield Strength, MPa	290
Tensile Strength, MPa	489

Table 4.7: Properties of S355JR taken from academic work [Dzi16]

Elasticty Modulus, GPa	197
Poisson's Ratio	0,30
Yield Strength, MPa	378
Tensile Strength, MPa	588 - 613

Depending on the mechanical properties given in the above **Table 4.7**, by the scientific work which examines S355JR steel, required fatigue strength coefficient, $\sigma f'$, is calculated as 99.

4.2.2 AISI 420

− Chemical composition and microstructure

The material of the stainless steel bar is an AISI 420 martensitic stainless steel, quenched and tempered at 700 C°, with the microstructural elements given in the below **Table 4.8**.

Table 4.8: Chemical properties of AISI 420 [Bir17]

C	Mn	P	S	Si	Cr
0,2	1,0 max.	0,04 max.	0,03 max.	1,0 max.	13,0
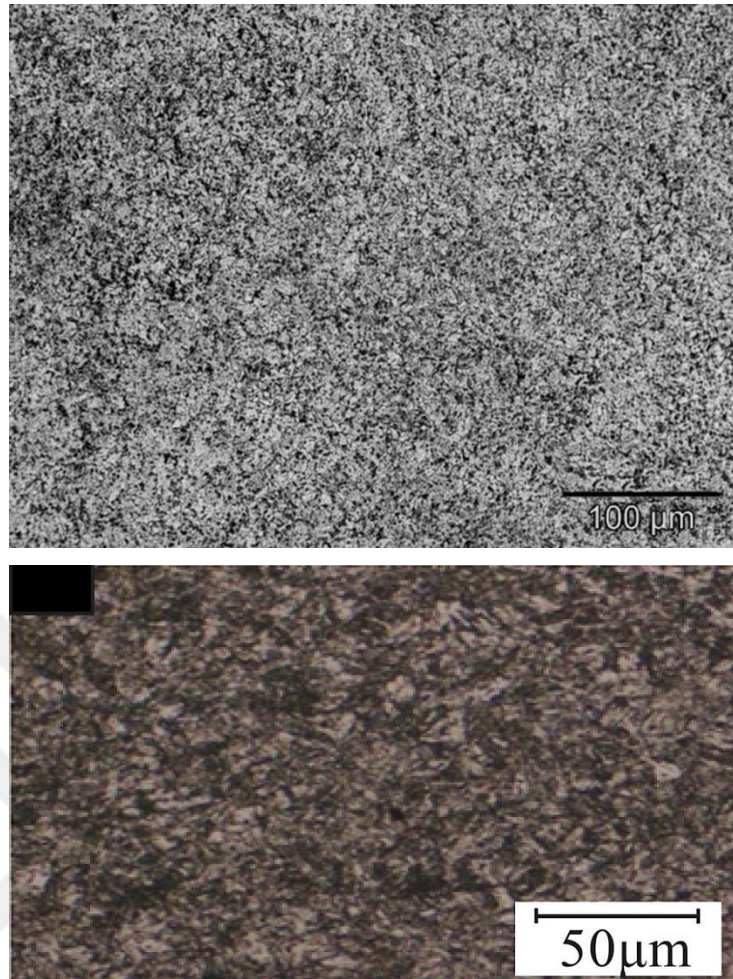
Figure 4.6 (a): Microstructure of annealed AISI 420 [Sch14], **Figure 4.6 (b):** Microstructure of AISI 420 QT700 [Sha15]

− Mechanical properties

The properties given below in **Table 4.9** are the averaged values given in the manufacturer catalogue.

Table 4.9: Properties from manufacturer [Bir17]

Yield Strength, MPa	600
Tensile Strength, MPa	800
Elasticty Modulus, GPa	200
Brinell Hardness, HB	257

As presented in the micrograph in **Figure 4.6 (b)**, AISI 420 steel bar has a martensitic microstructure which was formed after tempering at 700 C°. While the material is already

hardened and strengthened due to the alloying elements, (13 % Cr, and 1 % Si) and with 0,2% C content can be seen in the **Figure 4.6 (a)**, very high ultimate and yield tensile strengths and hardness were also obtained after the tempering process.

The mechanical properties for the same material tempered at temperature 648 °C are given in the research [Row07] as in the below **Table 4.10**.

Table 4.10: Properties of D420 taken from academic work [Row07]

Yield Strength, MPa	585
Tensile Strength, MPa	790
Rockwell Hardness, HRC	48

Depending on the mechanical properties given in the above tables, required fatigue strength coefficient, σf', is calculated as 1317,25.

4.2.1 Aluminium 5083-H111

- Chemical composition and the microstructure

Table 4.11: Chemical composition of aluminium 5083-H111 [Sey17]

Al	Mg	Mn	Fe	Si	Cr	Cu	Zn	Ti
Balance	4,0 - 4,9	0,4 - 1,0	0,4	0,4	0,25	0,1	0,25	0,15
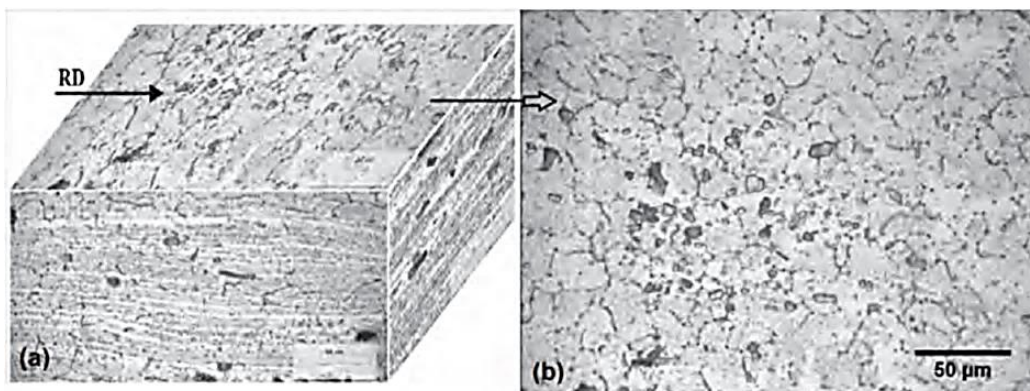
Figure 4.7 (a): Microstructure of aluminium 5083-H111, isometric view, **Figure 4.7 (b):** Top plane view [Mut11]

– Mechanical properties

Table 4.12: Properties of aluminium 5083 taken from manufacturer [Sey17]

Heat Treatment (Temper)	H111
UTS, MPa	270 - 345
Yield Strength, MPa	115
Elongation (min.), %	16
Shear Modulus, MPa	170
Young's Modulus	70

Even though the material, Al 5083 H111 has no special tempering treatment, the aluminium alloy has a yield strength of 115 MPa and an ultimate tensile strength between 270 and 345 MPa due to the alloying elements given in **Table 4.11**, within, Mg and Mn are the most effective with contents accordingly between 4,0 and 4,9 % and 0,4 and 1,0 %. The micrograph showing these microstructure can be seen in **Figure 4.7** above.

Table 4.13: Mechanical properties of Al 5083 taken from academic work [Hig78]

Hardness, HB	93
Elasticity Modulus, GPa	71
0.2% Offset Yield Strength, MPa	131
UTS, MPa	294
Fatigue Strength Coefficient, MPa	103
Fatigue Ductility Coefficient	0,405
Fatigue Strength Exponent	-0,122
Fatigue Ductility Exponent	-0,692

4.3 Surface retention factors

The surface retention factor, or surface factor, SRF, of such components made of construction steels, S235JR, S275JR and S355JR, which are tower and rope connection arm, is assigned as 0,7 depending on the SRF - UTS graph given in **Figure 2.14** [ASM08], since construction steels used in mooring station components are hot rolled profiles, which have UTS slightly lower or slightly higher than 500 MPa.

Depending on the same graph, a SRF of 0,9 is assigned for commercially polished AISI 420 steel bar, which is used in the sheave section of the tower, due to its UTS around 800 MPa.

Finally, the SRF of flying sheave component is set as 0,8 according to the same figure, since it is assembled by machined Al 5083 plates, which have UTS of 294 MPa.

5   CAE – fatigue analysis

Within the CAE – fatigue analysis, computer tools are used to estimate service life of the mooring station components under the worst possible dynamic loading case, of the both former 14 m and the new fatigue resistant 17 m balloons. For the CAE – fatigue analysis, specific fatigue analysis software nCode is used. First analysis will be applied onto the mooring station of 14 m balloon, then by the use of these results, the new larger mooring station for 17 m balloon will be designed. The last analysis will therefore be made for this larger mooring station design, which will undergo higher loads, and the SF results of its components are expected to be improved comparing to the SF results of the first analysis for the smaller mooring station.

The CAE analyses are done for each components of the mooring station separately. The reason of making CAE fatigue analysis separately for the components of the mooring stations is that it is very difficult, time consuming, and even impossible to do a single FEM analysis of the complete mooring station in one step.

5.1   Analysis setup

The principles and the setup of the CAE fatigue analysis, used for fatigue analysis of the mooring station components within this thesis project, is described in this section. Fatigue analysis of the mooring station components in the scope of this project is made by DesignLife module of nCode software, by which not only life and damage results but also fatigue safety factors (SF) depending on the preferred fatigue properties can be generated.
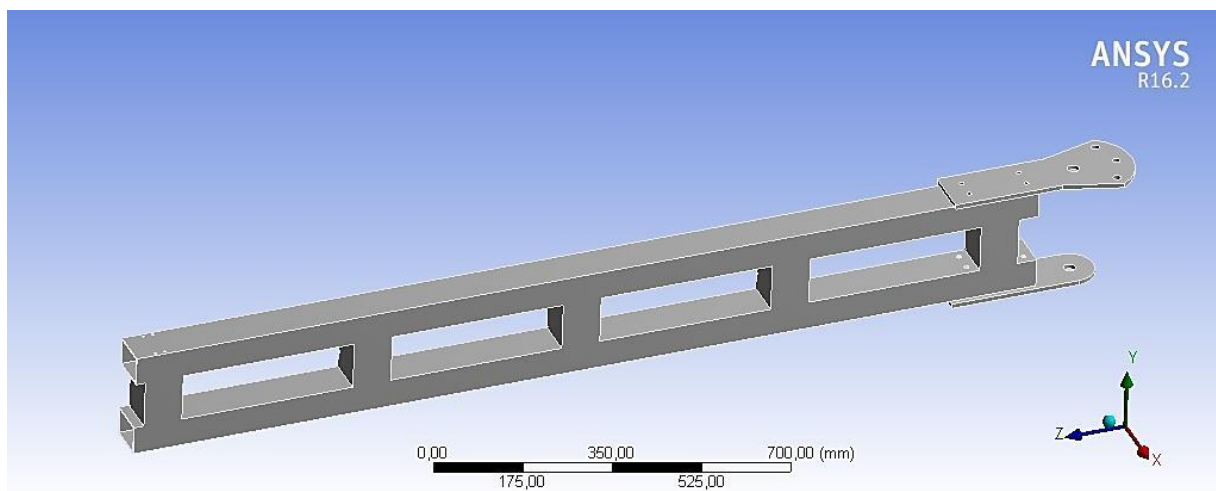
Figure 5.1: View of a component's geometry in Ansys

On the other hand, before making a fatigue analysis on nCode, first, FEM data from a static structural analysis is required, as this is a FEM dependent fatigue analysis software.

Therefore, FEM analyses of the components are firstly made by static structural module of ANSYS by adding 3D CADs, as presented in the above **Figure 5.1,** and the mechanical properties of materials. After preparing analysis setup in ANSYS static structural with 3D Geometry, boundary conditions, material assignments (Engineering Data), joints, temperature, mesh model, and loads, such stress results as Equilavent (Von-Misses), Max. Shear, or Max. Principal are then generated. In the generation of the stress results in static structural, display option is selected as "unaveraged" for the "integration point results". By this selection, the most exact solution will be shown on the elements, without averaging the values within. The most accurate maximum stress values will therefore be picked by analyzing the solutions within related elements.

The FEM result data can, not only be used to assess varying stress results depending on varying load conditions but also to connect to nCode DesignLife, as presented in the **Figure 5.2** below, and then to make fatigue analysis according to these data and required fatigue properties, which will be explained in detail later in this section.
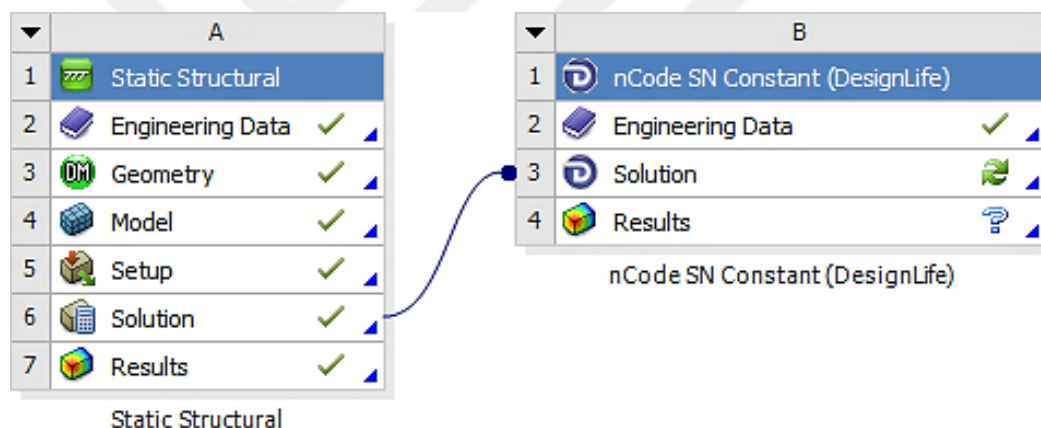
Figure 5.2: Static structural and nCode analysis connection on Ansys workbench

Within the FEM analysis on ANSYS, "fixed joints" are used to describe bolted connections, and for description of the bonded surfaces due to these bolted connections, "frictionless contacts" are used in order to be accurate with results of the FEM analysis.

5.1.1 Mesh quality

After setting up all the boundary conditions and loads, mesh quality is lastly checked and corrected. In case of too high skewness values more than 0,30 the meshing is corrected by refining the mesh sizes or manually removing meshes having bad quality. For generally meshing all the component geometries, body mesh with mesh sizes between 2-5 mm is used. The size is selected according to the optimum quality, which close to element quality value of 1.

Before the analysis of each of the components, a mesh convergence analysis method is applied to prove correctness of the analyses, with the parameters shown in the mesh convergence analysis results of the tower crane part below, in **Table 5.1**.

Table 5.1: Mesh convergence analysis of tower crane part of the new mooring station

Mesh [mm]	Skewness (avg.)	Orthogonal Q.	Element Q. min.	Max. Principal Stress [MPa]	Error %
20,00	1,00	0,01	0,38	69,00	
10,00	0,35	0,64	0,78	75,00	0,09
5,00	0,15	0,85	0,86	77,00	0,03
4,00	0,24	0,75	0,87	76,00	-0,01

The mesh convergence is applied as starting from a relevantly higher mesh size - generally 20 mm - and then remaking analysis by smaller mesh sizes step by step. When the error (% difference of result according to the previous) is approximately 0,01, then the mesh size is accepted to be adequate.
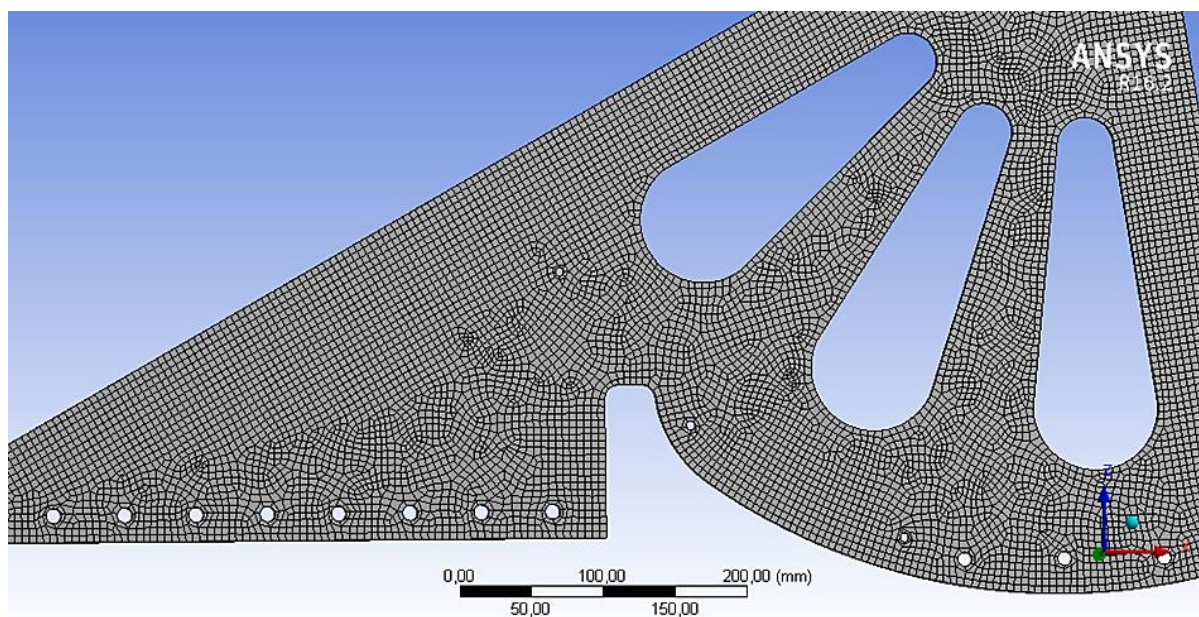
Figure 5.3: Meshed geometry

After getting the FEM data from ANSYS Static Structural, and transfering to NCode, as already described, lastly the setup of fatigue analysis is done under nCode DesignLife window, as seen in the **Figure 5.4** below.
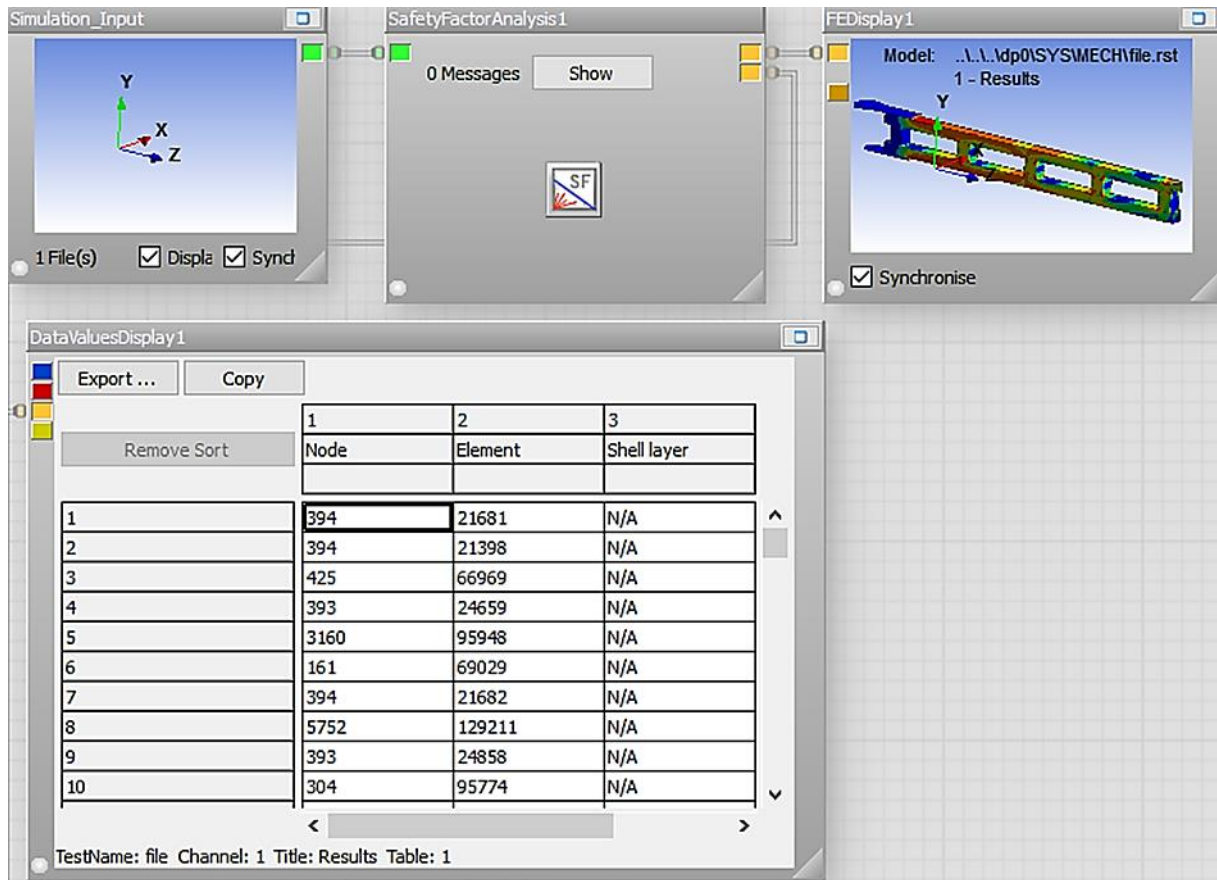
Figure 5.4: Glyphs in DesignLife

Since it is expected to see an infinite life without any fracture in the components, stress amplitudes must be low enough to obtain SFs over 1. Therefore, for the parts, which have shown no damage in the fatigue analysis, SF results, depending on related fatigue limits, will be presented instead of life or damage results. For the components made of steel, fatigue limits are accepted as max. possible stress amplitude at 10^6 cycle, and for the components made of Al-Alloy fatigue limit is taken as max. possible stress amplitude at 10^9 cycle, which are all input parameters in nCode setup screen as seen in the **Figure 5.5** below, named as TargetLife. If SF is above 1 then the component has a safe life according to the given limit, if it is under 1 then the component has a limited life. If SF is below 1, cycles to failure analysis would be required beside of the fatigue SF analysis.

Name	Value	Description
General		
LoggingLevel	Info	The amount of detail to output to the message window du
ResultsUpdateInterval	10	Time interval between processing result output
AnalysisGroup		
AnalysisGroup_GroupNames	*	Groups to process
AnalysisGroup_MaterialAssignmentGroup	Property	Sets the grouping type to be used for material mapping
AnalysisGroup_SelectionGroupType	Property	Sets the grouping type to be used for extracting results
AnalysisGroup_ShellLayer	TopAndBottom	Shell layer to use
AnalysisGroup_SolutionLocation	NodeOnElement	Solution location
AnalysisGroup_StressUnits	MPa	The units to use for stress values
Job		
Job_NumAnalysisThreads		The number of simultaneous analysis threads to use for th
Run1		
Run1_Gate	20	The gate value to apply during time history compression
Run1_TimeHistoryCompression	None	Specifies how to compress time history loading
SafetyFactorEngine		
SafetyFactorEngine_CertaintyOfSurvival	50	Required confidence level on damage results
SafetyFactorEngine_CheckStaticFailure	Warn	The action to take on static failure
SafetyFactorEngine_CombinationMethod	AbsMaxPrincipal	The method used to combine component stresses/strains
SafetyFactorEngine_EventProcessing	Independent	How to process separate events in duty cycles
SafetyFactorEngine_FactorOfSafetyType	ConstantMean	Method for calculating safety factor.
SafetyFactorEngine_MaxPrincipalPlaneStress	MostPositive	Use most positive or largest absolute value
SafetyFactorEngine_MeanStressCorrection	Goodman	The method used to correct the damage calculation for me
SafetyFactorEngine_OutputEventResults	False	Whether to output results per event or not for duty cycle
SafetyFactorEngine_SNFactorOfSafety	Standard	The method used to calculate the stress based safety fact
SafetyFactorEngine_TargetLife	1E6	Target life for safety factor calculation

Figure 5.5: Setting up fatigue analysis properties in NCode DesignLife

Within the fatigue analysis in nCode, maximum principal stress is preferred over others, since an area where a tensile principal stress with the highest value is the region where a possible fatigue fracture is expected the most, than an equivalent stress which include all other principal and shear stresses.

Solution location of the analysis is selected as "nodes on elements", rather than "averaged nodes on elements", since exact solutions on the elements are required. Thus, in the result screen, the solution in the elements will be comprehensively analysed and the most correct value will be picked to determine minimum SF of the component.
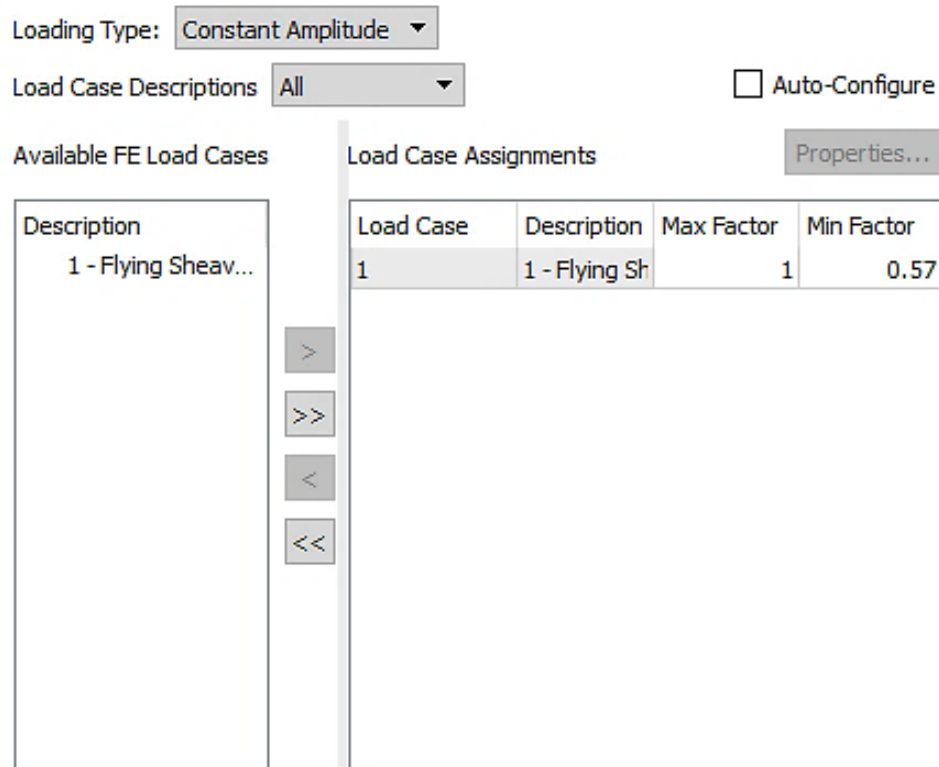
Figure 5.6: Describing the cyclic loading in DesignLife

In the next step, cyclic loading parameters are described in the nCode "Load Case" window. As seen in the **Figure 5.6** above, the max. and min. factors describe the max. and min. values of the cyclic loading according to the already given load in the static structural analysis. The load value given in static structural analysis is therefore the max. value in cyclic loading, which was set by wind speed calculations in previous section 4.1. Then min. value of cyclic loading is given to the analysis by this min. factor shown in the **Figure 5.6**, which is the ratio between max. and min. loads.

The setup of material generation in DesignLife is one of the most important steps, since depending on this information the software sets a computer generated S-N curve. In this module, DesignLife generates the S-N curve depending on such material properties as; type (Ferritic, Aluminum, etc.), UTS and standard error of log (N). Fatigue transition point (or fatigue limit) is also given in this step.
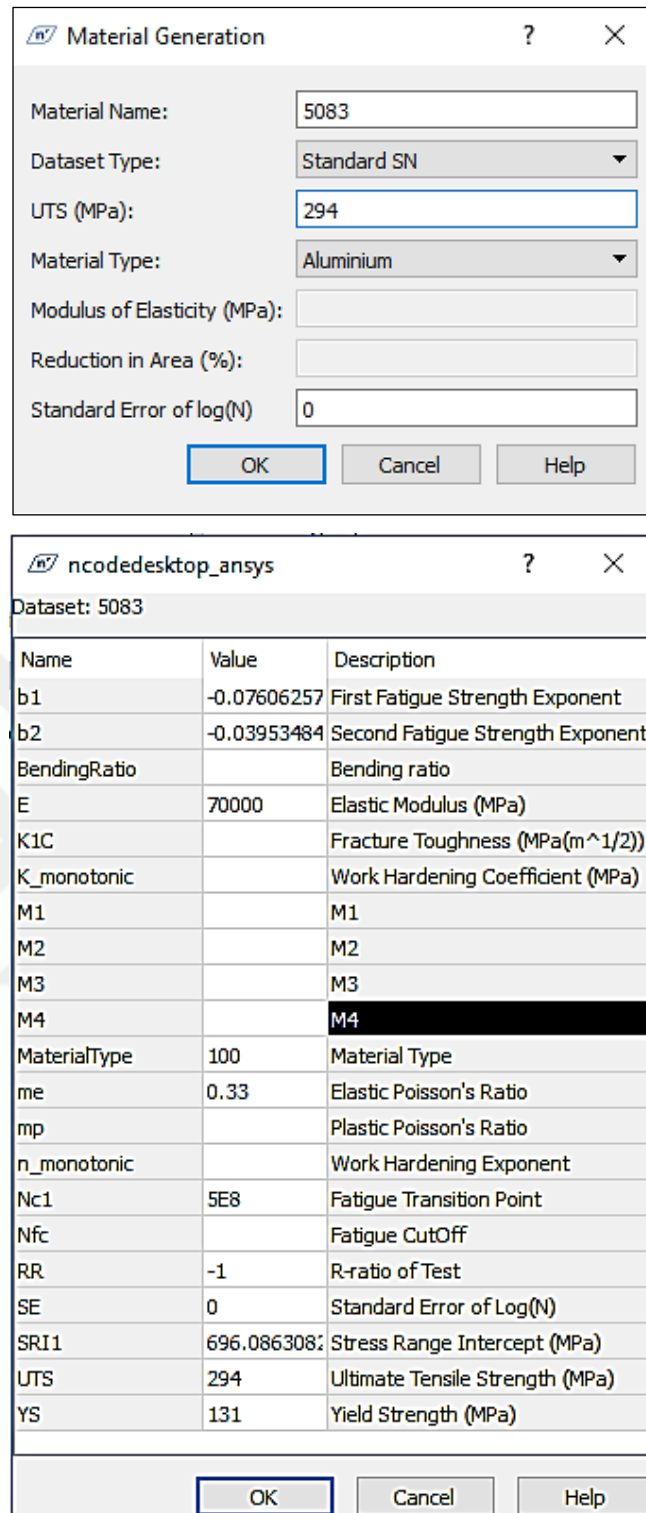
Figure 5.7: Material generation module windows in DesignLife

After setting all the material properties, then such material group parameters as surface factor related to surface roughness/quality, are entered to analysis setup which is already explained in previous factor as SRF, as seen in the **Figure 5.7** above. Finally, required S-N curves are generated according to given parameters by DesignLife as seen in the **Figure 5.8** below.
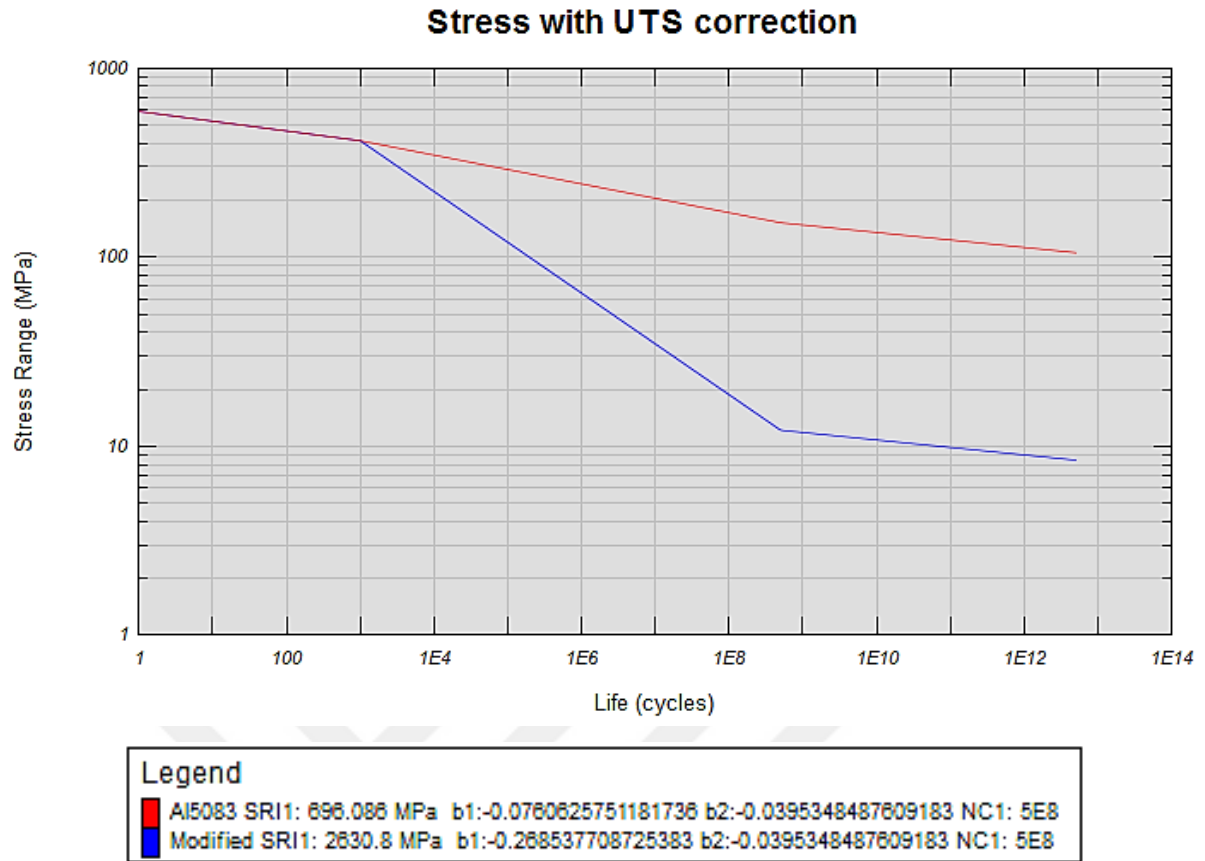
Figure 5.8: DesignLife generated S-N curve of a material

5.2 Predicted fatigue behaviour of the first mooring station

The first fatigue investigation of the thesis project is done for the mooring station of the 14 m balloon. For the analysis, the CAE methods which are described in the previous section as well as the parameters and loads found specifically for this mooring station design were used. Beside of the 3D CAD and material selection of the mooring station components, mechanical properties and surface quality information were also prepared as pre-requisites of the fatigue analysis by CAE. In the scope of the fatigue analysis of the mooring station of 14 m balloon, the designed main components, flying sheave, tower, tether crane and rope connection arm were analysed depending on the given CAE method and then results were presented according to the components.

5.2.1 Flying sheave

As said, the flying sheave is a mooring station component, which is directly affected by dynamic loads during the flight of the balloon. After setting up the parameters in ANSYS Static Structural as given in the **Figure 5.9** below, FEM results are generated. The 3D CAD geometry used in the FEM analysis is actually the side support plate in the component, which undergoes the half of the applied loads by itself.
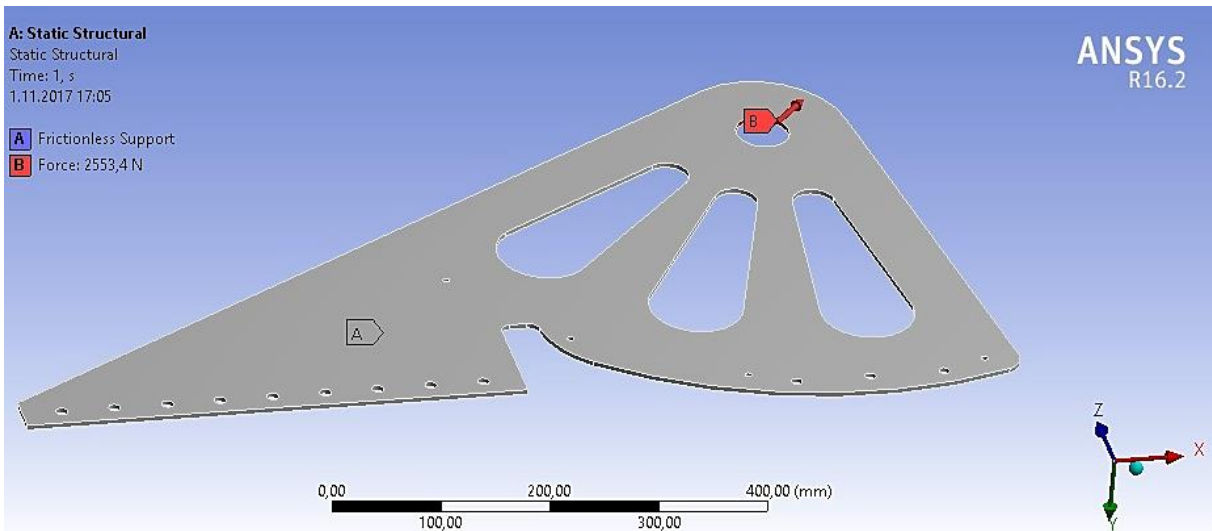
Figure 5.9: FEM setup of the flying sheave – 14 m balloon

The reason of analyzing only side plate of the component in the analysis is that, this piece is machined from an Al 5083 plate, while others ready taken parts or manufactured from thicker materials, which makes it the most sensitive part within the complete flying sheave.

The material used in the whole component is Al 5083, with the properties given in the previous chapter.
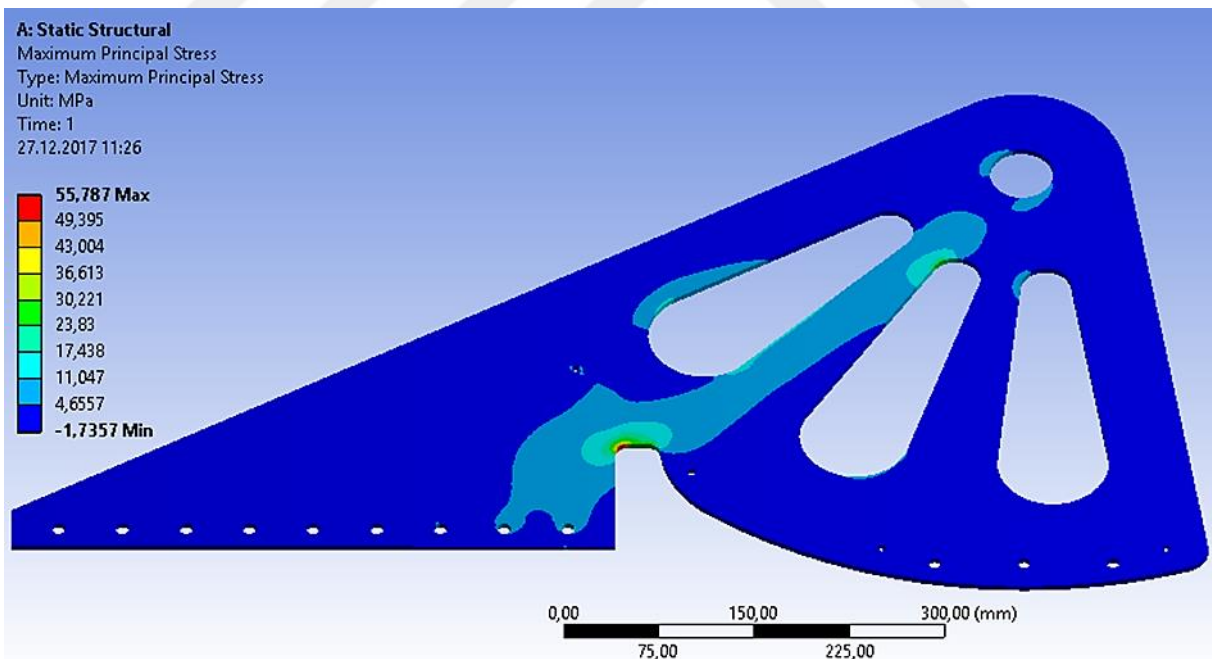
Figure 5.10: Max. principal stress distribution in the side plate of the flying sheave – 14 m balloon

According to the maximum principal stress result seen in the **Figure 5.10** above, a maximum stress of 55,79 was generated in the region shown in red colour when a maximum load of 3611,11 N is applied from the region where it will take dynamic loads during service.

Beside of the conventional static SF generated by Static Structural FEM analysis, a fatigue SF analysis was also required.
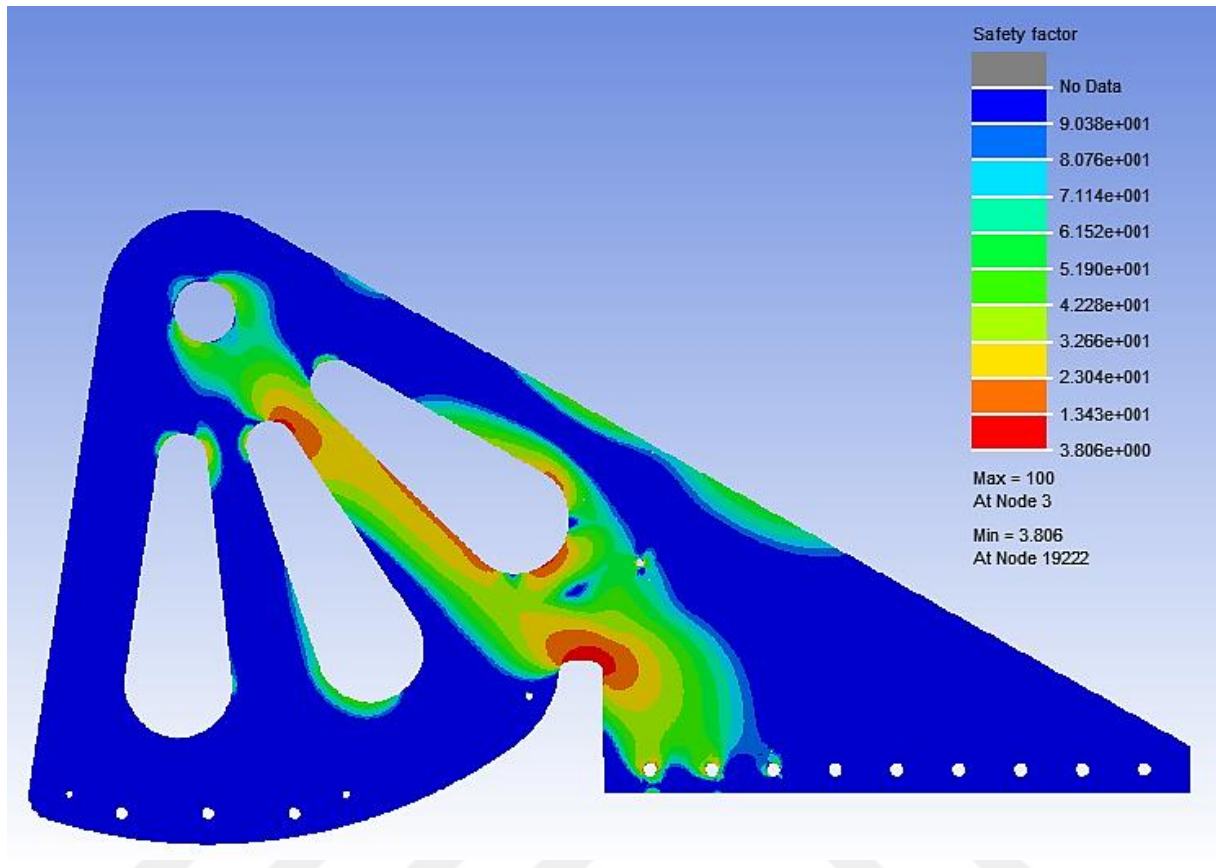
Figure 5.11: Fatigue SF of flying sheave generated by nCode – 14 m balloon

According to the analysis result given in the **Figure 5.11** above, the flying sheave has shown a fatigue SF of 3,81, which means that, it is almost four times safer for the applied cyclic load, according to the given fatigue strength limit at 10^9 cycles.

5.2.1 Tether Crane

Tether crane is the only component in the mooring station which is not designed and manufactured within the facility, shown in the **Figure 4.2** in detail, except the side support parts by which it is connected to the ground. However to be able to sure about results of the analysis, a CAE analysis for the tether crane was also completed specifically for the side sheet part while the drum and ball bearing parts were commercially bought parts, with a guaranteed SF and strength from supplier, manufactured from high strength materials. This thin support part machined from a S235JR steel plate, and actually connects the crane to the ground, on which the drum is connected with the help of a ball bearing. The setup of the support part can be seen in the **Figure 5.12** below.
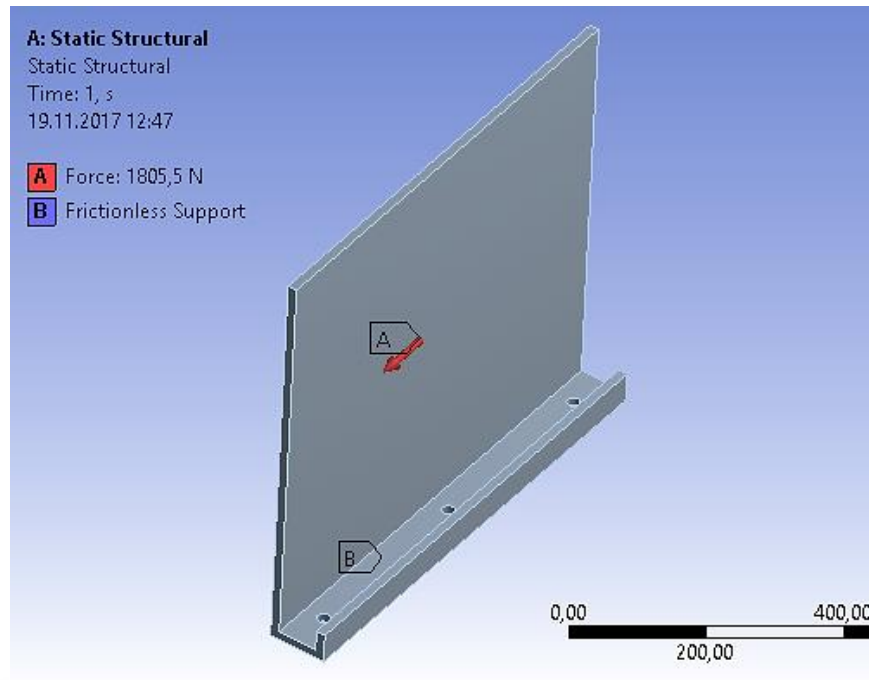
Figure 5.12: Analysis setup of tether crane – ground connection part – 14 m balloon

As presented in the **Figure 5.13** static structural result below, the maximum principal stresses on the component are too small, which even lead deciding not to do any further fatigue analysis since a possible stress amplitude even lower than 3,7 will be unessential for a potential fatigue failure within a component made of construction steel.
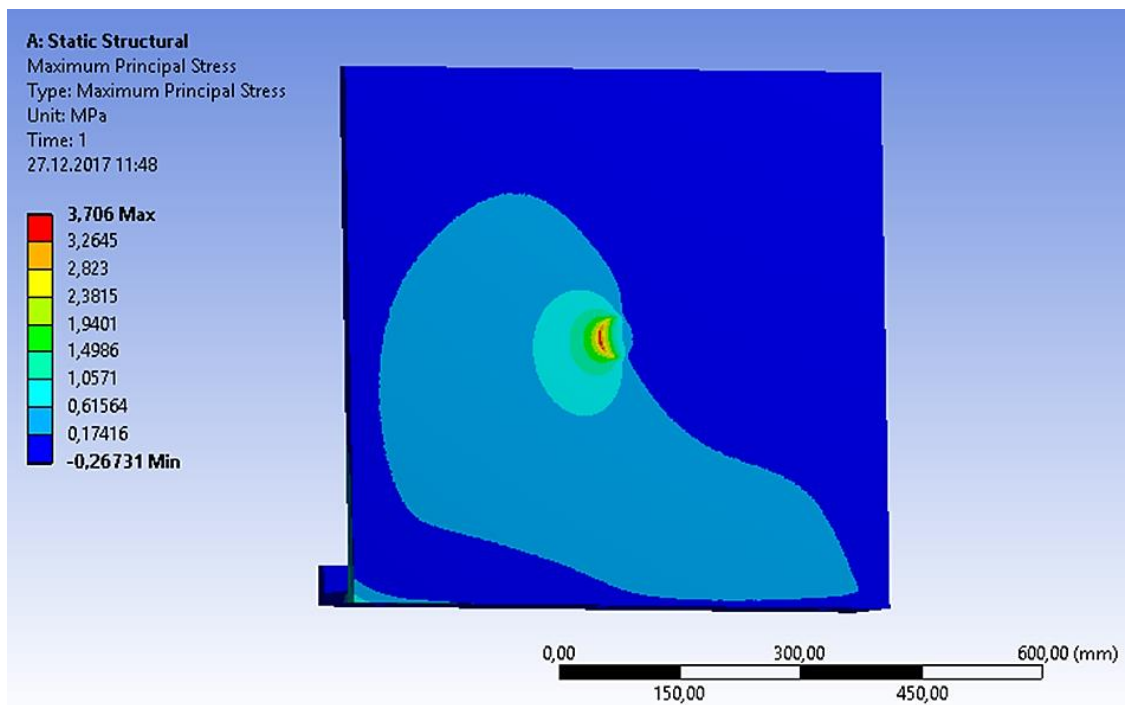
Figure 5.13: Max. principal stress distribution in the ground connection sheet of the tether crane – 14 m balloon

5.2.2 Tower

Tower is the biggest and the heaviest component in the mooring station. Beside of the dynamic loading generated by wind speed changes acting on balloon, tower also has an important factor, weight, to be considered within the analysis. Another aspect with this component is that it is affected by dynamic loads only when the balloon is in the parking position, on the ground level.
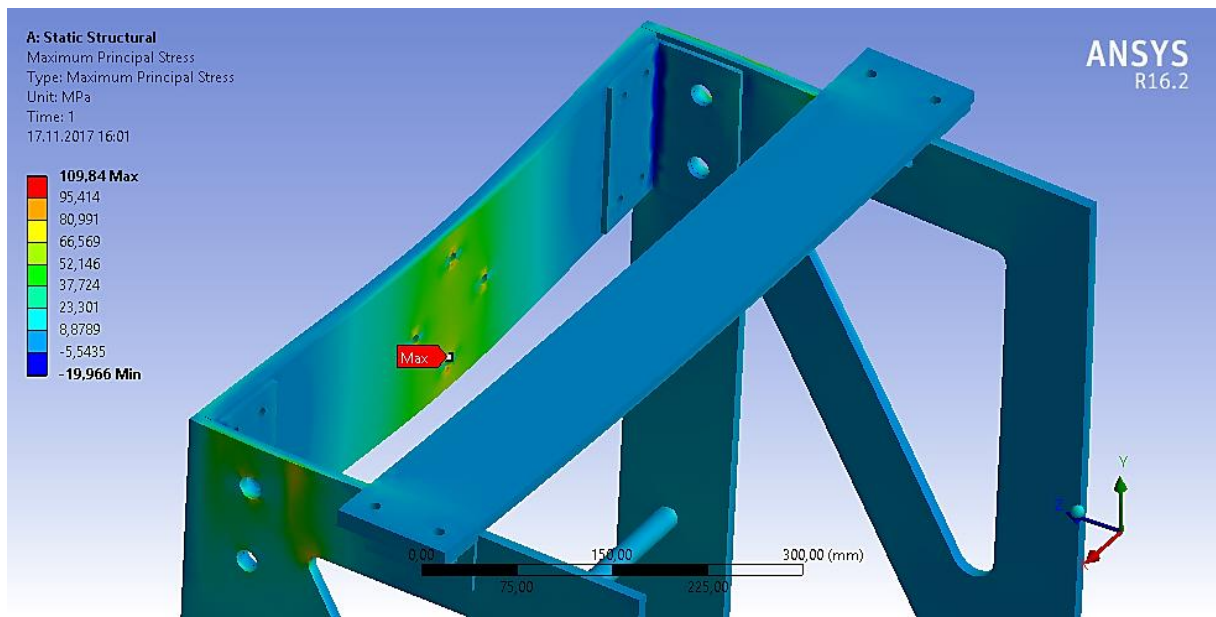
Figure 5.14: Max. principal stress distribution in the tower– 14 m balloon

Most of the parts used in this component are machined from S235JR steel, except steel bars or L-profiles made of S355JR. The highest stresses on the other hand are expected to reveal on the machined parts made of S235JR steel.

The highest averaged stress per element, under the maximum load within the structure is presented in the **Figure 5.14** above with a value of 110 MPa. The highest stress value is seen in the upper plate part, where balloon nose is directly connected, thus it takes the loads directly. According to these stress results, this part in the next step will solely be analysed for its fatigue SF.
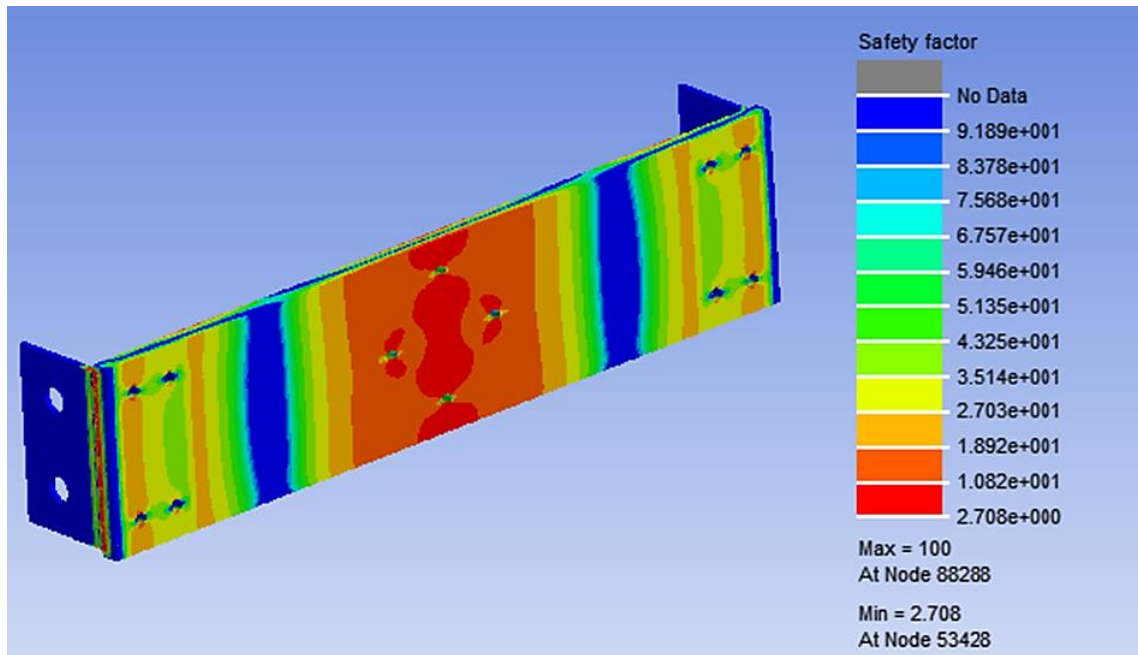
Figure 5.15: Fatigue SF of the tower– 14 m balloon

As given the reason as in the previous section, a fatigue SF analysis is done for the tower. According to the results presented in above **Figure 5.15**, it seems that fatigue SF of the component is 2,7 (shown as the regions with the yellow colours), of which factors are dependent on the fatigue limit at 10^6 cycles for a component made of steel. It means, the component would be considered as safe during the service life time.

5.2.3 Rope connection arm

There are two rope connection arms placed on the both left and right side of the mooring station. Balloon is connected to these components by ropes when it is on the ground for the maintenance. Therefore it is only affected by dynamic loads emerged from winds on the ground level. In order to analyse its fatigue strength under the worst wind condition, thus, the worst dynamic loading scenario, a fatigue analysis for the rope connection arm must be done to be able to sure about its failure-free service life.

The component is assembled by square profiles made of S235JR steel, with the properties given in the previous chapter.
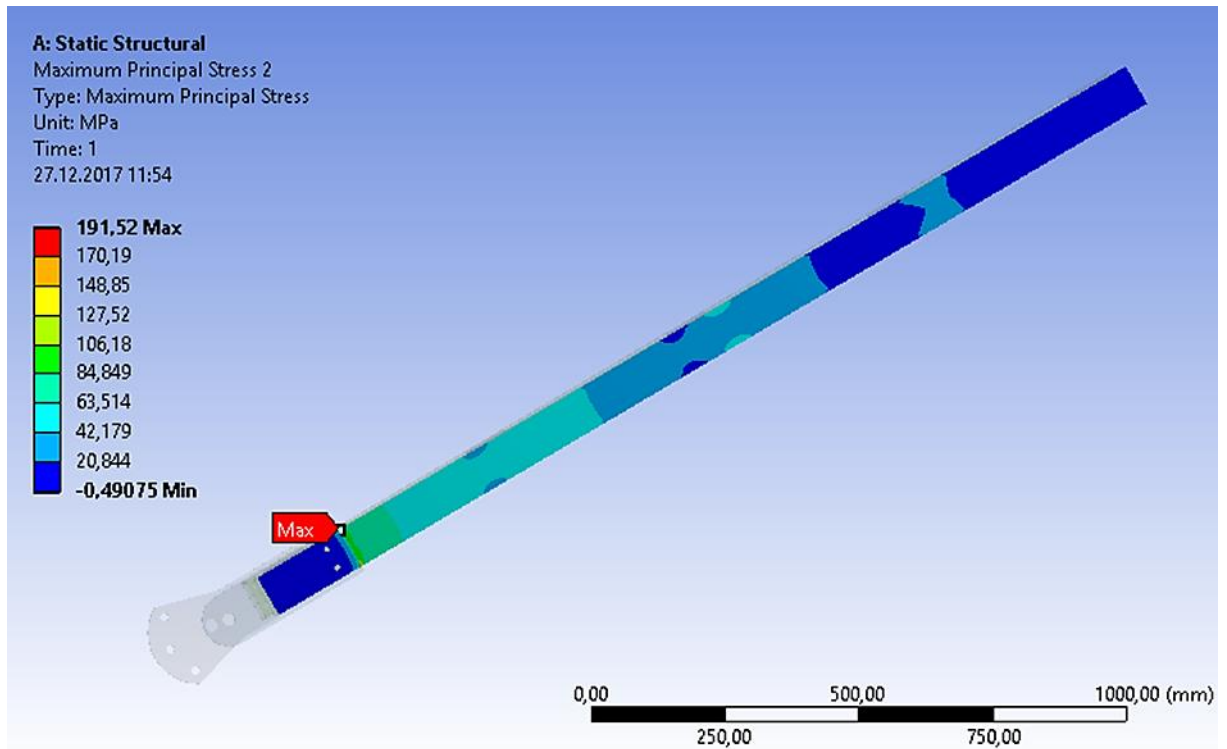
Figure 5.16: Max. principal stress distribution in the rope connection arm – 14 m balloon

According to the maximum principal stress results shown in **Figure 5.16** above, the maximum stress is obtained as 191,52 MPa, under the affecting maximum load.
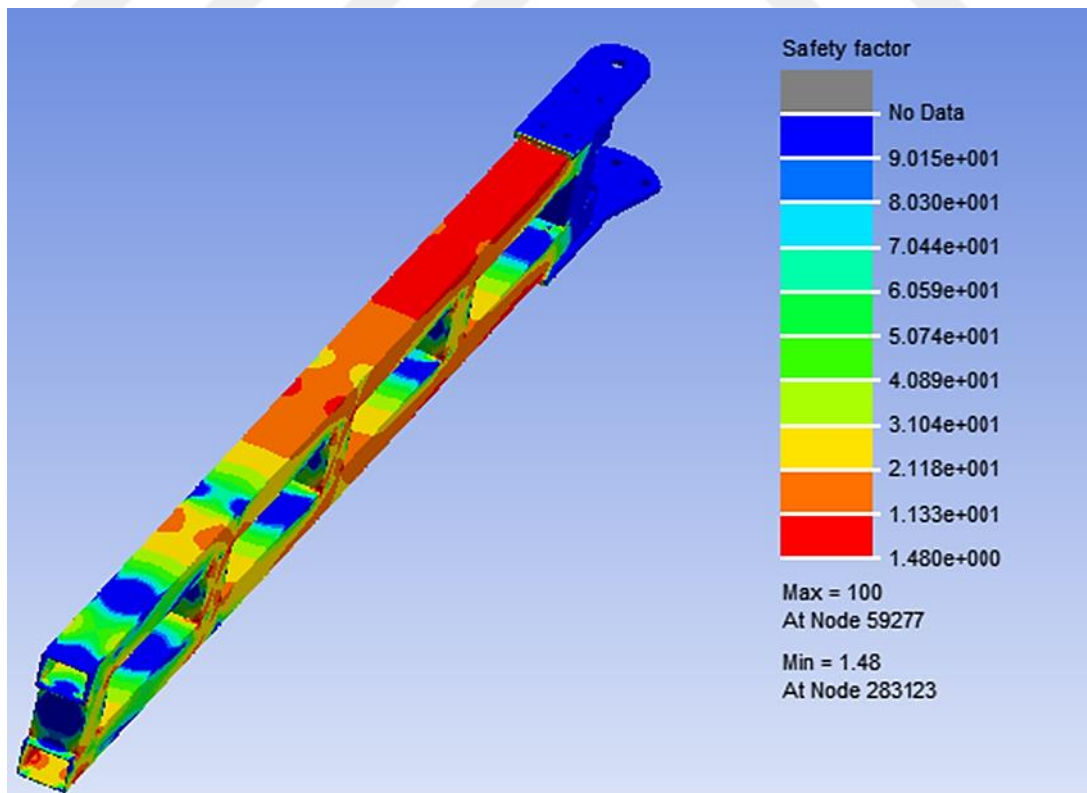
Figure 5.17: Fatigue SF analysis result of the rope connection arm – 14 m balloon

After having the static structural analysis results of the component, the fatigue SF analysis was completed with the results can be seen in **Figure 5.17** above. According to the results, a minimum SF factor of 1,48 is obtained, by a fatigue limit at the fatigue strength at 10^6 cycles to failure (Nf). With a SF of 1,48, the component seems to be designed slightly safe for the given fatigue limit at 10^6 cycles, which is under the determined safe limit of of 2,0.

5.3 Predicted fatigue behaviour of the second mooring station

After the first CAE fatigue analysis for the former mooring station of the 14 m balloon, the second CAE fatigue analysis is done for the fatigue resistant designed mooring station of the 17 m balloon. The same principles given in the previous chapter are also used in this analysis, while there were changes in load and material parameters which were specific for the bigger mooring station, which will undergo higher dynamic loads.

From the analysis results of the bigger fatigue resistant designed mooring station, it is expected to see SF values of the components over 2,0, while inhomogeneous SF values were obtained of from the previous smaller mooring station design even lower 2,0.

In the scope of the fatigue analysis of the mooring station of 17 m balloon, the main components, flying sheave, tower, tether crane and the rope connection arms were analysed depending on the given CAE method and then results were presented according to the components. Since the tower of this bigger mooring station is built according to several functional sections, analysis of this component is separated by these unique regions and analysed section by section.

5.3.1 Flying sheave

Just as in the first analysis of mooring station of the 14 m balloon, firstly the analysis results of flying sheave are presented. As seen in the analysis setup in **Figure 5.18**, a load applied on the component with a magnitude of 5308 N generates a reaction force up to 7506,6 N, which increases the failure risk of flying even more, compared to other components.

As in the maximum principal stress results, presented in **Figure 5.19** also below, the highest stress within the component structure is revealed as 52,02 MPa, which is 10 MPa higher than the maximum stress observed in the flying sheave of the 14 m balloon. However, as the main aim of the thesis work, fatigue SF analysis results should be more focused and used as a main comparison parameter.
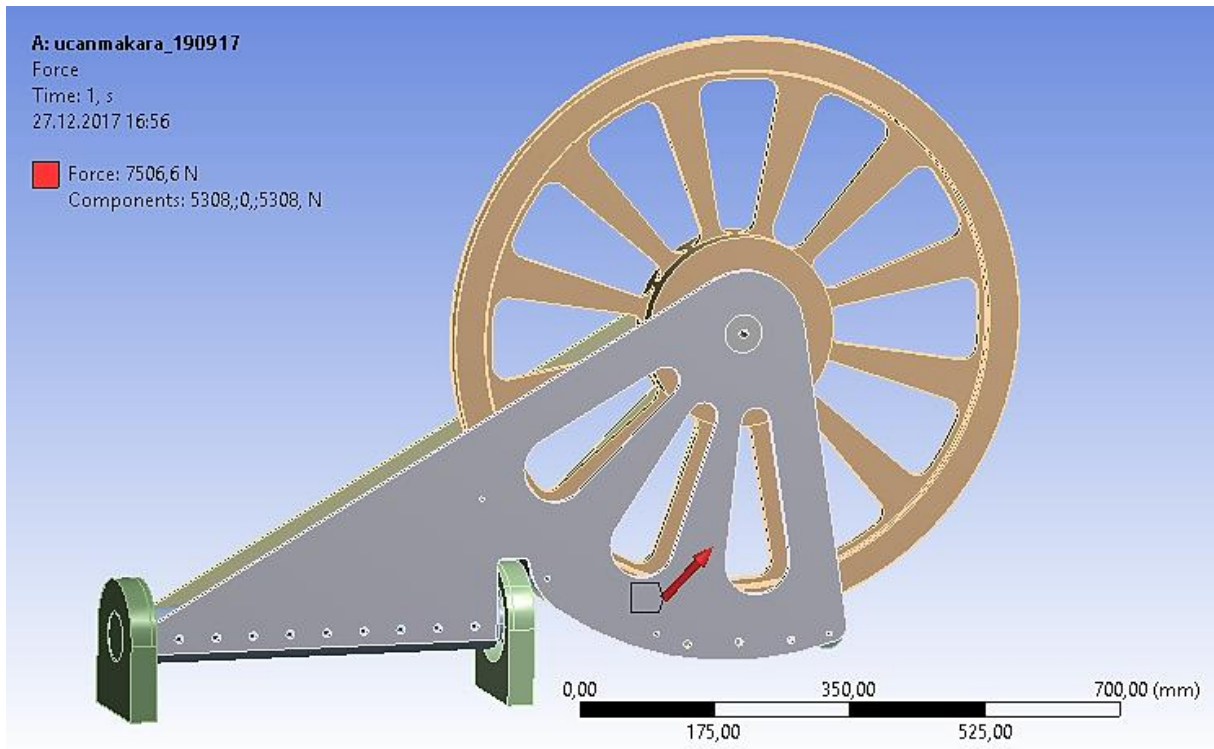
Figure 5.18: FEM analysis setup of flying sheave – 17 m balloon
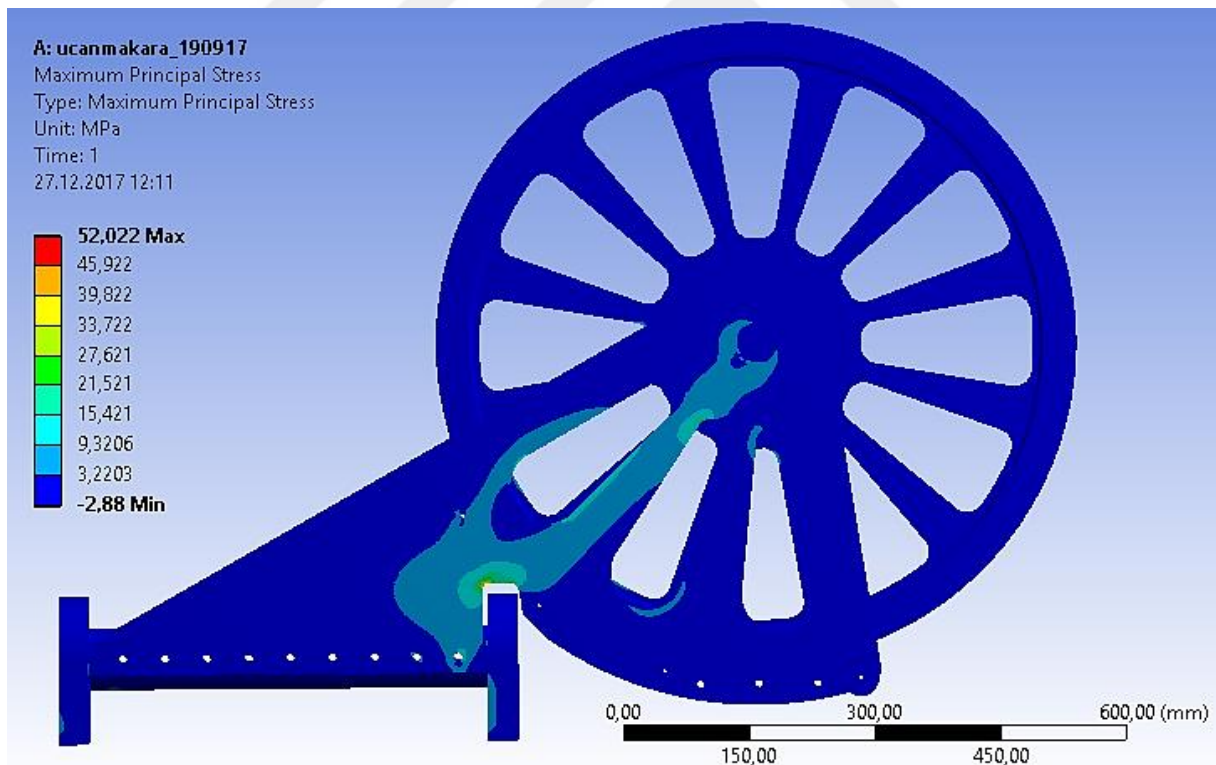
Figure 5.19: Max. principal stresses on the flying sheave – 17 m

As given in the **Figure 5.20** below therefore, fatigue SF analysis results of the flying sheave were observed with a maximum value of 3,55. Depending on this value, it can be said that, a SF factor of 3,55 by the fatigue limit at 10^9 cycles to failure (Nf) make the component three to

four times safe to be used under the worst dynamic load condition. The value is similar to the SF of 3,8, which was obtained by the flying sheave of the 14 m balloon.
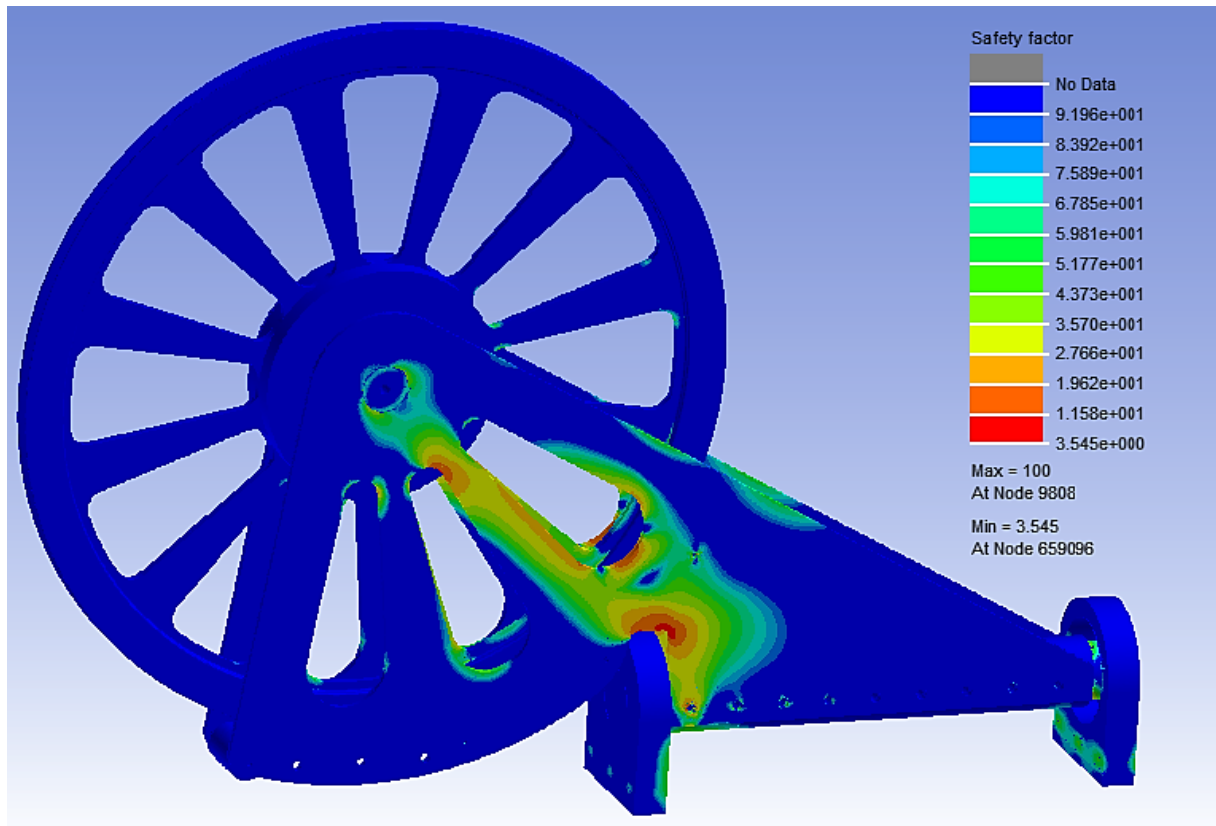
Figure 5.20: Fatigue SF analysis results for the flying sheave – 17 m balloon

5.3.1 Tether Crane

For the analysis of the tether crane, the same principle of the mooring station analysis of 14 m balloon was followed. Inside the tether crane component, only ground connection profiles were designed and produced within the facility, while the drum and ball bearings are the ready taken commercial components, which were already quality proven. Therefore, only the ground connection profile parts were analysed as if these were attached to the drum and undergo dynamic loading in the real situation.
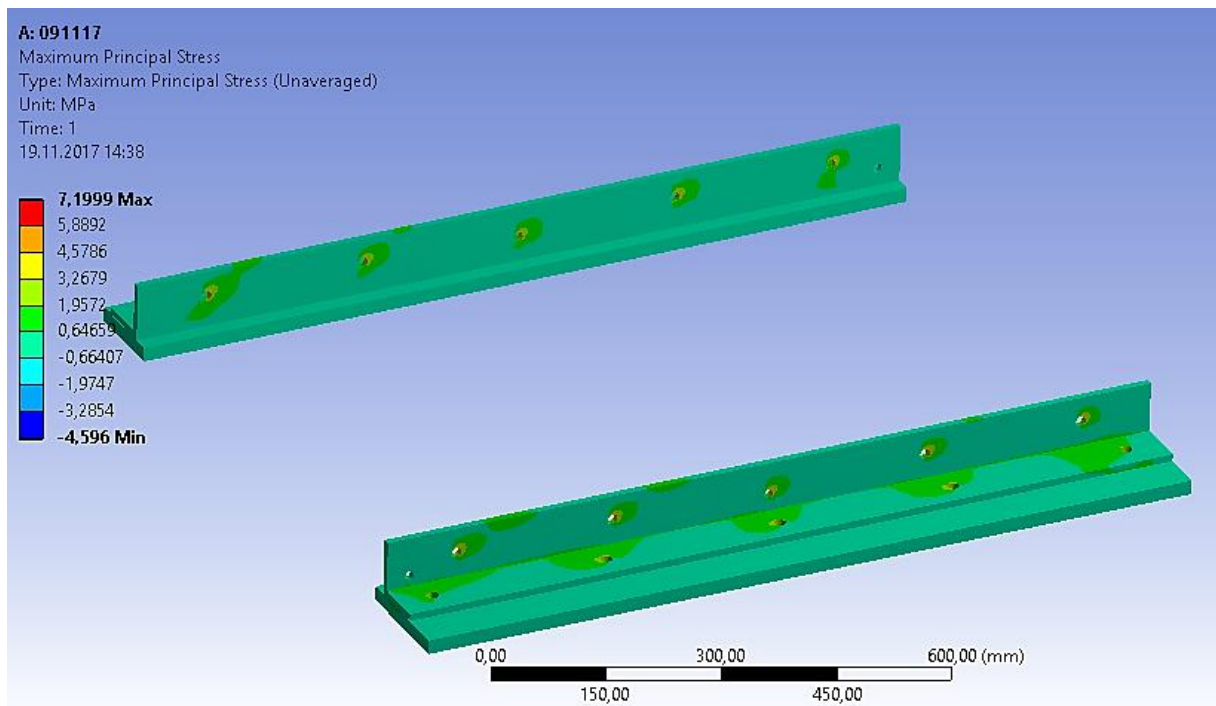
Figure 5.21: Max. principal stress results of the tether crane ground connection parts– 17 m balloon

The stress results by FEM static structural analysis can be seen in above **Figure 5.21**. The maximum stress under the maximum load seems to be around 7,2 MPa, which is an unessential value to consider within a fatigue analysis for a part made of construction steel. The part will therefore be considered as safe, and any further fatigue analysis will not be commenced.

5.3.2 Tower

As explained in the introduction of this chapter, the tower of the mooring station of 17 m balloon was not analysed as one structure, due to the size of the component with complex regions inside. Therefore, these several unique regions as joint section, sheave section and crane section will be analysed separately and the results will be presented accordingly.

− Joint section

The joint section is actually one of the most sensitive regions in the tower – or generally in the mooring station – since it connects upper and below parts together with a sensitive mechanism seen below in the **Figure 5.22**. Except the D420 stainless steel bar used for this connection mechanism, all other parts are assembled by profiles made of S235JR, S275 or S355JR construction steels.
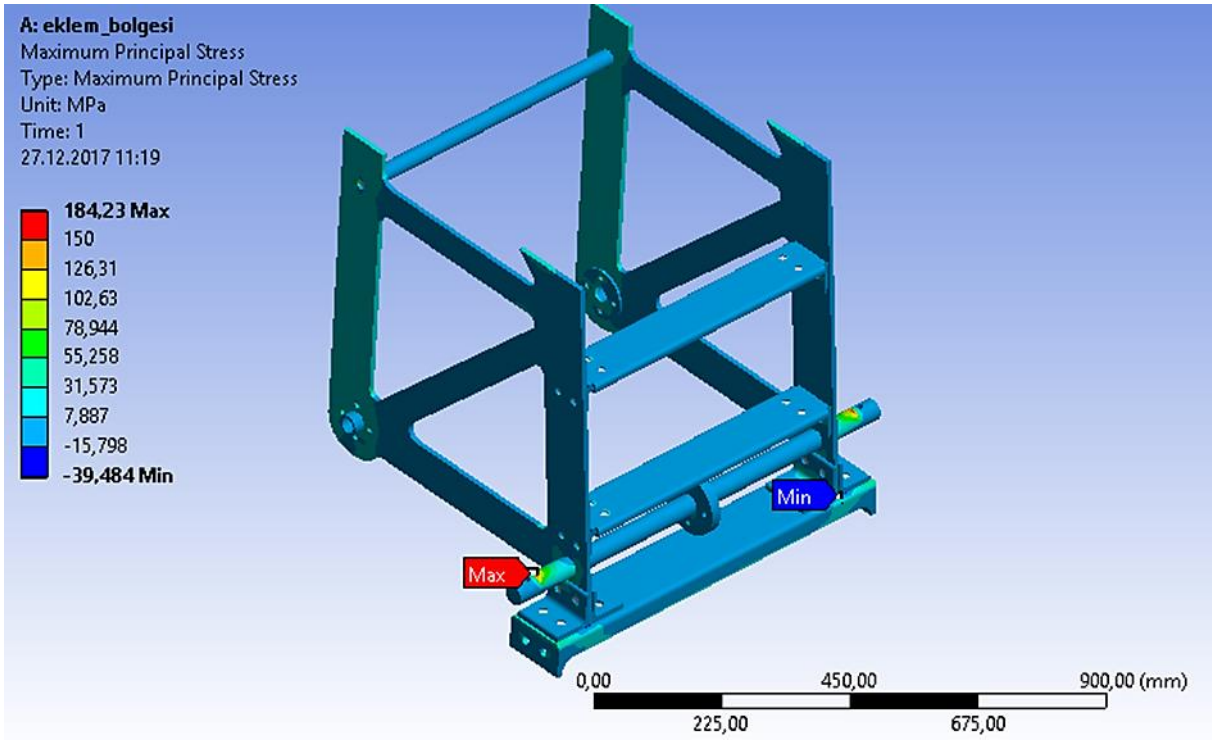
Figure 5.22: Max. principal stress results for joint section of the tower – 17 m
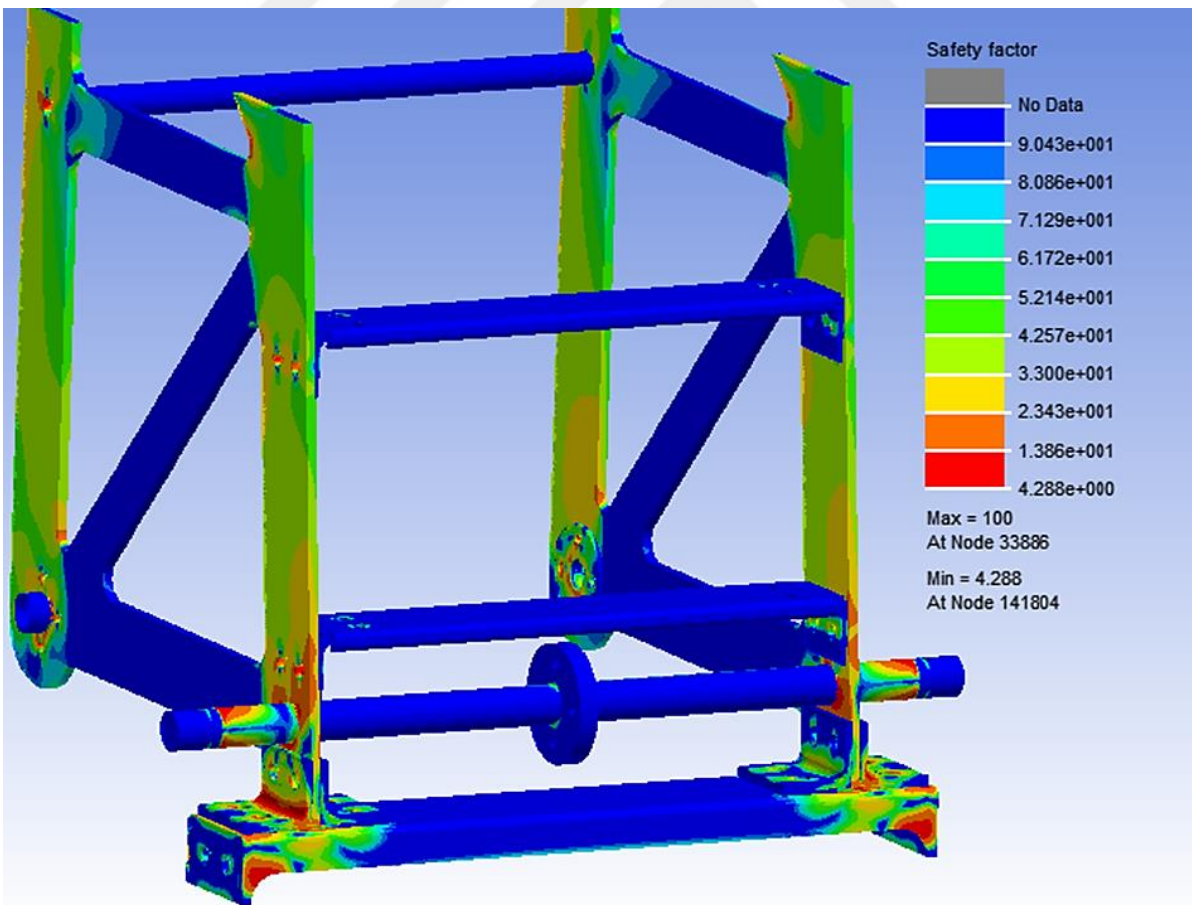
Figure 5.23: Fatigue SF analysis results for the joint section of the tower – 17 m

By the analysis of joint section of the tower, the maximum principal stress results are also presented above in **Figure 5.22**. According to the results, the highest stress per element under the maximum load is displayed as 184,23 MPa.

Finally, as the fatigue SF analysis results of the joint section are presented above in **Figure 5.23**, the min. value of SF is found as 4,29.

− Sheave section

The next CAE fatigue analysis was done for the sheave section of the tower, which includes a NPUx180 profile and two Lx100 profiles made of accordingly S275JR and S355 construction steels.

The maximum principal stress results are presented in the **Figure 5.24** below. The maximum stress under the maximum load is displayed as 124,5 MPa.
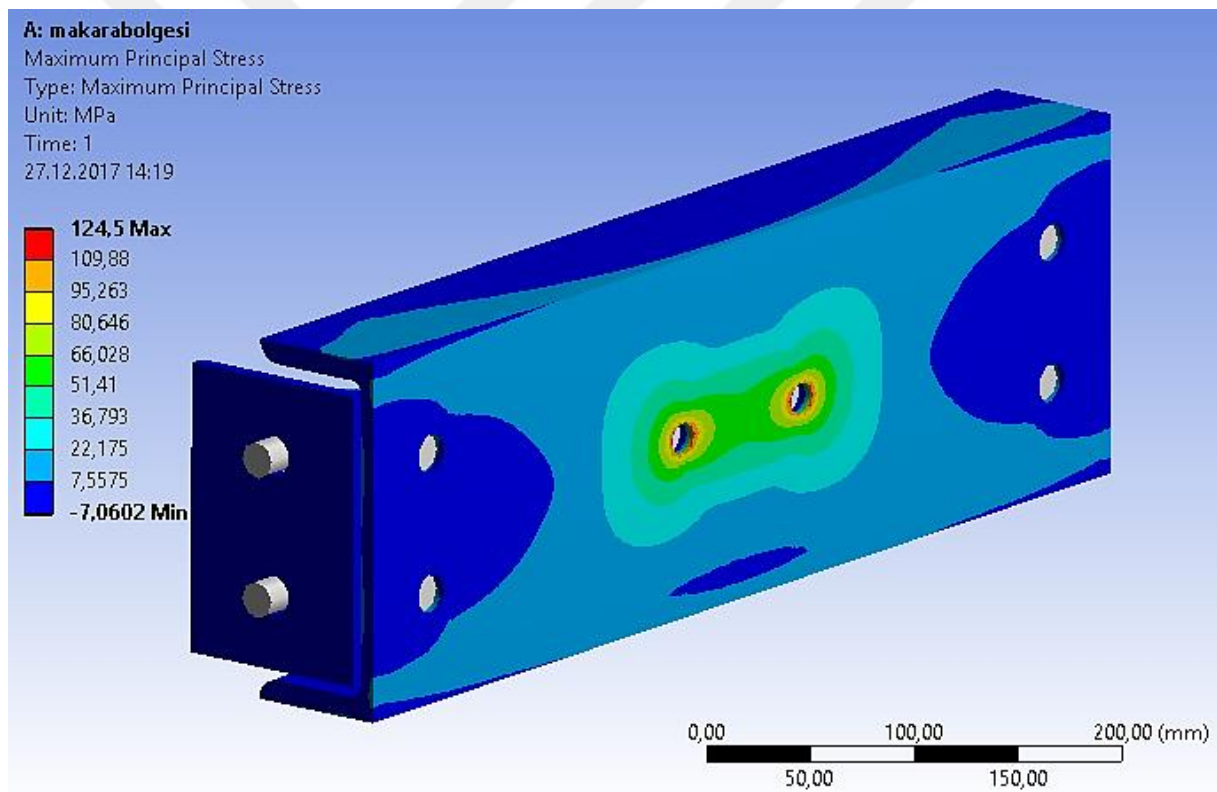
Figure 5.24: Max. principal stress result of sheave section of the tower – 17 m

After determining the maximum stress value, fatigue SF analysis was then utilized on nCode, with the results given below in **Figure 5.25**. According to the results, 3,87 is displayed as the min. SF value, depending on the unaveraged stress result from FEM analysis.
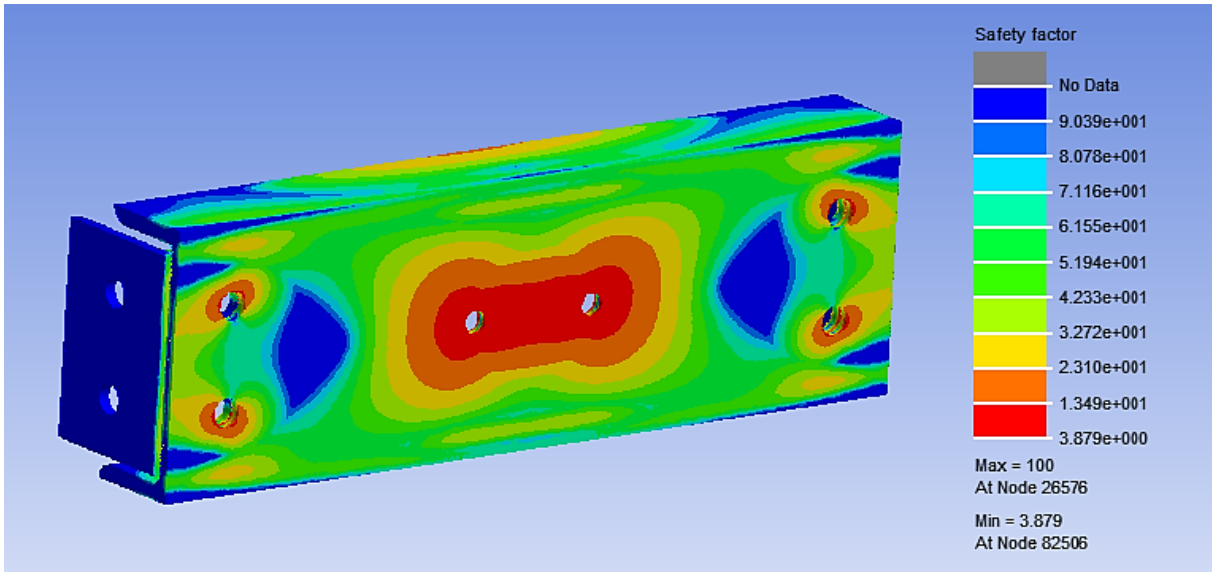
Figure 5.25: Fatigue SF analysis results for the sheave section of the tower – 17 m

– Crane section

The crane section of the tower, just as the sheave section, assembled by one NPU 180 and two L100 profiles made of accordingly S275JR and S355 construction steels, on which the rope crane is connected. The part must be resistant to fatigue, as it will undergo dynamic loads when the balloon is connected to the tower with a rope on this crane.
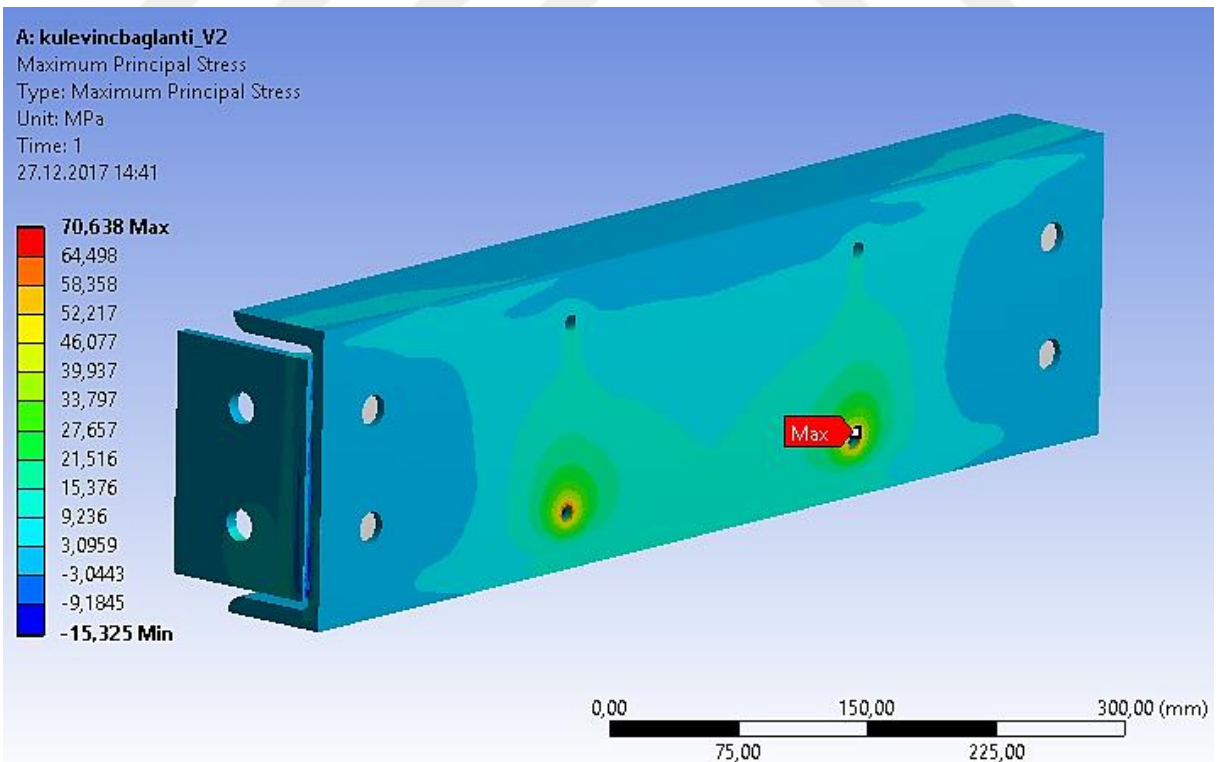
Figure 5.26: Max. principal stress result of crane section of the tower – 17 m

According to the maximum principal stress results from the static structural FEM analysis, given by **Figure 5.26** above, a stress value of 70,64 MPa is displayed the highest stress within elements under the maximum load.
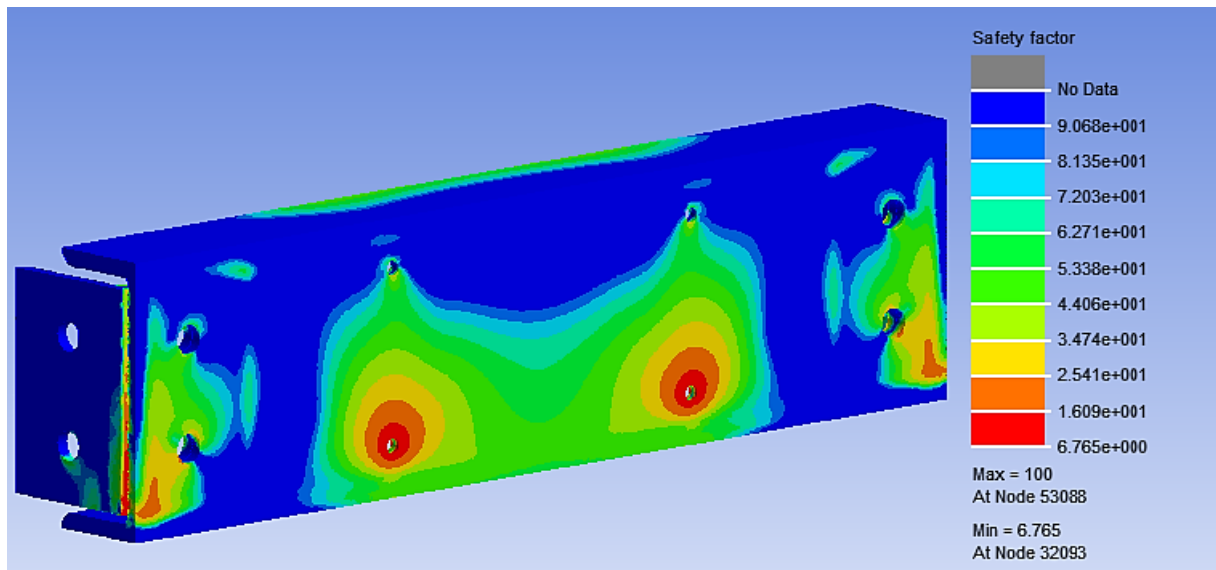
Figure 5.27: Fatigue SF analysis results for the crane section of the tower – 17 m

Depending on the fatigue SF analysis, presented in **Figure 5.27** above, the distribution of SF values within the structure can be seen. According to the results, the min. value of SF is chosen as 6,77.

5.3.3 Rope connection arm

Rope connection arms are assembled by 80x80 square profiles and L-profiles made of S235JR construction steel where the highest stresses are expected and additionally some steel plates made of S355JR.

Rope connection arm is one of the most important components in the mooring station design, since it undergoes dynamic loads when the balloon is connected by a rope on its crane during the maintenance on the ground level. The view of the component as well as the part, that has shown the highest maximum principal stress, can be seen in the below **Figure 5.3**

According to the maximum principal stress results from the static structural FEM analysis, given by the **Figure 5.28** below, a maximum stress value of 123 MPa is displayed depending on the maximum stress solution within elements under the maximum load. The results of the fatigue SF analysis, besides, can also be seen below in **Figure 5.29**, by the distribution of values within the structure.
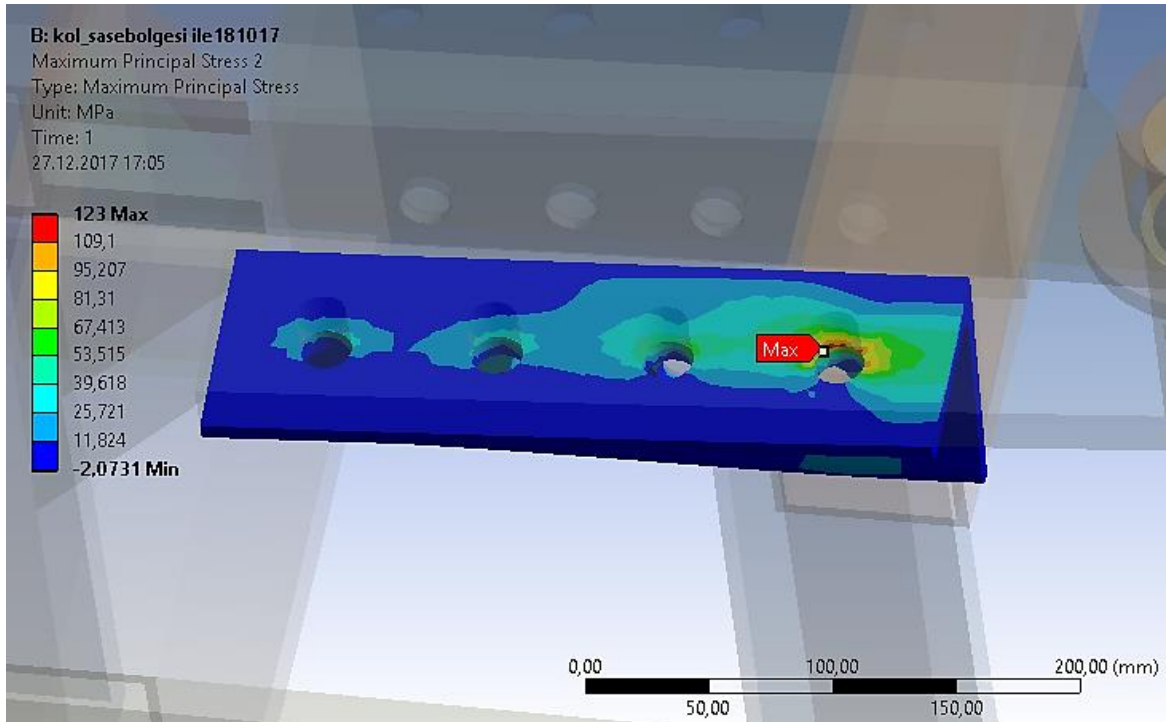
Figure 5.28: Maximum principal stress solution within elements, rope connection arm – 17 m
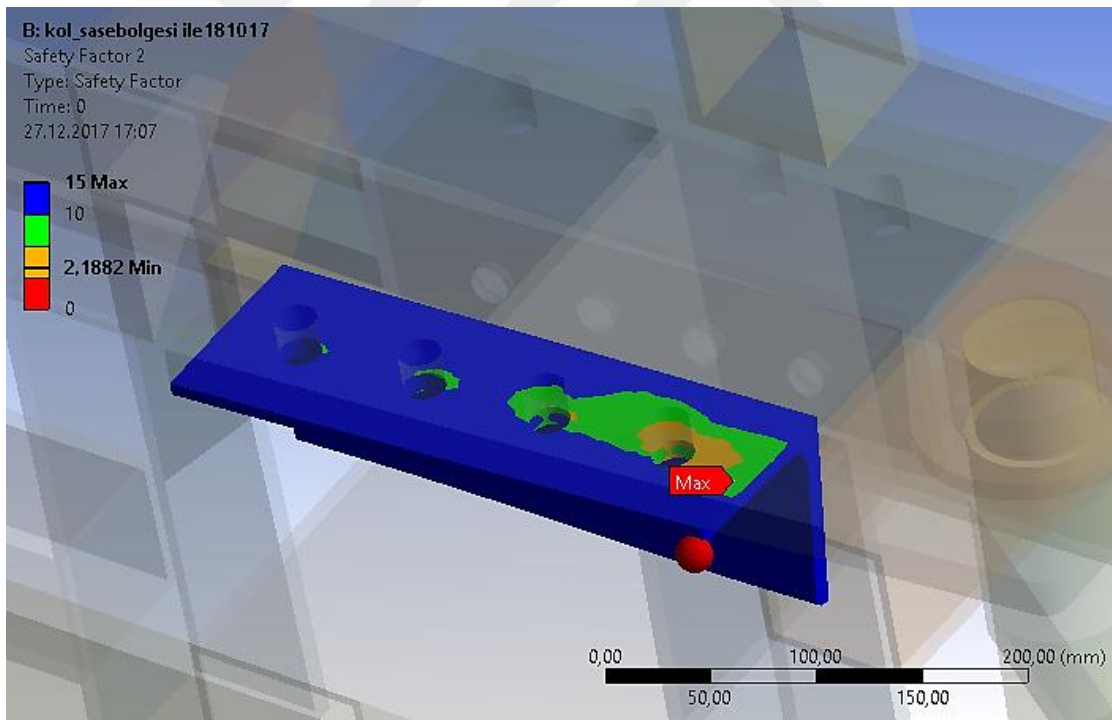
Figure 5.29: Fatigue SF analysis results for the rope connection arm – 17 m

In **Figure 5.29** above, which represents SF values within the structure which have shown the most critical values, the value of 2,19 is determined as the min. SF in the structure.

6 Analytical prediction of the fatigue behaviours

In this section, analytically created S-N curves, which are specifically generated for the components in the new mooring station of 17 m balloon which are tower components, flying sheave and the rope connection arm, are presented. The generated curves are used to verify the results found by CAE – fatigue analysis, before any fatigue tests, in order to decide if the CAE – fatigue analyses are reliable. For generating the curves, former researches on the used materials or generally on the fatigue technology were used.

6.1 Principles

After determination of the material related constants of the Basquin equation, already presented by **Equation 4.1**, fatigue strength coefficient and fatigue strength exponent, which are shown in **Section 4.2**, stress amplitudes per cycles to failures (Nf) up to 10^{10} are found. Depending on these data, curves are generated. The curves are then modified by mean stress corrections (MSC) and surface retention factors (SRF) (which are explained in detail in **Section 4.3**).

The maximum and minimum stresses, stress amplitudes and the mean stresses of the life curves are calculated depending on the point where the highest unaveraged maximum principal stress occurs on the component, found by the FEM analysis.

As given in the state of the art section, there are three major MSC methods used in life curve generations as Goodman, Gerber and Soderberg. Also known, most of the experimental fatigue data fall between Goodman and Gerber curves where Soderberg is too conservative and not too much realistic. To generate S-N curves for mooring station components of 17 m balloon, therefore, Goodman method is preferred over the others, since Goodman generates more conservative curves than Gerber, which is a better aspect for a fatigue-resistant therefore safe design work, while most of the experimental data lie between Goodman and Gerber.

Beside of the generated curves, the fatigue limits of the components made of steel are also calculated by three different fatigue limit calculation methods for steels, **Equations 2.15** and **2.16** for steels in gigacycle regimes, FLE1 and FLE2, and 0,45 x UTS condition for axial cyclic loading, depending on the graph shown in **Figure 2.15**.

6.2 Flying sheave

Beside of the CAE – fatigue analysis, life curves were also generated for the flying sheave of the mooring station of 17 m balloon, as presented in **Figure 6.1** below. By the calculation of

analytic data, presented in **Table 6.1**, the curves are generated according to three different mean stress correction methods with and without SRF correction.

The mean stress (σ_m) and stress amplitude (σ_a) values are calculated depending on the maximum principal stress results by FEM static structural analysis as shown in **Table 6.1** below.

Table 6.1: Cyclic loading parameters of the flying sheave – 17 m

Max Load, N	Min Load, N	σ_{max}, MPa	σ_{min}, MPa	σ_a, MPa	σ_m, MPa	R
5308,00	3006,00	52,02	29,65	11,18	40,84	0,61

Table 6.2: Stress – Life data of flying sheave – 17 m, with and without MSC and SRF

		Max. allowable stress amplitude, MPa					
		MSC			MSC – SRF (0,8)		
Log Nf	Basquin	Goodman	Gerber	Soderberg	Goodman	Gerber	Soderberg
0	653,35	562,60	640,74	449,68	450,08	512,59	359,75
1	493,34	424,81	483,82	339,55	339,85	387,06	271,64
2	372,52	320,77	365,33	256,39	256,62	292,26	205,11
3	281,28	242,21	275,86	193,60	193,77	220,69	154,88
4	212,39	182,89	208,30	146,19	146,32	166,64	116,95
5	160,38	138,10	157,28	110,38	110,48	125,83	88,31
6	121,10	104,28	118,76	83,35	83,42	95,01	66,68
7	91,44	78,74	89,68	62,94	62,99	71,74	50,35
8	69,05	59,46	67,71	47,52	47,57	54,17	38,02
9	52,14	44,90	51,13	35,88	35,92	40,90	28,71
10	39,37	33,90	38,61	27,10	27,12	30,89	21,68
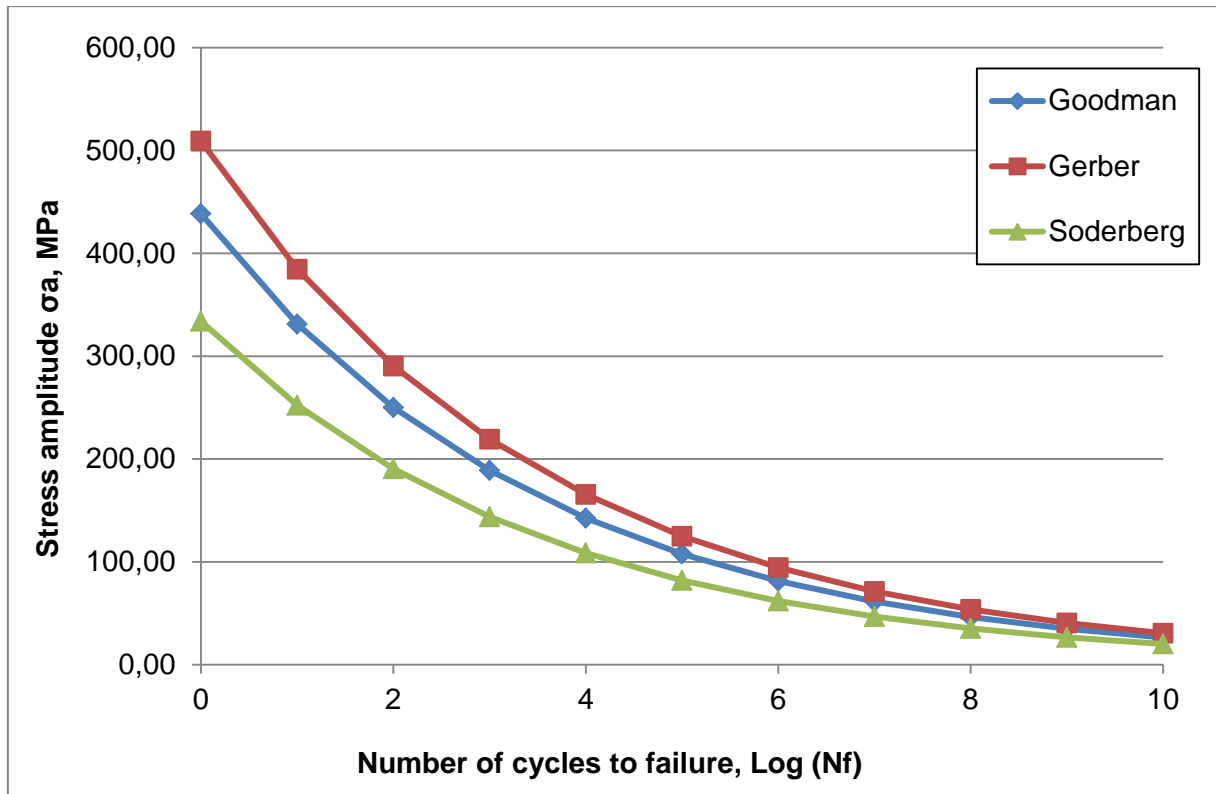
Figure 6.1: Stress – life curve of flying sheave – 17m according to three MSC methods

According to the calculated life curves data and corresponding fatigue limits at 10^9 cycles to failure, the analytical SF values are found as in given in the **Table 6.3** below. While the fatigue SF according to fatigue limit at 10^9 cycles to faiure of Goodman and SRF corrected curve is obtained as 2,7, the SF according to the Gerber and Soderberg corrected curves are found accordingly as 3,14 and 2,06.

Table 6.3: SFs depending on three different MSC methods

Goodman	Gerber	Soderberg
3,21	3,66	2,57

6.3 Tower

Beside of the CAE – fatigue analysis, life curves were also generated for the three main tower sections of the mooring station of 17 m balloon, which are joint, sheave and crane sections, as presented in **Figure 6.5 Figure 6.3, Figure 6.4** below. By the calculation of analytic data, given accordingly in **Table 6.5**, **Table 6.8**, **Table 6.11** the curves are generated according to the three different mean stress correction methods, Goodman, Gerber and Soderberg with and without SRF corrections.

The mean stress (σ_m) and stress amplitude (σ_a) values are calculated depending on the maximum principal stress results by FEM static structural analysis as shown accordingly in **Table 6.4**, **Table 6.7**, Table **6.10** below.

– Joint section

Table 6.4: Cyclic loading parameters of the tower joint section – 17 m

Max Load, N	Min Load, N	σ_{max}, MPa	σ_{min}, MPa	σ_a, MPa	σ_m, MPa
5308,00	3006	184,23	105,01	39,61	144,62

Table 6.5: Stress – Life data of the tower joint section – 17 m, with and without MSC and SRF

		Max allow. stress amplitude, MPa					
		MSC			MSC – SRF (0,9)		
Log Nf	Basquin	Goodman	Gerber	Soderberg	Goodman	Gerber	Soderberg
0	1237,59	1013,86	1197,14	939,29	912,47	1077,43	845,36
1	1005,95	824,10	973,07	763,48	741,69	875,77	687,13
2	817,67	669,85	790,94	620,58	602,87	711,85	558,52
3	664,62	544,48	642,90	504,43	490,03	578,61	453,98
4	540,23	442,57	522,57	410,01	398,31	470,31	369,01
5	439,11	359,73	424,76	333,27	323,76	382,29	299,94
6	356,92	292,40	345,26	270,89	263,16	310,73	243,80
7	290,12	237,67	280,64	220,19	213,90	252,57	198,17
8	235,82	193,19	228,11	178,98	173,87	205,30	161,08
9	191,68	157,03	185,42	145,48	141,33	166,87	130,93
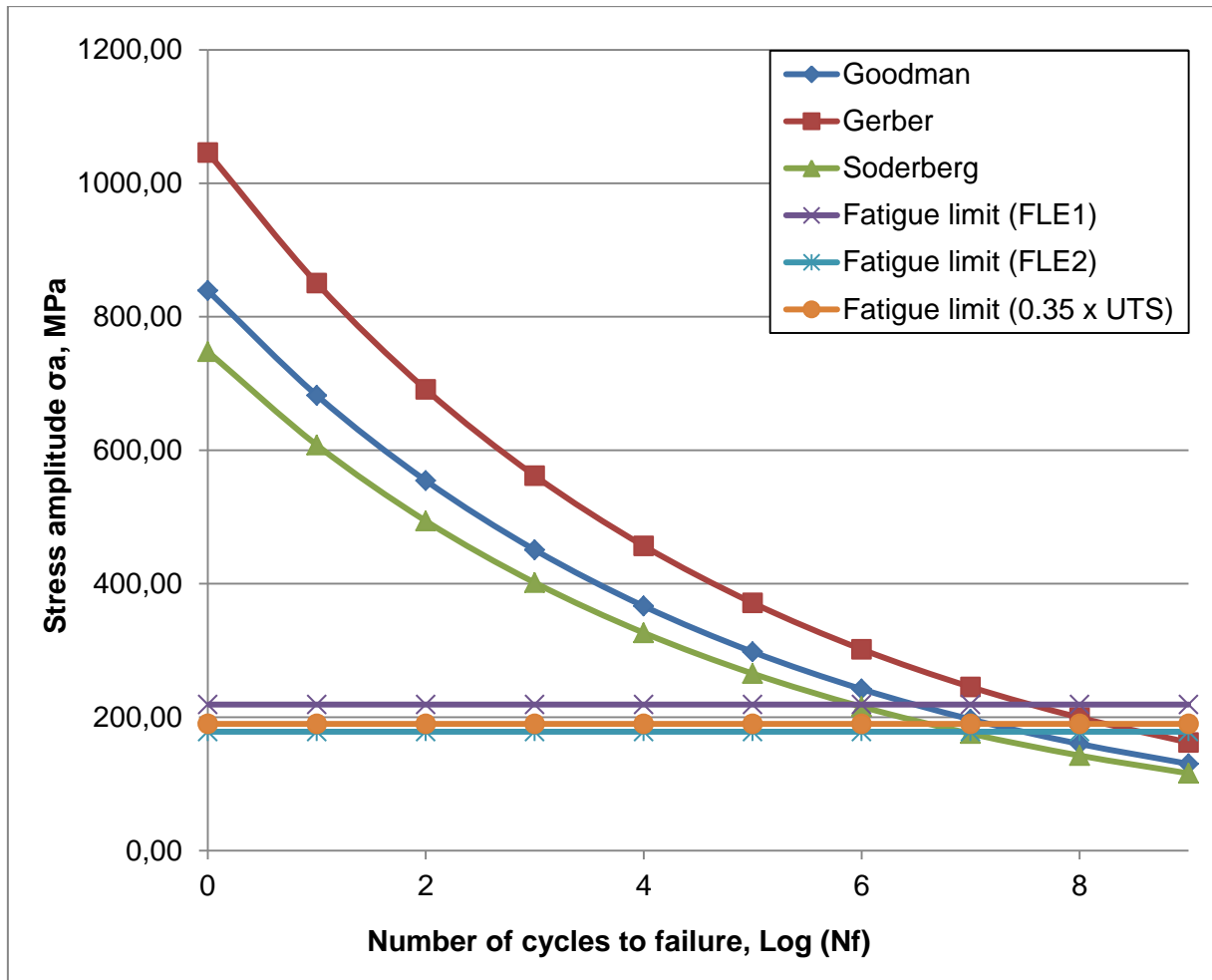
Figure 6.2: Stress – life curves and fatigue limits of the tower joint section – 17 m, according to varying methods

According to the calculated life curves data and corresponding fatigue limits at 10^6 cycles to failure, alternative analytical SF values of the tower joint section are found as in given in the **Table 6.12** below. While the fatigue SF according to fatigue limit at 10^6 cycles to failure of Goodman and SRF corrected curve is obtained as 2,35, according to the two different analytical fatigue limit equations (FLE) for steels at gigacycles it is found accordingly as 3,14 and 2,06, and depending on 0,45 x UTS method found as 2,38.

Table 6.6: Fatigue limits and SFs of tower joint section – 17 m, according to varying methods

|	Goodman Nf 10^6, SRF 0,7	FLE1	FLE2	0,45 x UTS
Fatigue limit, MPa	263,16	238,02	193,72	265,43
SF	6,64	6,01	4,89	6,70

–   Sheave section

Table 6.7: Cyclic loading parameters of the tower sheave section – 17 m

Max. Load, N	Min. Load, N	σ_{max}, MPa	σ_{min}, MPa	σ_a, MPa	σ_m, MPa
5308,00	3006,00	124,50	70,97	26,77	97,73

Table 6.8: Stress – life data of the tower sheave section – 17 m, with and without MSC and SRF

		Max allow. stress amplitude, MPa					
		MSC			MSC – SRF (0,7)		
Log Nf	Basquin	Goodman	Gerber	Soderberg	Goodman	Gerber	Soderberg
0	810,34	647,05	777,43	522,35	452,93	544,20	365,65
1	658,67	525,94	631,92	424,58	368,16	442,35	297,21
2	535,39	427,50	513,65	345,11	299,25	359,55	241,58
3	435,18	347,48	417,51	280,52	243,24	292,25	196,36
4	353,73	282,45	339,36	228,01	197,71	237,55	159,61
5	287,52	229,58	275,84	185,34	160,71	193,09	129,74
6	233,70	186,61	224,21	150,65	130,63	156,95	105,45
7	189,96	151,68	182,25	122,45	106,18	127,57	85,72
8	154,41	123,29	148,14	99,53	86,30	103,70	69,67
9	125,51	100,22	120,41	80,90	70,15	84,29	56,63
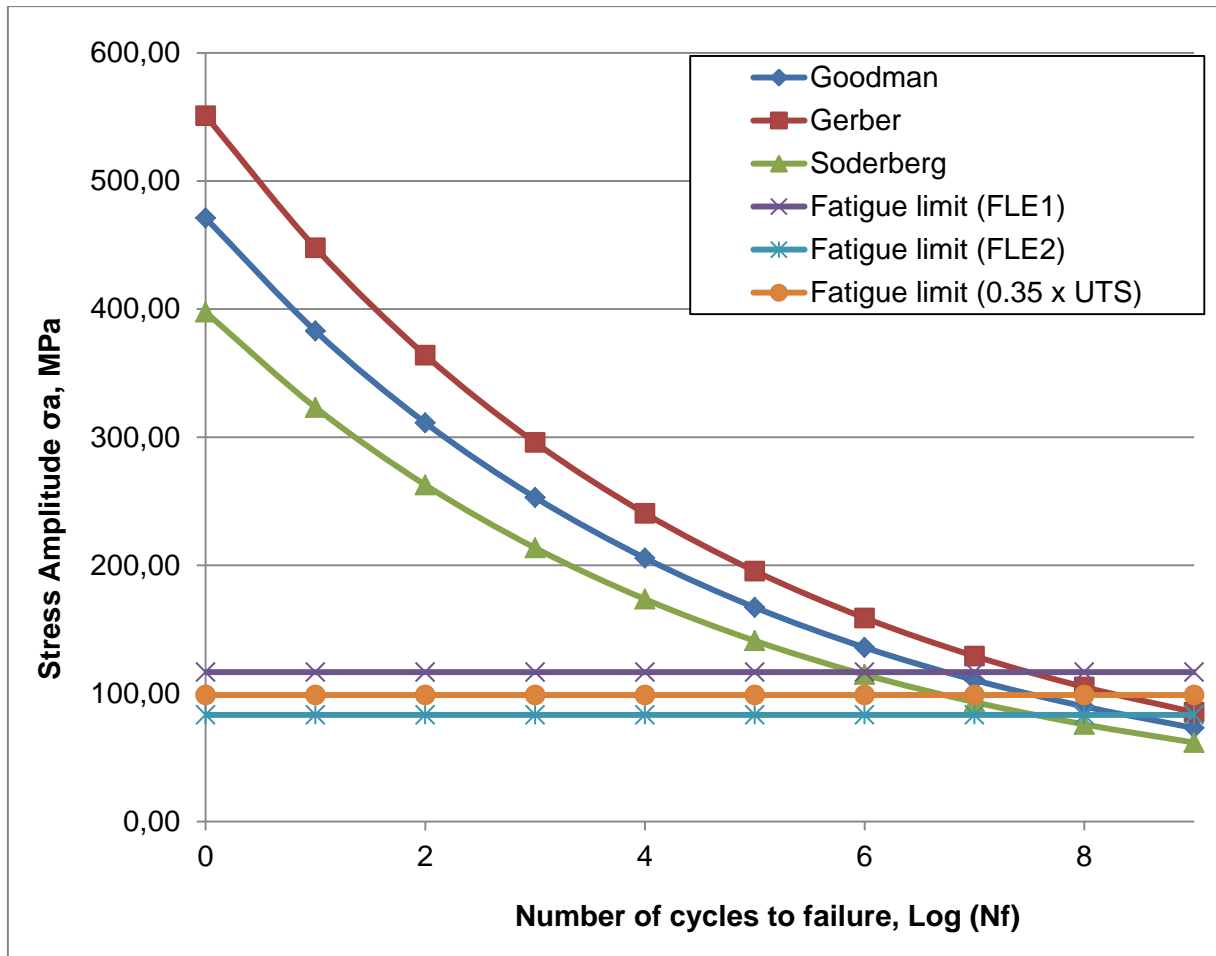
Figure 6.3: Stress – life curves and fatigue limits of the tower sheave section – 17 m, according to varying methods

According to the calculated life curves data and corresponding fatigue limits at 10^6 cycles to failure, alternative analytical SF values of the tower sheave section are found as in given in the **Table 6.9** below. While the fatigue SF according to fatigue limit at 10^6 cycles to failure of Goodman and SRF corrected curve is obtained as 3,17, it is obtained according to the two different analytical fatigue limit equations (FLE) for steels at gigacycles found accordingly as 2,72 and 1,94, and depending on 0,45 x UTS method found as 2,96.

Table 6.9: Fatigue limits and SFs of the tower sheave section – 17 m according to varying methods

	Goodman Nf 10^6, SRF 0,7	FLE1	FLE2	0,45 x UTS
Fatigue limit, MPa	130,63	112,12	79,99	121,99
SF	4,88	4,19	2,99	4,56

– Crane section

Table 6.10: Cyclic loading parameters of the tower crane section – 17 m

Max Load, N	Min Load, N	σ_{max}, MPa	σ_{min}, MPa	σ_a, MPa	σ_m, MPa
5308,00	3006,00	70,64	40,26	15,19	55,45

Table 6.11: Stress – Life data of the tower crane section – 17 m, with and without MSC and SRF

		Max allow. stress amplitude, MPa					
		MSC			SRF (0,9)		
Log Nf	Basquin	Goodman	Gerber	Soderberg	Goodman	Gerber	Soderberg
0	810,34	717,69	799,75	646,94	502,38	559,82	452,86
1	658,67	583,36	650,06	525,85	408,35	455,04	368,10
2	535,39	474,17	528,39	427,43	331,92	369,87	299,20
3	435,18	385,42	429,49	347,43	269,80	300,64	243,20
4	353,73	313,28	349,10	282,40	219,30	244,37	197,68
5	287,52	254,65	283,76	229,54	178,25	198,63	160,68
6	233,70	206,98	230,65	186,58	144,89	161,45	130,61
7	189,96	168,24	187,48	151,66	117,77	131,24	106,16
8	154,41	136,75	152,39	123,27	95,73	106,67	86,29
9	125,51	111,16	123,87	100,20	77,81	86,71	70,14
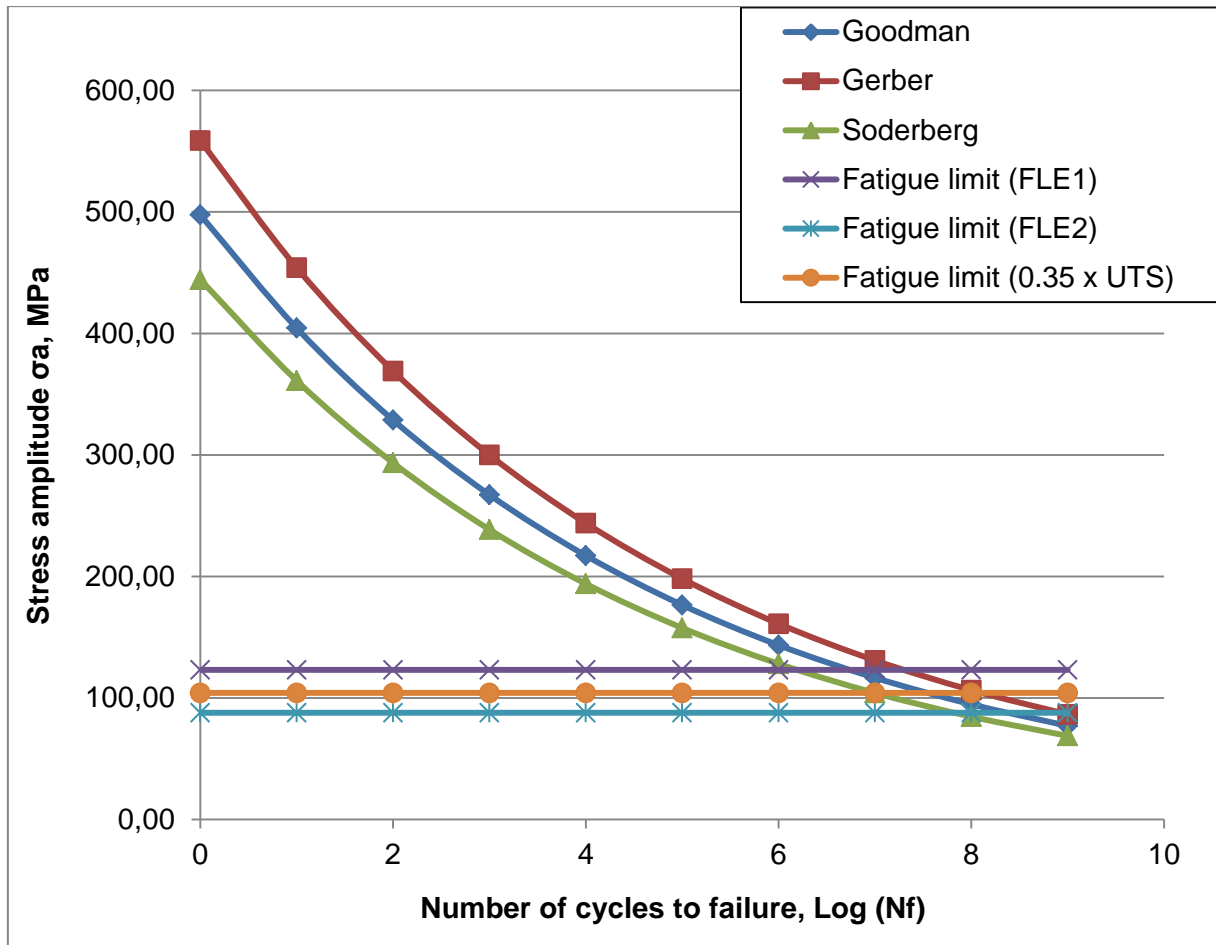
Figure 6.4: Stress – life curves and fatigue limits of the tower crane section – 17 m, according to varying methods

According to the calculated life curves data and corresponding fatigue limits at 10^6 cycles to failure, alternative analytical SF values of the tower crane section are found as in given in the **Table 6.12** below. While the fatigue SF according to fatigue limit at 10^6 Nf of Goodman and SRF corrected curve is obtained as 8,79, it is obtained according to the two different analytical fatigue limit equations for steels at gigacycles as 7,55 and 5,38 and depending on 0,45 x UTS method as 8,21.

Table 6.12: Fatigue limits and SFs of the tower crane section – 17 m according to varying methods

	Goodman Nf 10^6, SRF 0,7	FLE1	FLE2	0,45 x UTS
Fatigue limit, MPa	144,89	124,36	88,72	135,31
SF	9,54	8,19	5,84	8,91

6.4 Rope connection arm

Table 6.13: Cyclic loading parameters of the rope connection arm – 17 m

Max Load, N	Min Load, N	σ_{max}, MPa	σ_{min}, MPa	σ_a, MPa	σ_m, MPa
5308,00	3006,00	70,64	40,26	15,19	55,45

Table 6.14: Stress – life data of the rope connection arm – 17 m, with and without MSC and SRF

		Max allow. stress amplitude, MPa					
		MSC			Surface retention factor (0,7)		
Log Nf	Basquin	Goodman	Gerber	Soderberg	Goodman	Gerber	Soderberg
0	726,49	717,69	799,75	646,94	502,38	559,82	452,86
1	590,51	583,36	650,06	525,85	408,35	455,04	368,10
2	479,98	474,17	528,39	427,43	331,92	369,87	299,20
3	390,15	385,42	429,49	347,43	269,80	300,64	243,20
4	317,12	313,28	349,10	282,40	219,30	244,37	197,68
5	257,77	254,65	283,76	229,54	178,25	198,63	160,68
6	209,52	206,98	230,65	186,58	144,89	161,45	130,61
7	170,30	168,24	187,48	151,66	117,77	131,24	106,16
8	138,43	136,75	152,39	123,27	95,73	106,67	86,29
9	112,52	111,16	123,87	100,20	77,81	86,71	70,14
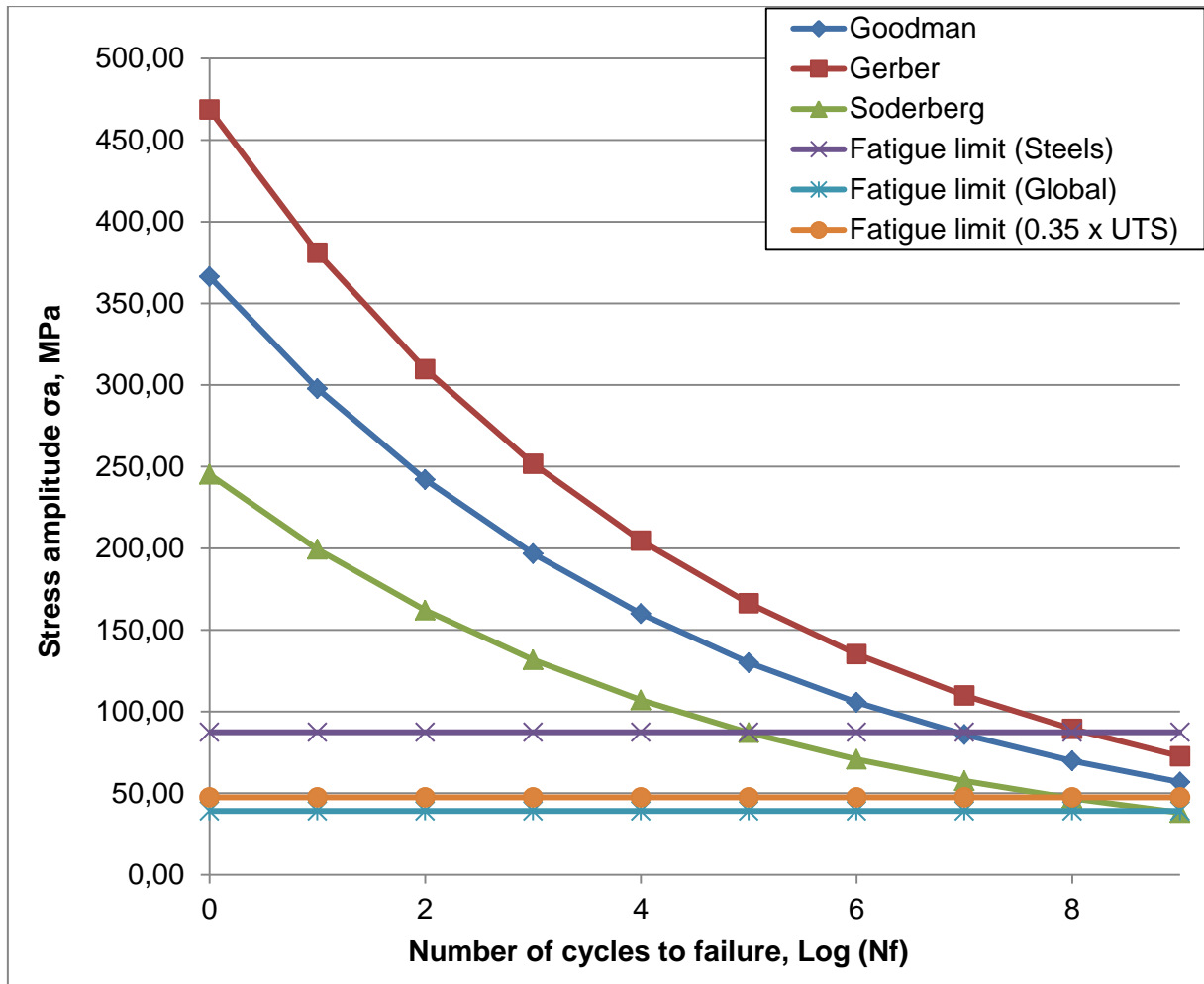
Figure 6.5: Stress – life curves and fatigue limits of the rope connection arm – 17 m, according to varying methods

According to the calculated life curves data and corresponding fatigue limits at 10^6 cycles to failure, the analytical SF values are found as in given in the **Table 6.15** below. While the fatigue SF according to fatigue limit at 10^6 Nf of Goodman and SRF corrected curve is obtained as 3,79, it is found according to the two different analytical fatigue limit equations for steels at gigacycles accordingly as 3,22 and 2,75 and according to 0,45 x UTS as 3,54.

Table 6.15: Fatigue limits and SFs of the rope connection arm – 17 m, according to varying methods

	Goodman Nf 10^6, SRF 0,7	FLE1	FLE2	0,45 x UTS
Fatigue limit, MPa	144,89	124,36	88,72	135,31
SF	9,54	8,19	5,84	8,91

7 Cylic loading tests

In the last stage of the thesis project, two mooring station components of 17 m balloon, the tower crane and the flying sheave were tested under the maximum possible cyclic loading, which was already determined during the analysis section. These cyclic loading tests are planned as service test of the components, but not fatigue tests which are used to determine a material's fatigue behaviour by creating fatigue fractures on the specimens in varying stress amplitudes. The test is used to verify component behaviour against fatigue under the maximum possible loading within the planned service life. It is expected to obtain from the test results, basically, if the products will function in the given life under the maximum possible dynamic loading (the worst case) without any failure, and therefore if the results found by analytical and CAE methods are reliable.

As attached to a test machine with a steel rope and to the ground with a specific component platform, which was also manufactured for the aim of the thesis work, tests for these two components were completed. The reason of choosing the components tower crane and flying sheave for the cyclic loading tests is that, the main parameter within CAE and analytical fatigue analyses, and also the main difference between them, was actually the materials and the determined mechanical properties. Therefore, one component, made of steel, and one component made of aluminium were chosen in order to see the effect of material difference onto fatigue behaviour of the components.

7.1 Test specifications

A cyclic loading range of 5308 N to 3000 N was used within the component tests, which was found by the maximum possible dynamic load calculations for 17 m aerostat in the **Section 4.1**. On the other hand, the load was applied in the most correct position, how exactly components will be affected during the service.

Since the fatigue limit of the components made of steel is accepted as the fatigue strength at 10^6 life cycles in the HCF region, the tests were planned to be conducted for 10^6 life cycles. The frequency parameter used in the cyclic loading tests was taken according to the maximum available speed of the testing device in the facility, working with a linear movable screw, is capable of applying frequencies between 0,25 and 1 Hz, and therefore not frequently used for fatigue tests for specimens with high frequencies up to 20 Hz but for component service tests. From the demo tests of the test setup, it is observed that the machine can apply the required cyclic loading case on the components with a frequency value of 0,7 – 0,8 Hz at its maximum. By looking to the **Figure 2.18**, as any frequencies between 0,2 and 2 Hz will not affect the results of fatigue tests seriously [Gue13], a

frequency value 0,75 Hz within the cyclic load tests is aimed, even though the calculated maximum frequency, caused by winds, which the mooring station will be affected in service, was 0,25 Hz.

7.2   Test setup

The test setup with the test machine, and other units can be seen in the below **Figure 7.2** and **Figure 7.3** from different angles. The test machine, movable screw, is attached to the load cell and steel rope. The load is applied onto the component, which is connected to the component platform, by the steel rope. The test machine is controlled by a Raspberry card which reads load values created by the load cell simultaneously and then controls the machine. Also, a temperature sensor obtains the temperature of a specific region on the component during the tests.

7.2.1   Test device

The cyclic loading during the tests was applied onto the components, which were connected to ground with a test platform, by a linear movable screw device with the specs below:

- − Tr 40x7 Screw
- − Stroke length: 500 mm
- − Screw material: AISI 1040 Steel
- − Gear material: Bronze
- − Max. Load: 25 kN
- − Reduction ratio: 1/6
- − Service position: Horizontal
- − Drive: DC
- − Input rotation: 100 RPM
- − Feeding speed: 110 mm/dk
- − Engine reducer: 0,75 kW, EV50 reducer
- − Reducer out: 100 RPM

A load cell is attached to the movable screw in order to read the load value, and it is attached to the steel ropes via a carabiner, which can function under loads up to 20 kN.
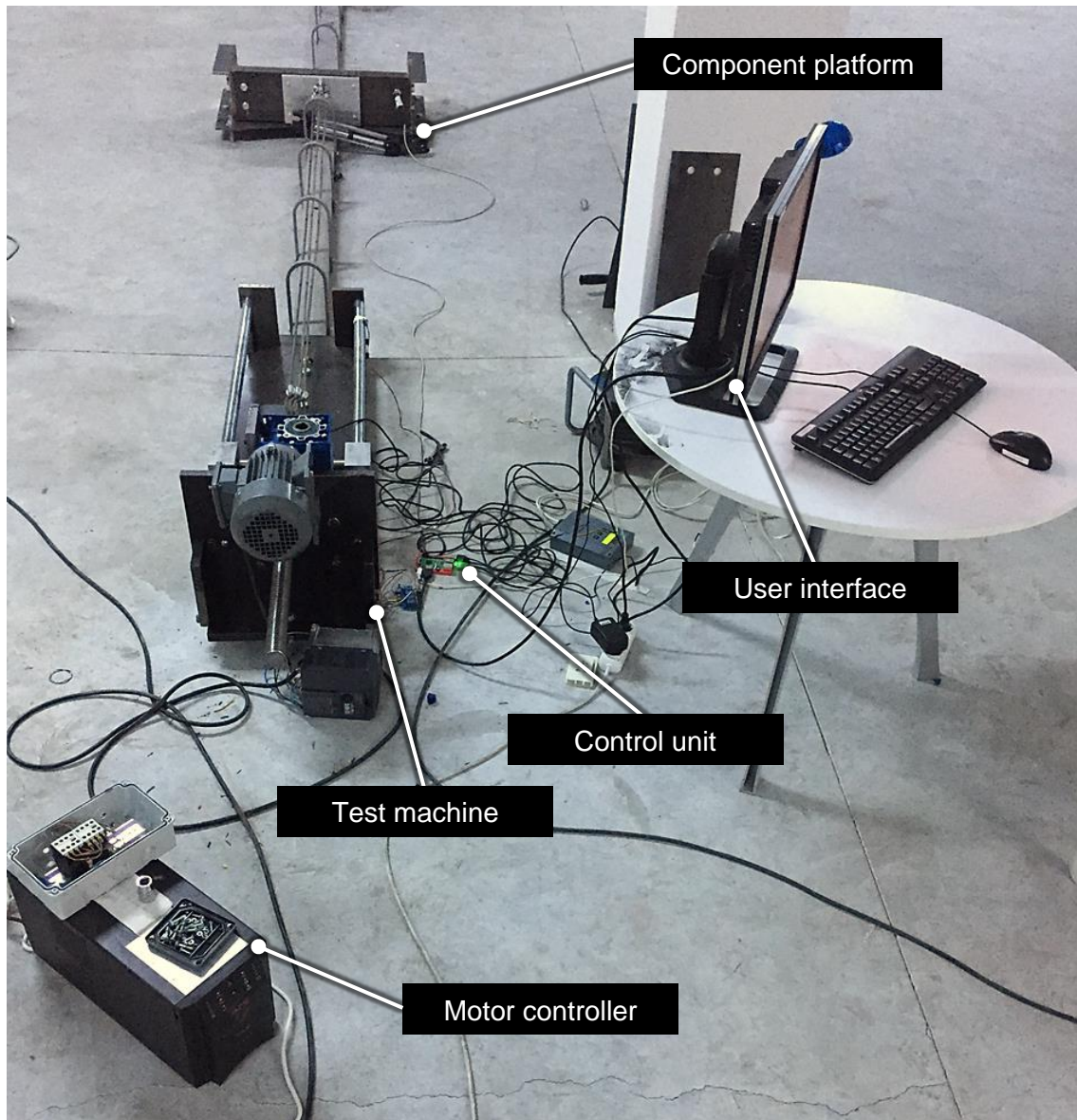
Figure 7.1: Test platform view from above

7.2.2 Control unit

As seen next to the movable screw device in below **Figure 7.2**, a Raspberry card with the 5 N of control sensitivity is used to control the movable screw, by reading the load data from load cell and also the data from temperature sensor during the cyclic loading tests up to 10^5 life cycles. The test parameters, maximum and minimum load values, are logged into the Raspberry card in Newton, via a computer interface, which is specifically built for the aim of the tests. The card applies then cyclic loading onto the test machine.

During the tests, all the cycles, seconds and load values were no able to be logged due to the too high amount of cycle lines, however the load cycles were simultaneously controlled via temporary log data on the raspberry card. Temperature values are also simultaneously monitored to determine daily environment temperature change and any dramatic

temperature increase within the component. Any rapid temperature change within the component is of the great importance, since it is a sign of fatigue growth or failure, while a great temperature change of the test environment will affect quality of the tests.
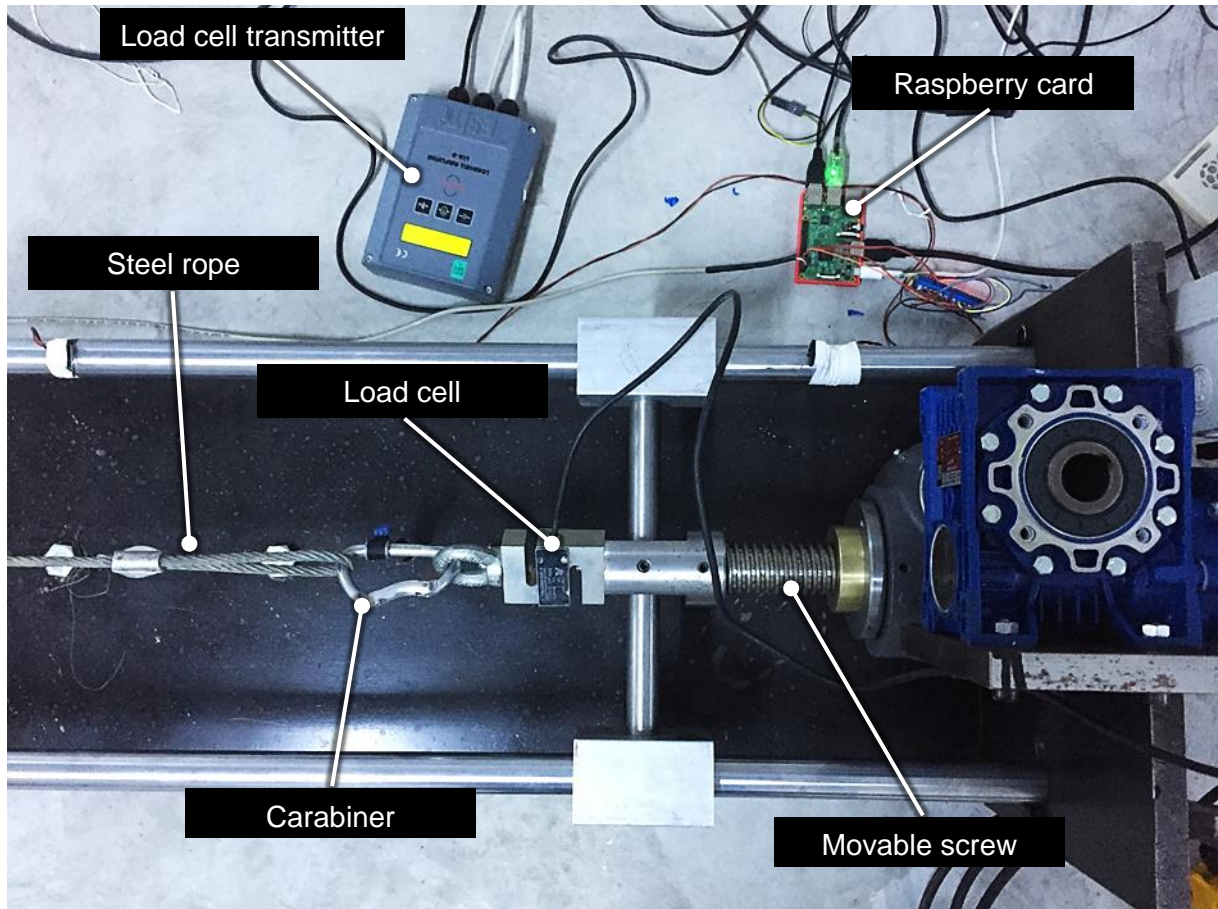
Figure 7.2: Test setup top view

7.2.3 Component platform

To be able to apply cyclic loading onto the components, a common ground connection platform and workpiece holder parts for each component were first designed and manufactured, and were connected to the ground by bolts and nuts. The component platform is built by NPU 180 profiles made of S275 steel, L x 100 profiles made of S355JR and a 8 mm steel plate made of S355. The parts are specifically joined by bolts and nuts and spring lock washers for the usage under dynamic loading. As well as, the steel ropes are attached to the components by these M8 eyebolts, nuts and spring lock washers. For the complete component platform, presented in the **Figure 7.3** below, CAE – Static structural and fatigue analyses were also made, as it will be used for cyclic loading tests of the mooring station components. The platform itself therefore must be even tougher and resistant to dynamic loads more than the tested components. Moreover, the platform is designed in a way that all the parts can be tested in the same loading direction.
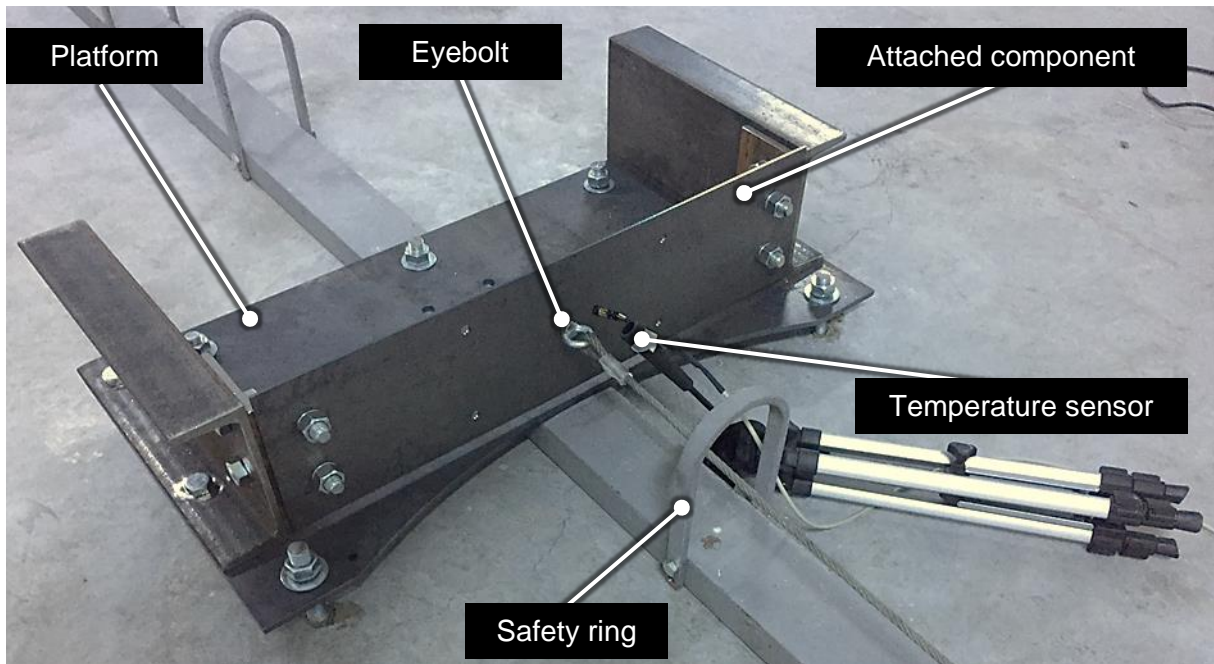
Figure 7.3: Component platform

As also seen in the **Figure 7.3**, an infrared temperature sensor is placed on the platform, to be able to monitor temperature within region of the component where the highest stress is expected, to be able to do a fatigue inspection by thermoelasticity effect [Nis12].

Another equipment of the platform is the safety rings, which were placed on the route of the steel rope by 50 cm gaps in order to protect test attendants as well as other machine and equipment in the environment from a possible fracture risk of the loaded steel rope during the cyclic load tests.

Figure 7.4: Closer view of steel rope attachment and temperature sensor

Beside of the main holders and equipment, a special workpiece holder made of Al 5083 plate, presented below in **Figure 7.5**, was also produced for the flying sheave tests and a FEM static structural analysis was also completed for this test equipment. The static structural FEM analysis of the component platform, test machine and other equipment were completed by ANSYS, and depending on the results the reliability of the parts were discussed. The maximum stress generated on the parts under the maximum load is compared with the maximum principal stress result of the mooring station components, to decide whether the test equipment is appropriate for the cyclic loading tests.
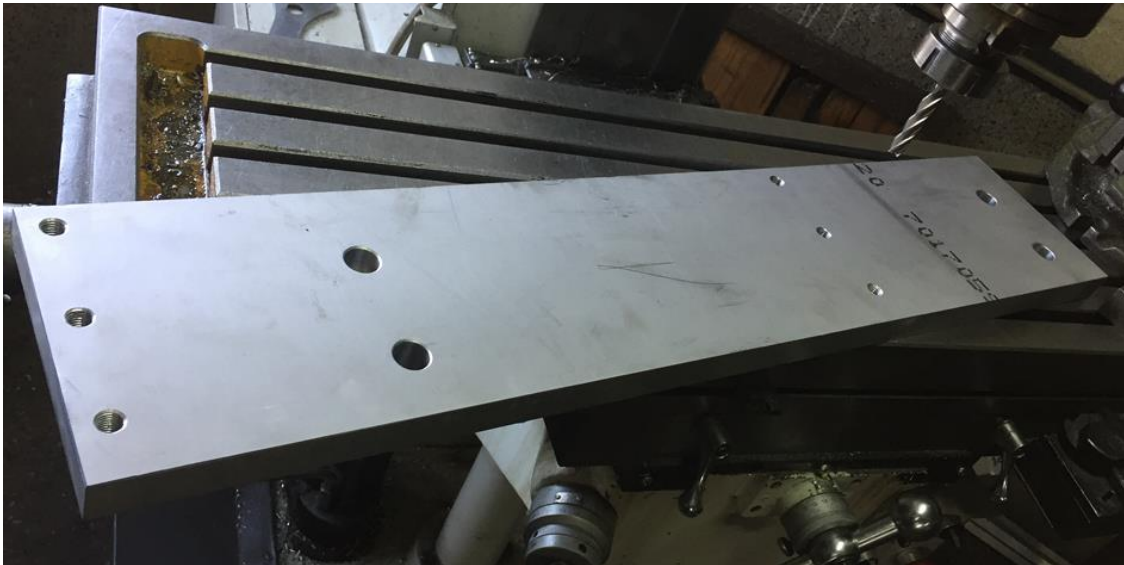
Figure 7.5: Flying sheave holder
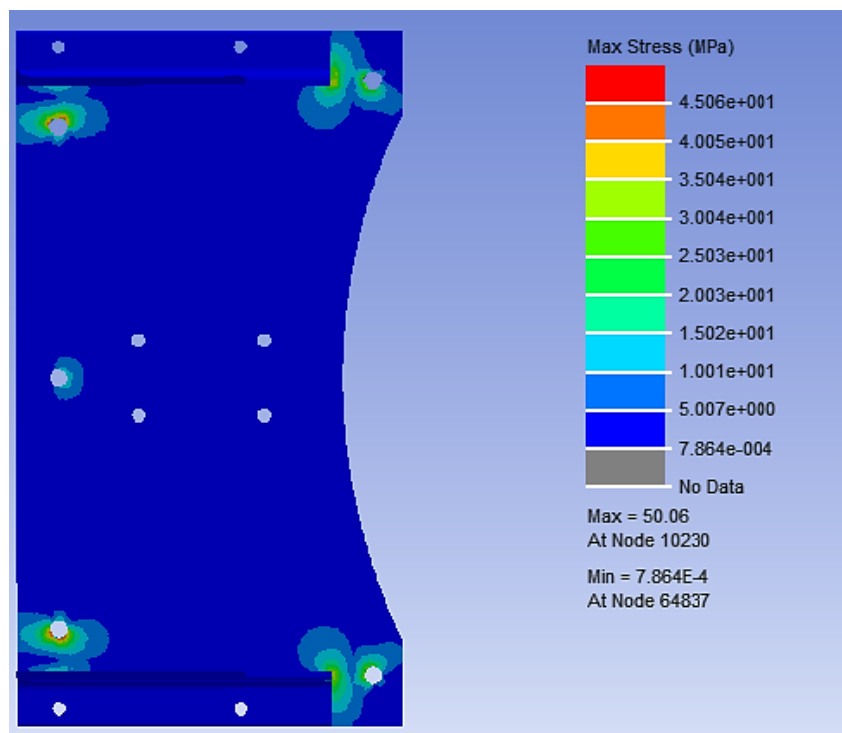
Figure 7.6: FEM static structural result of the component platform

The maximum principal stress result of the static structural analysis of the component platform is presented in **Figure 7.6** above. The maximum stress is displayed as 50,06 MPa under the maximum load. The highest maximum principal stress generated on the tower sheave component was in fact around 140 MPa under the same amount of load. As it is known, both the components and the test platform parts will be loaded under the same cyclic loading case, and the maximum stress result of the platform is less than the maximum stress result generated in the tower sheave section under the same loading case, the platform can be defined as reliable for cyclic load tests.

Also, the FEM static structural analysis results of the test machine is given below in the **Figure 7.7**. Most of the platform, especially the regions with the highest stresses, is made of S235JR steel. As the highest maximum principal stress is observed as 47 MPa, which is again less than those found in the FEM static structural analysis of the main mooring station components made of S235JR steel which undergo the same cyclic loading case, the machine platform can also be defined as to be used in cyclic loading tests.
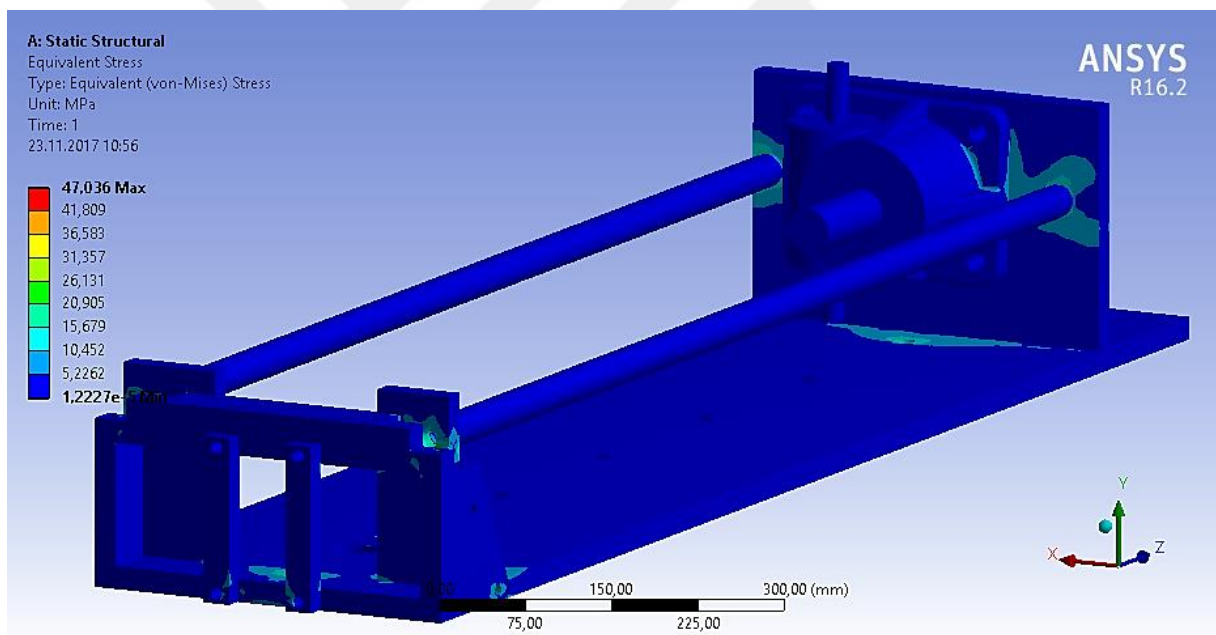
Figure 7.7: Static structural FEM analysis of the test machine platform

Depending on the unaveraged maximum principal stress result presented in **Figure 7.8** below, a maximum stress of 35 MPa is observed within the flying sheave holder part under the maximum load of 5308 N. As the highest maximum principal stress under the maximum load was observed as 66, 26 MPa in the flying sheave component in the previous chapter, the static structural result of this aluminium 5083 holder part has proven, it will be more resistant to loads than the flying sheave and therefore be appropriate to function as component holder in the cyclic loading tests.
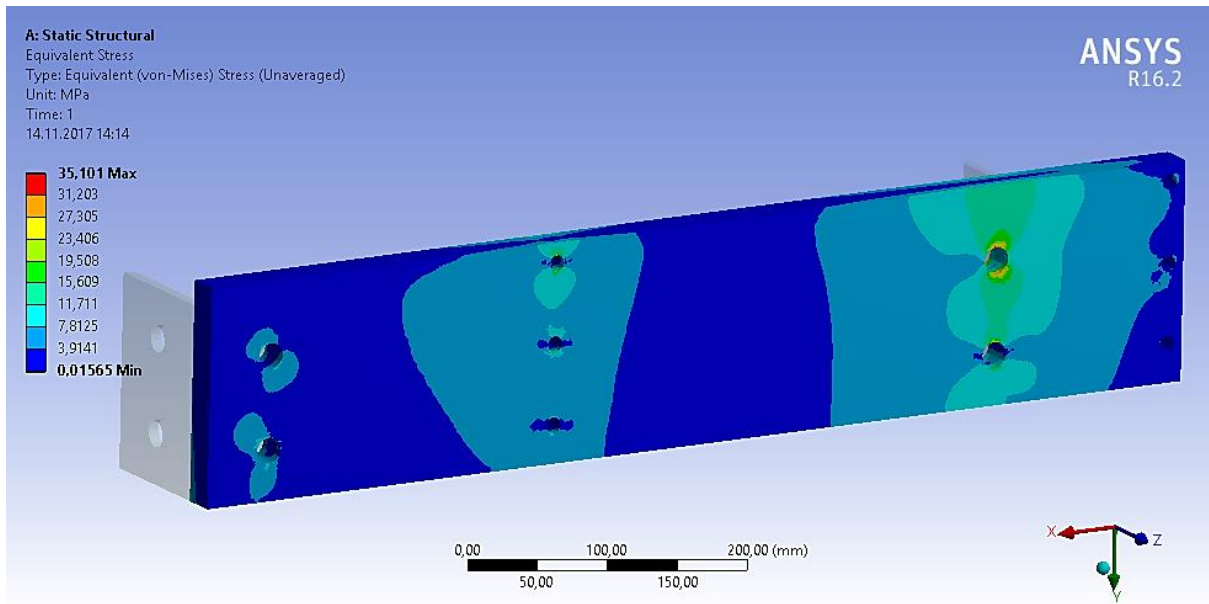
Figure 7.8: Static structural FEM analysis of the flying sheave attachment

7.3 Test procedure

Before the cyclic loading test, the component is assembled to the component platform by bolts, nuts and spring lock washers. The temperature sensor and steel rope is placed onto the determined section of the component. Then loading parameters are entered to the control card, by the user interface screen which can be seen in below **Figure 7.10**, which are load tolerance, safety factor, maximum and minimum loads as well as number of cycles.

After starting the test, temperature was watched every day, and the average daily temperatures were logged. Besides, the pretension of the bolted joints were daily controlled, and were screwed if there was any loss of torque due to the dynamic loading as presented in the **Figure 7.9** below.

Figure 7.9: Daily control of bolted joint pre-tensions
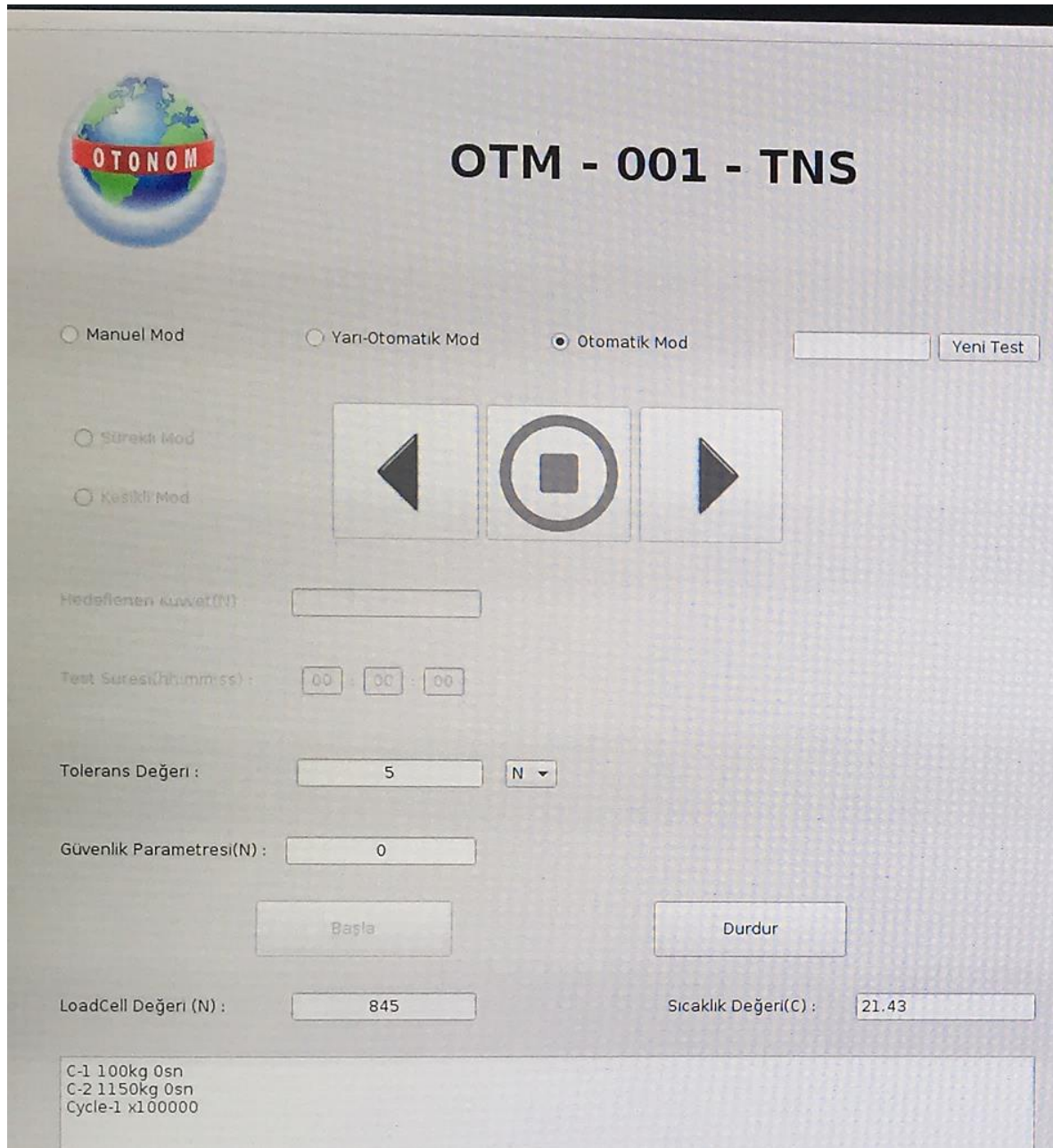
Figure 7.10: Control card user screen

Since temperature increase is a sign of a fatigue mechanism within the material, it is periodically controlled if there is any dramatic temperature increase.

7.4 Modifications

Within the first trial of the cyclic load tests, the seized gear defect has occurred on the bronze section of the gear inside the engine reducer, due to the unwanted frictional torques generated on sliding support regions, where movable screw is joined to the support bars on both sides. Since the cyclic load tests have required too many back and forth movement of

this sliding support on the bars, a vibrated frictional motion, and then high frictional torques were generated on the sliding support after one week from the test begin, which caused this bronze in the gearbox to damage.
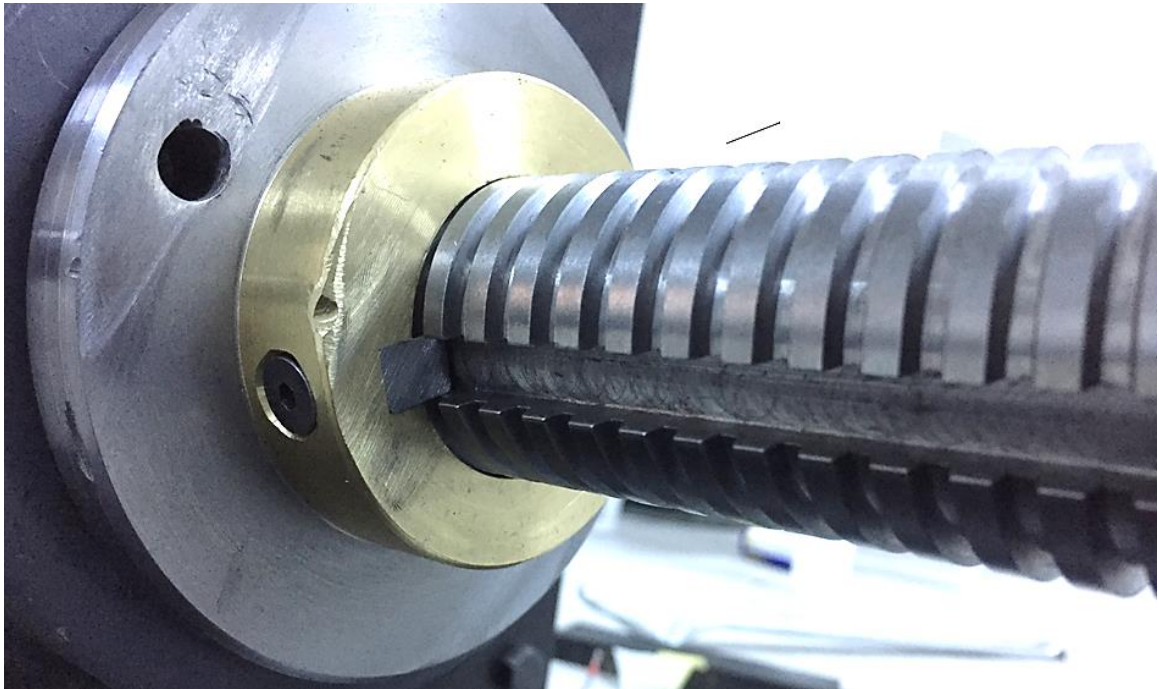
Figure 7.11: Machined wedge on reducer and keyway on the movable screw

In order to solve this problem, a keyway is machine cut on the movable screw as seen in the **Figure 7.11** above, and any possible rotational torques generated by frictions were directed into this wedge, which was machined on the reducer. Besides, the regions where sliding support is joined to bars which generate friction after cyclic movement are periodically (every eight hours) oiled and the risk of any frictional torque was eliminated.

After the final solution, the tests were completed without failure and the results in the following chapter are obtained.

7.5 Test results

7.5.1 Flying sheave

The cyclic load test of the flying sheave was conducted with a frequency of 0,7 Hz and in 19 days with the test setup seen in the **Figure 7.12** below.
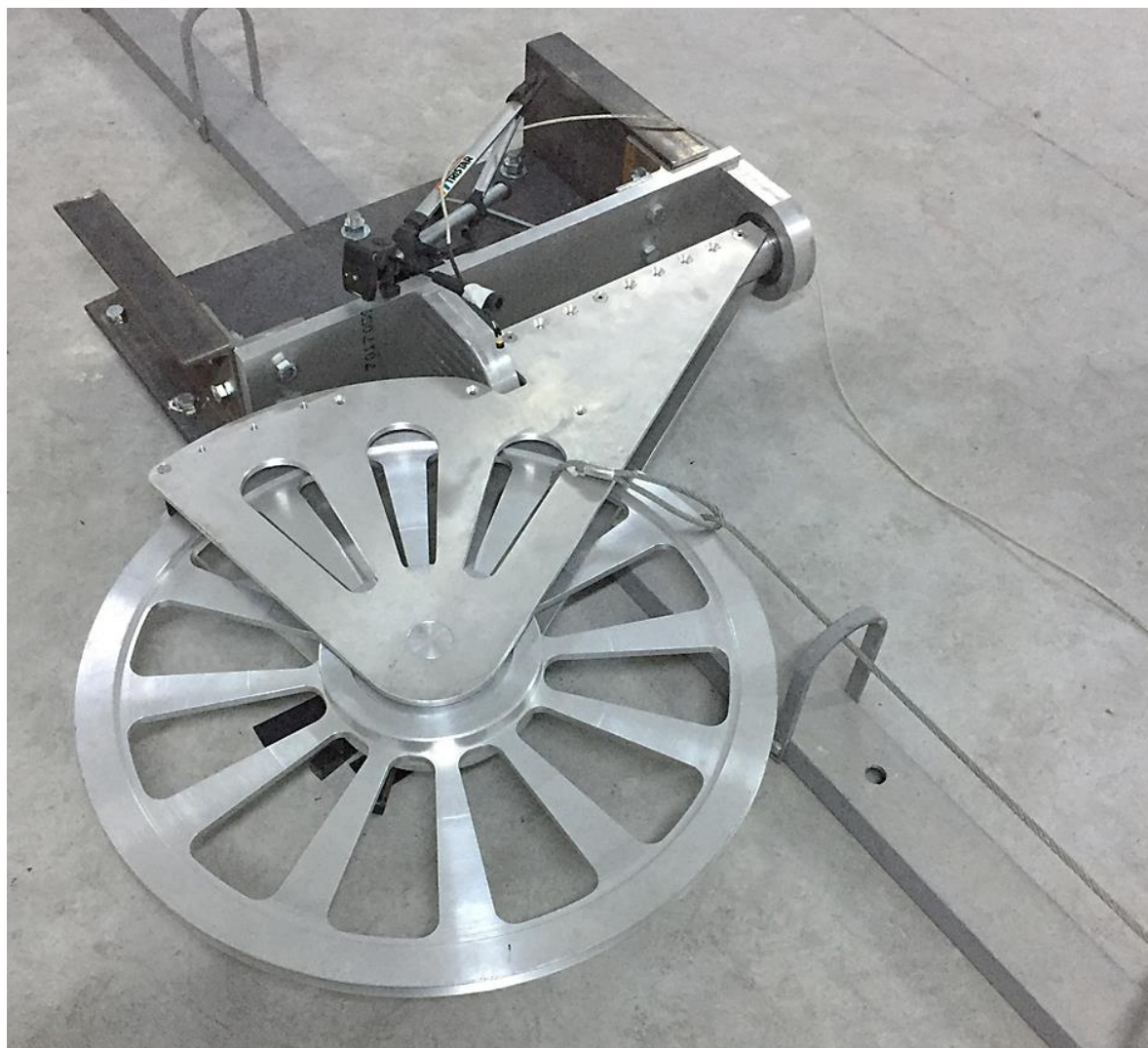
Figure 7.12: Test setup of the flying sheave

After applying the test, with the procedure given in the previous section, neither a failure within the flying sheave component nor in the joints was observed during the duration of cyclic loading test. Besides, no fatigue crack growth related temperature increase was seen during the whole test cycles within the monitored section. All the bolted connections were tight, and the component geometry was not deformed in any area. The picture in the **Figure 7.13** below is taken after the cyclic loading test.

According to the temperature measurements of the temperature sensor during the test, a daily average temperature of 11,5 C°, and a daily temperature range of 8 C° were obtained. As no fatigue related failure during the cyclic loading tests had occurred, the effect of temperature, its difference between room temperature, was irrelevant to discuss. If there was a fatigue related failure, occurred in this temperature range, another test under the room temperature would be essential.

Figure 7.13: View of the flying sheave holder after test

7.5.2 Tower – Crane section part

The 3D design of the tower crane section part can be seen in the **Figure 7.14** presented below. By this part a crane is attached on the tower, which is used to attach a rope coming from the nose of the balloon during the landing. Therefore it will be affected by dynamic loads which are emerged by the rope, attached to the crane on the part. The crane will be attached onto the part by the presented joint holes in the figure, and the loads will act on these joint regions, from where the rope is attached to the crane.
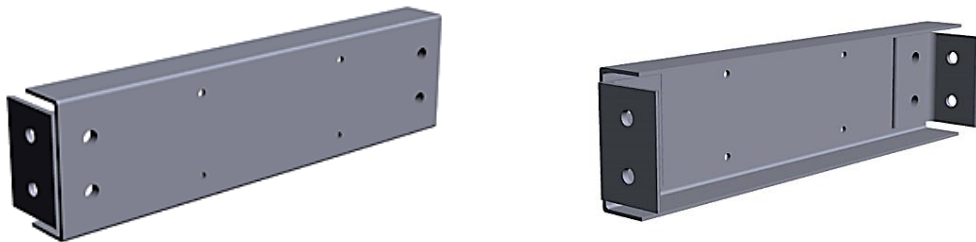
Figure 7.14 (a): "Tower – Crane section" front view, **Figure 14 (b):** Behind view

The cyclic load test of the tower crane section part was completed within 17 days, under a frequency value of 0,75 Hz, on the test setup seen in **Figure 7.15** below. By attaching the ropes to a 30 mm thick aluminium plate on the points where load is precisely expected, the dynamic load and its moments affecting the part via the crane was applied on the part. The temperature sensor was also placed to the region where the highest stress is expected, in order to monitor any sudden temperature increase.

Figure 7.15: "Tower – Crane section" component attached to the test platform

The picture in the **Figure 7.16** was taken after the cyclic load test of the component. After applying the test procedure given in the previous section was followed, neither a failure within the tower crane part nor in the joints was observed during the test. Besides, no fatigue crack growth related temperature increase was seen during the whole test cycles within the monitored section. Some friction affected wears were on the other hand, seen between the contact surfaces between part and bolted joints in which the pretension was always remained. All the bolted joints were tight, and the component geometry was not deformed in any area. According to the temperature measurements of the temperature sensor during the test, a daily average temperature of 14,7 C°, and a daily temperature range of 8 C° were observed. As no fatigue related failure was observed during the cyclic loading tests, the effect of temperature range and magnitude, its difference between room temperature, was irrelevant to discuss. If any fatigue damage has occurred during the test under this temperature range, another test specifically under the room temperature would be essential to compare.

Figure 7.16: Tower crane section part after the test

8 Discussions

In this chapter, the results obtained by the CAE fatigue analyses, analytically generated curves and also cyclic load tests are compared and discussed for the new -fatigue resistant – and the former mooring station designs, respectively of 17 m and 14 m long aerostats.

In the **Table 8.1** below, SF results by CAE fatigue analysis of the two different mooring stations are presented. As seen, the expected maximum dynamic load range for the mooring station of 17 m balloon is approximately 50% higher than the maximum dynamic load range for the mooring station of 14 m balloon. Therefore, the mooring station of 17 m balloon had to be bigger and designed with components which are even more resistant to repetitive loads. Depending on the presented results, as fatigue resistant designed, mooring station components of 17 m aerostat have all shown SF values above 2,0 despite these load range increase. It is also observed that, the former mooring station design of 14 m balloon has shown close values to the new fatigue resistant designed one, except the rope connection arm, of which fatigue SF is appeared to be 1,48, less than the acceptable SF value.

Table 8.1: Comparison of the component fatigue SFs of 14 m and 17 m balloon mooring stations

Mooring Station Type	Cyclic Loading, N	Load range, N	Flying Sheave	Tower	Rope Connection Arms
14 M	3611 - 2059	1552,00	3,81	2,71	1,48
17 M	5308 - 3006	2322,00	3,55	4,98	2,19
% Change		49,61	-6,96	83,64	47,97

Beside of the CAE fatigue analysis results of the two different mooring stations, compared above, the SF values, generated by four different fatigue limit determination methods for the mooring station components of 17 m balloon are also presented and also compared with the already given CAE fatigue SF below, in **Figure 8.1**. The analytical fatigue limit determination methods include firstly the limit determination by fatigue strength from the S-N curves (for steels according to the fatigue strength at 10^6 number of cycles to failure (Nf) and for Al-alloys according to the fatigue strength at 10^9 number of cycles to failure (Nf)). The S-N curves were generated by Basquin's equation with the material related parameters, and were corrected by Goodman MSC and component dependent SRFs. Other two fatigue limit determination methods were based on the **Equations 2.15** and **2.16,** FLE1 and FLE2, which are used to determine fatigue limits of steels and steel alloys at gigacycle regimes. Moreover,

as a safe-design recommendation taken from the literature, an analytical fatigue limit of UTS x 0,45 depending on the fatigue limit of axially cyclic loaded steels, presented in **Figure 2.13**, was also used and compared with the other analytical approaches.
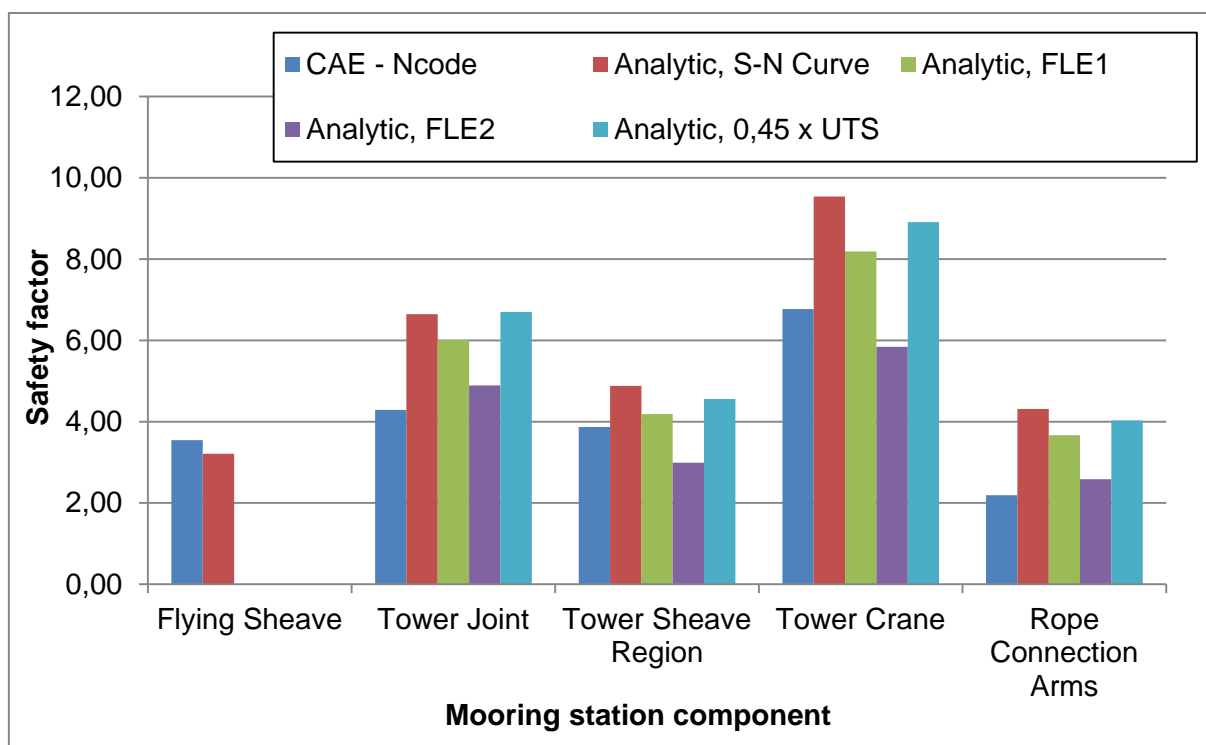
Figure 8.1: Comparison of safety factors obtained by CAE and analytical methods

According to the comparison data in the **Table 8.2**, except the flying sheave, the CAE fatigue analysis generated safety factors were appeared to be the most conservative, and the safety factors by analytical limit determination methods were appeared to be the less conservative with higher SF values. However, the analytical SF results are accepted as more reliable than the results obtained by CAE fatigue analyses, due to the more comprehensive parameters and more detailed theoretical equations. In fact, within the CAE fatigue analyses, rougher curves were generated by nCode during the material generation section, in order to make fast and simple fatigue analysis of the structures. It however, resulted in more conservative and less accurate results, when compared to analytical methods. This aspect of CAE must be well considered, since it will result in heavier and unnecessarily costly designs in the future.

Among the analytical generated values, FLE2 equation has shown the most conservative values for each of the components, while the values obtained by the S-N curve fatigue strength dependent method seem to be the highest, which presented therefore the least conservative analytical results.

Table 8.2: 17 M Aerostat – Fatigue SFs calculated by varying methods

	Flying Sheave	Tower Joint Section	Tower Sheave Section	Tower Crane Section	Rope Connection Arms
CAE - Ncode	3,55	4,29	3,87	6,77	2,19
Analytic, S-N Curve	3,21	6,64	4,88	9,54	4,31
Analytic, FLE1	-	6,01	4,19	8,19	3,67
Analytic, FLE2	-	4,89	2,99	5,84	2,58
Analytic, 0,45 x UTS	-	6,70	4,56	8,91	4,03
CAE vs S-N Curve, %	10,44	-35,43	-20,70	-29,04	-49,25
CAE vs FLE1, %	-	-28,61	-7,60	-17,32	-40,28
CAE vs FLE2, %	-	-12,28	29,50	15,89	-15,20
CAE vs 0,45 x UTS, %	-	-35,98	-15,08	-24,01	-45,68

As seen in the data table, among all of the analytical limit determination methods, the analytical SFs obtained from FLE2 method is the most similar to the SF results taken by the CAE fatigue analysis for all of the mooring station components of the 17 m balloon. Besides, as expected, the results depending on the limits determined by gigacycle regimes (FLE1 and FLE2), were appeared as more conservative than the results according to the accepted fatigue limit at 10^6 (for steels) and 10^9 (for Al) number of cycles of the predicted component S-N curves. Moreover, a similarity –especially for tower parts- was observed between the S-N curve and 0,45 UTS based analytical approaches.

When considering the safety factors obtained by the each of the analytical fatigue limit determination methods, the S-N curve, FLE1 and FLE2 dependent, all of the components seem to be designed adequately fatigue resistant with safety factors above 2, while the tower crane and joint section parts with safety factor much above 2 seems to be even designed over safe. Considering the decrease in fatigue limits, therefore fatigue safety factors, of steels in gigacycles, FLE1 and FLE2 are however recommended more, of which FLE2 seems to present too conservative results which may result in too heavy designs, FLE1 would be more appropriate. The underestimation of gigacycle affects especially in the S-N curve based analytical determination method, on the other hand, may result in damages of

the components, which are accepted as safe but will be used under dynamic loads at gigacycle regimes.

As all of the components were designed according to the infinite life criteria with fatigue safety factors above 2 calculated by varying fatigue limit methods, it was planned to test the two components under cyclic loading with determined parameters for the worst possible case according to high cycle fatigue (HCF), conducted up to 1 000 000 life cycles, in order to verify the designs. Since no such fatigue related failure or damage was observed within the flying sheave and tower crane section parts after the tests, the designs were accepted as reliable and the analyses were verified for the worst dynamic loading condition which will take approximately one and a half months with the highest frequency caused by winds. Even though the flying sheave component is made of aluminium 5083 alloy, and has an accepted fatigue limit of the fatigue strength of the component at 10^8 life cycles, the test duration was found adequate, since one and a half months under the highest possible wind condition was thought not possible to experience in the service time. On the other hand, a test system, which can test the flying sheave component made of 5083 Al alloy, or the material specimens, for the material testing and S-N curve generation, under the same cyclic loading up to 10^8 or even 10^9 number of cycles would make the verification of this component design much more reliable.

9 Summary and outlook

Within this thesis work, primarily a fatigue resistant design of a 17 m long aerostat was done by a comprehensive literature research and safe-life fatigue design criterion. Furthermore, fatigue behaviours of the mooring station components accordingly of a former 14 m and the new 17 m aerostats were analysed through CAE using FEM software ANSYS and nCode DesignLife, as well as analytical life predictions and cyclic load tests at the firm Otonom Teknoloji. While the fatigue investigation for the mooring station design of the 14 m balloon was only limited by CAE fatigue analysis with nCode, for the mooring station design of the larger 17 m balloon, the further described steps, analytical approach, and cyclic load tests were additionally applied and the results were discussed. The comparison between the CAE analysis and analytical determinations was done using fatigue safety factors, which were calculated by the ratio of the stress amplitude to the predicted fatigue limit of the related component.

After the CAE fatigue analyses for the two different mooring stations, the safety factor values of the components for the fatigue resistant mooring station design were found above 2, which was the aimed value before the analyses, despite the increase of the dynamic load range between the former and the new fatigue resistant mooring stations approximately up to %50.

The safety factors found by varying analytical methods, which are fatigue strength at 10^6 life cycles for steel components 10^9 for aluminium components, fatigue limit equations FLE1 and FLE2 and lastly 0,45 X UTS for steel components, have shown variated results compared to the results of CAE fatigue analyses, while the highest similarity to the CAE results was observed by FLE2 analytical method. Among analytical methods, the highest similarity was seen between the S-N curve dependent method, in which the fatigue limit is taken according to the fatigue strength of the steel components at 10^6 and of the aluminium components at 10^9 life cycles, and 0,45 x UTS method. Although results by CAE were more conservative, analytical methods, which are considered to be more accurate, especially FLE1 was recommended to be more focussed in order to make a reliable safe-life, or infinite-life design for metallic components at gigacycle regimes without too heavy and costly designs. By FLE1 method, both the possible effects of gigacycle regime are considered, which are not taken into consideration in the method of fatigue limit prediction on S-N curve, and also the design is not too conservative -over-safe- as in FLE2.

Lastly, in the cyclic loading tests for the flying sheave and the tower crane section part, which were applied for the verification purposes, no fatigue related failure or damage has occurred. Depending on these tests, therefore, the analyses were accepted to be reliable.

For further aerostat mooring station design projects, which take dynamic loads and metal fatigue into consideration, it is recommended to apply the steps used in this thesis work as a guideline and improve the works by applying more advanced cyclic testing approaches with machines which may test components or specimens with higher frequencies, up to 20 Hz, and up to 10^8 life cycles, in order to verify analytical or CAE analysis results with a higher correctness and to make fatigue resistant design approach much more reliable. If possible, besides, it would even be better to test components made of such non-ferrous metals as Al-alloys, which have definitely no such certain fatigue limit, under cyclic loading up to 10^9 life cycles, in order to generate much more dependable test results.

Another important improvement would be applying cyclic loading tests not only for the components but also for the specimens made of component materials to obtain experimental S-N curves of the materials before all of the analysis stages, to be able to generate more accurate life curves, therefore, more reliable designs.

Finally, if the inspection costs are proportionally adequate compared to other costs within a design project, a fail-safe design may be applied instead of safe-life design, which is in order to achieve the weight disadvantage and thus to produce lighter components with minimized costs. This type of design methodology, on the other hand, would require periodical inspections with special measurement equipment during the service.

10 References

[ASM08]   ASM International: Elements of Metallurgy and Engineering Alloys. Chapter 14: Fatigue, 2008, Doc. No.: 05224G, Available online at: www.asminternational.org

[Bad14]   Bader, Qasim.; Kadum, Emad.: Mean stress correction effects on the fatigue life behaviour of steel alloys by using stress life approach theories. International Journal of Engineering & Technology. 14 No: 04 (143804-5656-IJET-IJENS), 2014

[Bap11]   Baptista, C. A. R. P.; Versuto, B. C. B. V.; Oliveira, F. P.; Torres, M. A. S.; Costa, D. H. S.: Mechanical and microstructural characterization of flash-welded joints in HSLA Steels. 21th Brazilian Congress of Mechanical Engineering October 24-28, 2011, Natal, RN, Brazil

[Ban13]   Bandara, C. S.; Siriwardane, S. C.; Dissanayake, U. I.; Dissanayake, R.: Preliminary study on an offshore wind energy resource monitoring system. International Journal of Materials, Mechanics and Manufacturing, 2013

[Bir17]   Bircelik: Technical Catalogue 2017 Available online at: https://bircelik.com/tr/kategori/420-1-4021-

[Boa90]   Boardman, B: Fatigue resistance of steels. ASM Handbook, Volume 1: Properties and Selection: Irons, Steels, and High-Performance Alloys ASM Handbook Committee, Doc. No.: 06181G, p 673-688, 1990

[Coo06]   Cook, C. D.: Finite element modeling for stress analysis. University of Wisconsin – Madison John Wiley & Sons, Inc., 1995 ISBN 0-471-10774-3

[Cra10]   http://craftsmenindustrial.com/wp-content/gallery/aerostat/ci-platform_product-shot.jpg

[DIN ISO 68-1]   Norm DIN ISO 68-1: Gewinde allgemeiner Anwendung – Grundprofil. Beuth Verlag, Berlin, 1999

[Dzi16]   Dzioba, I.; Lipiec, S.: Testing the mechanical properties of S355JR steel with different types of microstructure. 2016

[Erd15]   Erdemir Group: Product Catalogue 2015, Available online at: https://www.erdemir.com.tr/Sites/1/upload/files/Erdemir-Group-Product-Catalogue-2015-62.pdf

[GAO-13-81]   U.S. Government Accountability Office: DEFENSE ACQUISITIONS: Future Aerostat and Airship Investment Decisions Drive Oversight and Coordination Needs. Report to the Subcommittee on Emerging Threats and Capabilities, Committee on Armed Services, U.S. Senate Report to the Subcommittee on Emerging Threats and Capabilities, Committee on Armed Services, U.S. Senate, GAO-13-81, 2012, Available online at http://www.gao.gov.

[Gaw07]   Gawande, V. N.; Bilaye P.; Gawale, A. C.; Pantt, R. S.; Desai, U. B.: Design and fabrication of an aerostat for wireless communication in remote areas. American Institute of Aeronautics and Astronautics, 2007

[Gue13]   Guennec, B.; Ueno, A.; Sakai, T.; Takanashi, M.; Itabashi, Y.: Effect of loading frequency in fatigue properties and micro-plasticity behaviour of JIS S15C low carbon steel. 2013

[Hig78]   Higashida, Y.; Burk, D.; Lawrance JR, F. V.: Strain-controlled fatigue behaviour of ASTM A36 and A514 Grade F Steels and 5083-0 aluminum weld materials. 1978

[Kos93]   Koshal, D.: Manufacturing Engineer's Reference Book. Butterworth-Heinemann., pp. 1/6-1/7., 1993

[Kos12]   Kossakowski, P. G.; Trampczynski, W.: Microvoids evolution in S235JR steel subjected to multi-axial stress state. Kielce University of Technology, Faculty of Civil Engineering and Architecture, 287–314, 2012

[Kra11]   Krausman, J. A.; Petersen, S. T.: The 22M Class Aerostat: Increased Capabilities for the Small Tethered Aerostat Surveillance System. AIAA 11th Aviation Technology, Integration, and Operations (ATIO) Conference, AIAA 2011-7069

[Kta12]   Ktari, A.; Zied, A.; Haddar, N.; Elleuch, K.: Modeling and computation of the three-roller bending process of steel sheets. 2012

[Kuk14]   Kukla, D.; Balkowiec, A.; Grzywna, P.: Evaluation of microstructural changes of S235 steel after rolling on the basis of microscopic observations and eddy current non-destructive method. Advances in Materials Science, Vol. 14, No.4 (42), December 2014

[Kum09]   Kumar, S. R.; S, Kumar.; Kumar, A. R. S.: Fatigue of steel structures. Chapter 1.7, Design of Steel Structures, Indian Institute of Technology Madras, 2009, Available online at: nptel.ac.in

[Mil05]	Miller, J. I.: The design of robust helium aerostats. A thesis submitted to McGill University in partial fulfilment of the requirements for the degree of Master of Engineering. McGill University, Montreal, August, 2005
[Mit09]	MIT OpenCourseWare: Finite Element Analysis of Solids and Fluids I. Fall 2009, Available online at: http://ocw.mit.edu
[Mut11]	Mutombo, K.; Toit, M.: Corrosion fatigue behaviour of aluminium 5083-H111 welded using gas metal arc welding method. University of Pretoria, 2011
[Nis12]	Nishina, Yoshiaki.; Imanishi, Daisuke.; Shibuya, Kiyoshi.: Various measurement technologies (Temperature/Stress/Fatigue/Crack) with highly precise infrared thermography and their applications. JFE Techical Report, No. 17, 2012
[Ost07]	Ostermann, F.: Anwendungstechnologie Aluminium. Springer-Verlag, Berlin und Heidelberg, 2007
[Pen13]	Penning, B.; Walther, F.; Dumke, D.; Künne, B.: Einfluss der Verformungsgeschwindigkeit und des Feuchtegehaltes auf das quasistatische Verformungsverhalten technischer Vulkanfiber. MP Materials Testing 55, 4 (2013) 276-284
[Pet05]	Petersen, S. T.: The small aerostat system: Field tested, highly mobile and adaptable. AIAA 5th Aviation, Technology, Integration, and Operations Conference (ATIO), AIAA 2005-7444
[Poe11]	Poeppelman, C. M.: Comparison of Axial and Torsion Fatigue of a High Hardness Steel. Submitted to the Graduate Faculty as partial fulfillment of the requirements for the Master of Science Degree in Mechanical Engineering. The University of Toledo, 2011
[Qi06]	Qi, H. J.: Finite element analysis. MCEN 4173/5173 University of Colorado, 2006
[Ram14]	Ramamutry, U.: Fatigue: Total Life Approaches. Fatigue Course, Laboratory for Micro and Nano mechanics of Materials, 2014, Available online at: materials.iisc.ernet.in
[Roe00]	Roessle, M. L.; Fatemi, A.: Strain-controlled fatigue properties of steels and some simple approximations. International Journal of Fatigue, Vol. 22, pp. 495-511, 2000

[Row07]   Rowlands, D. P.: The mechanical properties of stainless steel. Southern africa stainless steel development association. Stainless steel information series No.3, 2007

[Sch14]   Scheuer, C. J.; Fraga, R. A.; Cardoso, R. P.; Brunatto, S. F.: Effects of heat treatment conditions on microstructure and mechanical properties of AISI 420 steel. 21th CBECIMAT, November 13th, 2014

[Sey17]   Seykoc Aluminyum: Aluminum-alloys 5083. Available online at: http://www.seykoc.com.tr/icerik/5083?dil=tr

[Sha15]   Sharifi, H.; Kheirollahi-Hosseinabadi, I.; Ghasemi, R.: The effect of tempering treatment on the microstructure and mechanical properties of DIN 1.4021 martensitic stainless steel. International Journal of ISSI, Vol. 12, 2015, No.1, pp. 9-15

[Shi00]   Ship Structure Committee: Fatigue of aluminum structural weldments. NTIS #PB2000-108442, pp. 44, 2000

[Sko14]   Skowronski, W.; Wloka, A.; Chmiel, R.: Modelling of strength processes of S235JR steel at increased temperature. 2014

[Tho05]   Thompson, B. S.; Müller, N.: ME 471 Engineering Design II. Michigan State University, Spring 2005.

[Wec04]   Weck, O.; Kim, I. Y.: Engineering design and rapid prototyping. Lecture 4: Finite element method,16.810. Massachusets Institute of Technology, 2004

11 Appendix of figures

12 Appendix of tables